Mechanisms Underlying Biphasic Synaptic Vesicle Acidification in Glutamatergic Synapses

Inaugural-Dissertation

zur Erlangung des Doktorgrades
der Mathematisch-Naturwissenschaftlichen Fakultät

der Heinrich-Heine-Universität Düsseldorf

vorgelegt von

Felix Ralf Michael Beinlich
aus Münster

Jülich, Juni 2018

aus dem Institute of Complex Systems – Zelluläre Biophysik
des Forschungszentrums Jülich

Berichterstatter:
1. Prof. Dr. Christoph Fahlke
2. Prof. Dr. Karl-Erich Jaeger
Tag der mündlichen Prüfung: 12. Oktober 2018

"Nature is showing us only the tail of the lion, but I have no doubt that the lion belongs to it even though, because of its large size, it cannot totally reveal itself all at once. We can see it only the way a louse that is sitting on it would."

Albert Einstein, 1914

Abstrakt

Signalübertragung und Informationsverarbeitung einer chemischen Synapse während neuronaler Aktivität beruht auf der regulierten Freisetzung von Neurotransmittern. Diese Art der chemischen Erregungstransmission basiert auf der repetitiven Fusion von synaptischen Vesikeln mit der Plasmamembran. Um die Verfügbarkeit beladener synaptischer Vesikel zu gewährleisten, werden diese durch Recycling regeneriert. Dieser Prozess beinhaltet Endozytose, Neurotransmitterbeladung und Exozytose. Da die Anzahl der freigesetzten Neurotransmittermoleküle direkt die Stärke der synaptischen Transmission moduliert, ist deren Beladung der kritischste Schritt während des Recycling. Obgleich mehrere Mechanismen und regulatorische Prozesse bereits identifiziert wurden ist die Regulation des Grades der Vesikelbeladung noch nicht vollständig verstanden. Der wichtigste exzitatorische Neurotransmitter im Nervensystem der Wirbeltiere ist Glutamat. Vesikuläre Glutamattransporter nutzen den protonenelektrochemischen Gradienten als treibende Kraft für die Glutamatakkumulation in synaptische Vesikel. Die vesikulare Glutamataufnahme wird darüber hinaus durch niedrige millimolare $[Cl^-]_{Cytosol}$ stimuliert und durch hohe millimolare $[Cl^-]_{Cytosol}$ inhibiert. Abwesenheit des Cl^-/H^+ Austauscher ClC-3 führt zu schwerwiegender Degeneration des zentralen Nervensystems. Die genaue Funktion von ClC-3 in der Regulation der Glutamatbeladung ist noch nicht vollständig untersucht und wird gegenwärtig diskutiert. In dieser Thesis konnte mittels des fluoreszierenden Proteins Cerulean, als neuartiger Biosensor und Fluoreszenzlebenszeitmikroskopie, der absolute pH Wert in synaptischen Vesikeln von kultivierten Primärneuronen des Hippocampus bestimmt werden. Es wurde gezeigt, dass nach der Endocytose synaptische Vesikel erst bis zu pH 4.5 ansäuern und dann wieder auf den Ruhe pH alkalisiert. Mittels *knock-out* Mausmodellen und pharmakologischen Blockern konnte der molekulare Prozess hinter diesem biphasischem Prozess der Ansäuerung aufgeklärt werden. Es konnte gezeigt werden, dass die anfängliche Ansäuerung des synaptischen Vesikels unabhängig von der V-ATPase Aktivität, aber in Abhängigkeit der luminalen $[Cl^-]$ stattfindet. Die luminale $[Cl^-]$ ist anfangs im Vergleich zur $[Cl^-]_{cytosol}$ hoch. Der dadurch entstehende ΔCl^- wird genutzt durch den Cl^-/H^+ Austauscher ClC-3, um luminales Cl^- gegen cytosolische H^+ auszutauschen. Dies führt zu einer bisher unbekannten, ATP unabhängigen, Ansäuerung des synaptischen Vesikels. Der dadurch entstehende protonenelektrochemische Gradient wird dann von VGLUT1 genutzt, um Glutamat im synaptischen Vesikel zu akkumulieren. Es konnte weiterhin gezeigt werden, dass die Alkalisierung abhängig ist von VGLUT Aktivität. Die Ergebnisse dieser Arbeit liefern einen neuen Einblick in die Bedeutung des Cl^-/H^+ Austauschers ClC-3 in der Regulation des pH_{SV}.

Abstract

During neuronal activity signal transmission and information processing at a chemical synapse relies on the regulated release of neurotransmitters which are stored in synaptic vesicles. This type of chemical neurotransmission is based on the repetitive fusion of a high number of synaptic vesicles with the plasma membrane. In order to refill the pool of neurotransmitter-loaded synaptic vesicles they are regenerated by recycling. This process involves endocytosis, neurotransmitter loading and exocytosis of synaptic vesicles. Because the amount of neurotransmitter molecules stored in synaptic vesicles directly modulates the strength of synaptic transmission the filling of synaptic vesicles with neurotransmitters is the most critical step in synaptic vesicle recycling. The regulation of the degree of vesicle filling is not fully understood yet, although several mechanisms and regulatory processes have been identified already. The major excitatory neurotransmitter in the vertebrate nervous system is glutamate. Glutamate uptake into synaptic vesicles is mediated by vesicular glutamate transporters (VGLUTs) that utilize the electrochemical gradient of protons for vesicular glutamate accumulation. Moreover, vesicular glutamate uptake is stimulated by low millimolar $[Cl^-]_{cytosol}$ and inhibited by high millimolar $[Cl^-]_{cytosol}$. Removal of the Cl^-/H^+ exchanger ClC-3 leads to severe neurodegeneration. The exact function of ClC-3 in regulation of glutamate uptake is not fully understood yet and controversially discussed. By use of the fluorescent protein Cerulean as a novel biosensor for pH-sensing and fluorescence lifetime imaging microscopy the absolute pH in synaptic vesicles in primary hippocampal neurons could be measured. It is shown for the first time that after endocytosis synaptic vesicle first over-acidify to a pH similar to that of lysosomes, and then alkalize to the resting pH. By a combination of *knock-out* mice models and pharmacological blocking the molecular process behind this biphasic acidification process could have been unraveled. The initial acidification is independent of V-ATPase activity but strongly depends on the luminal Cl^- concentration. It could be demonstrated for the first time that the initial ΔCl^- with high luminal Cl^- concentration is utilized by the Cl^-/H^+ exchanger ClC-3 to rapidly accumulate cytosolic H^+ in exchange to luminal Cl^- in the synaptic vesicle lumen. This, hitherto unknown process of acidification mediated by Cl-3 enlightens an ATP-independent, energy saving pathway of synaptic vesicle acidification promoting the exhibition of the driving force which regulates neurotransmitter loading in recycled synaptic vesicles. The re-alkalization process, furthermore, is mediated by VGLUT1 activity. The findings in this thesis thus provide a new insight into the importance of the luminal $[Cl^-]$ and the Cl^-/H^+ exchanger ClC-3 in the regulation of pH_{SV} after endocytosis of recycled synaptic vesicles.

Contents

List of Figures

List of Tables

Chapter 1

Introduction

1.1 Neurotransmission in a Chemical Synapse

The nervous system is build up of nerve cells and supporting glial cells. Nerve cells, also called neurons, have the unique ability to respond to stimuli with an electrical discharge, the exhibition of a nerve impulse, and by their fast conduction of the nerve impulse over long distances. This allows a fast transmission of nerve impulses in milliseconds either within the central nervous system or organs of the body. A single neuron typically can be distinguished by three major compartments, the cell body or soma, the dendrites and the axon. In the soma, nucleus, protein synthesis machinery and various organelles (ER, lysosomes, mitochondria) are located. Synaptic input from other cells is collected on the large surface of the dendrites which form extensive branches, the 'dendritic tree'. In contrast, nerve impulses from the cell body to other nerve cells are conducted via the axon. Therefore, in the axonal branches specific regions are formed, the synaptic boutons, which are club-shaped enlargements in close proximity to the cell body or the dendrites of other nerve cells [1].

Signal transmission and information processing at a chemical synapse in the central nervous system relies on the regulated release of soluble mediators. Already in the late 1960s Katz and colleagues have shown that synaptic transmission at the neuromuscular junction is quantized, and proposed that the underlying unit or quantum is a neurotransmitter-filled synaptic vesicle [2]. Hereby, a nerve impulse in form of an

electrical discharge, an action potential, depolarizes the presynaptic membrane by interfering the distribution of positively and negatively charged particles across the membrane. This leads to opening of voltage-gated Ca^{2+} channels thus elevating the cytosolic Ca^{2+} concentration. Ca^{2+} then triggers the fusion of synaptic vesicles with the presynaptic membrane, a process called exocytosis, resulting in the release of neurotransmitter molecules into the synaptic cleft, the space between pre- and postsynapse. The released neurotransmitter diffuses across the synaptic cleft at the postsynaptic membrane and binds to neurotransmitter receptor proteins. Once activated, they lead to a transient alteration in the postsynaptic membrane permeability to certain ions which in turn triggers a subsequent series of events [3]. This results in the conversion of the chemical signal back into an electrical signal which is activating or inhibiting, respectively, depending on the neurotransmitter type. In this signal transmission pathway several neurotransmitter are utilized, e.g. glutamate, aspartate, nucleotides, GABA (γ-aminobutyric acid), glycine and monoamines. These neurotransmitters are actively accumulated into synaptic vesicles by vesicular neurotransmitter transporters which differ in their substrate specificity and tissue distribution. This type of chemical neurotransmission is based on the repetitive fusion of a high number of synaptic vesicles with the plasma membrane. In order to refill the pool of neurotransmitter-loaded synaptic vesicles they are regenerated by recycling. This cycle of exocytosis and compensatory endocytosis at the synapse has been termed synaptic vesicle cycle [3].

1.2 Synaptic Vesicle Recycling in the Synapse

In the classical model three distinct synaptic vesicles pools can be distinguished which differ in number and stimulus required for exocytosis [4, 5]. Synaptic vesicles docked in the active zone, forming the readily releasable pool (RRP), are typically released first and are compensatory substituted either by endocytosis or by synaptic vesicles from the recycling pool when endocytosis is not sufficient. Utilization of synaptic vesicles from the reserve pool only occurs when the recycling pool is depleted which can be achieved by prolonged low frequency stimulation [5] (Figure 1.1A). Recent work has demonstrated that the synaptic vesicle pools differ in the composition of their SNARE proteins, the proteins involved in docking and release of synaptic vesicles at the active zone [6]. A crucial step for sustaining synaptic transmission during intense activity is the rapid replenishment of synaptic vesicles through endocytosis. Before subsequent reuse, synaptic vesicles undergo several recycling steps including endocytosis, acidification,

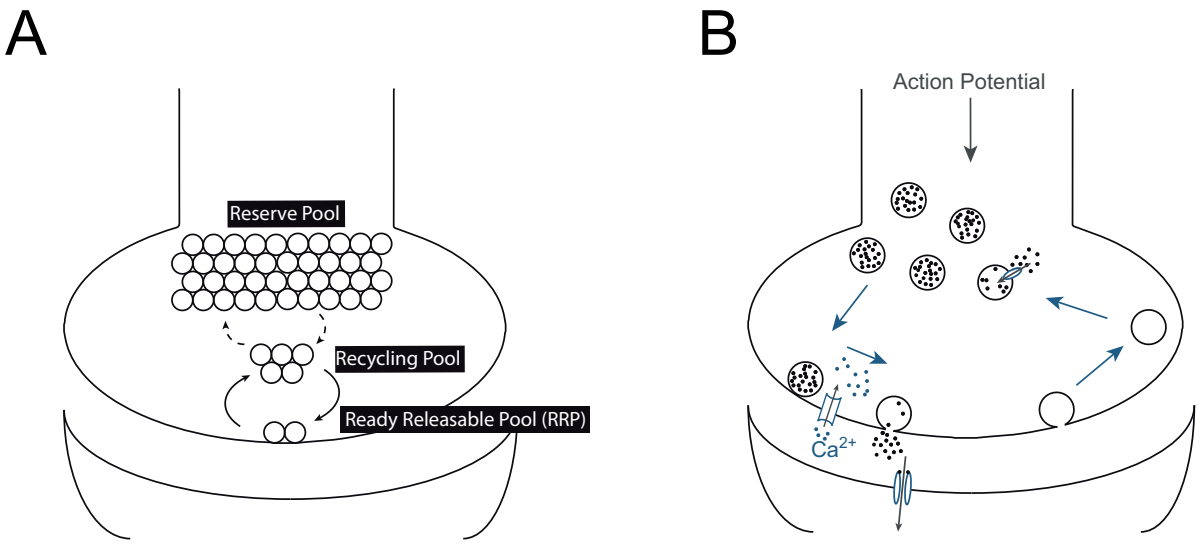

Figure 1.1: **Neurotransmitter loading into synaptic vesicles.** (A) The classic model of three distinct synaptic vesicle pools. With the reserve pool (80 – 90 %), the recycling pool (10 – 15 %), and the readily releasable pool (RRP, ∼1 – 5 %) (adapted from [4]). (B) Recycling process of synaptic vesicles in a single synapse (adapted from [3]).

neurotransmitter loading, docking, release-priming and exocytosis ([3] (Fig. 1.1B). Because the amount of neurotransmitter molecules stored in synaptic vesicles directly modulates the strength of synaptic transmission [7, 8, 9, 10, 11, 12, 13, 14] the filling of synaptic vesicles with neurotransmitters is the most critical step in synaptic vesicle recycling [15, 16]. The regulation of the degree of vesicle filling is not fully understood yet, although, several mechanisms and regulatory processes have been identified already.

1.3 Neurotransmitter Filling into Synaptic Vesicles

To date it is widely accepted that neurotransmitter storage into newly endocytosed synaptic vesicles is maintained by neurotransmitter transporters which harness the electrochemical gradient for protons $\Delta\mu_{H+}$. $\Delta\mu_{H+}$ is composed of a H^+ gradient (ΔpH) and an inside-positive membrane potential ($\Delta\psi$). Typically the ΔpH and $\Delta\psi$ of acidified vesicles are $\sim$ 1.8 pH units [17, 18] and $\sim$ 80 mV [19, 20], respectively. This has been determined in the the RRP of cultured hippocampal neurons, isolated synaptic vesicles and the RRP of chromaffin cells.

Distinct neurotransmitter transporters employ these two types of driving forces to variable extends due to the charge of the neurotransmitter at cytoplasmic pH and its proton-coupled stoichiometry of the import process. Proton-coupled transporters of

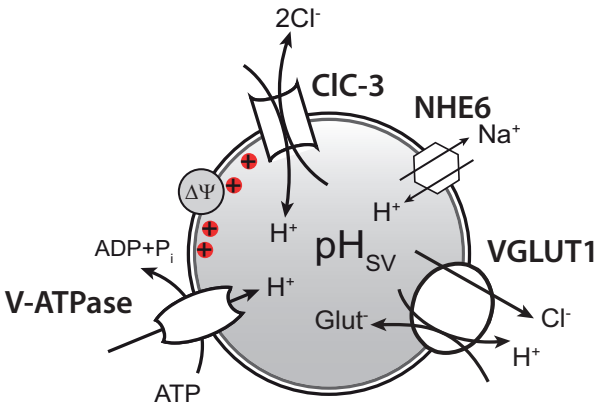

Figure 1.2: **Simplified model of a single synaptic vesicle and its transport proteins.**

electroneutral neurotransmitters such as GABA or glycine are electrogenic and thus utilize both components of $\Delta\mu_{H+}$ [21, 22, 23]. Electroneutral transporters of cationic neurotransmitters are only driven by the transmembrane proton gradients [24, 25, 26], whereas uptake of glutamate by vesicular glutamate transporters (VGLUTs) is primarily dependent on $\Delta\psi$ [27, 28, 29, 30, 31, 32, 33]. A generic model for a single glutamatergic synaptic vesicle and the most important proteins participating into the loading process is shown in figure 1.2. Since vesicular transporter will start the moment a driving force has built up, the amount of accumulated neurotransmitter is critically dependent on the time course of $\Delta\mu_{H+}$ development after endocytosis. This makes the formation and regulation of $\Delta\mu_{H+}$ in synaptic vesicles after endocytosis a matter of high importance.

1.4 Formation and Regulation of the Electrochemical Gradient

$\Delta\mu_{H+}$ describes the H^+ gradient across the vesicular membrane. The total free energy is the sum of the electrical ΔG_ψ and chemical energy ΔG_{pH}:

$$\Delta G_{total} = \Delta G_\psi + \Delta G_{pH} \tag{1.1}$$

and according to Farsi et al., 2017 [34] described as:

$$\Delta G_\psi = z_{H+} \times F \times \Delta\psi \tag{1.2}$$

$$\Delta G_{pH} = R \times T \times ln\left(\frac{[H^+]_{SV}}{[H^+]_{cytosol}}\right) \tag{1.3}$$

where z_{H+} is the proton valence, F is Faraday's constant, $\Delta\psi$ is the membrane potential, R the universal gas constant and T the absolute temperature. The electrochemical gradient ($\Delta\mu_{H+}$) can be calculated as follows:

$$\Delta\mu_{H+} = \Delta\psi + 2.30\frac{RT}{F}\Delta pH \tag{1.4}$$

However, calculation of the electrical component is quite difficult while the chemical component of $\Delta\mu_{H+}$ is mainly determined by $[H^+]_{SV}$ and $[H^+]_{cytosol}$. The $\Delta\psi$ depends not only on the concentration of free protons, but also on the net accumulation of charged ions in the lumen of the compartment and is described by the following equation [35, 36]:

$$\Delta\psi = \frac{FV}{C}\left[\sum_i n_i\,[cation] - \sum_j n_j\,[anion] + \beta \times \Delta pH - B\right] \tag{1.5}$$

where C is the membrane capacitance, V is the SV volume, i and j are all cation and anion species with n_i and n_j are their respective valences, β is the buffering capacity, B represents the Donnan particles, which are primarily fixed negative protein charges trapped in the synaptic vesicle lumen [37]. The dependence of $\Delta\psi$ on these factors means that all variations in volume, protein composition, ion flux and luminal buffering capacity can change $\Delta\psi$ and thus $\Delta\mu_{H+}$.

The regulation of $\Delta\mu_{H+}$ in synaptic vesicles is affected by net proton movement across the membrane: proton pumping activity and proton efflux. All synaptic vesicles independent of the type of neurotransmitter stored inside contain a vacuolar-type H^+-ATPase (V-ATPase). Through energy released by the hydrolysis of ATP to ADP + P_i the V-ATPase translocates protons into the lumen of the SV forming an $\Delta\mu_{H+}$ across the vesicular membrane. Since the V-ATPase is an electrogenic proton pump its efficiency to pump H^+ is dependent on the movement of a counterion which would dissipate the voltage developed from the proton transport [38]. *In vitro* studies showed that the addition of ATP is not sufficient enough to ensure the exhibition of a substantial pH gradient (ΔpH), since activation of the proton pump rapidly increases $\Delta\psi$ and arrests the activity of the proton pump. Dissipation of $\Delta\psi$, by anion entry, allows the V-ATPase in return to pump protons and exhibit a sizable ΔpH.

In contrast, proton efflux from the synaptic vesicle lumen affects the extent of the ΔpH as well. Protons can leave the synaptic vesicle lumen either via passive leakage by the membrane surface of the synaptic vesicle and the physical state of the membrane [39], or through all the transporters and ion exchanger of the synaptic vesicle whose activity is coupled to the translocation of protons for external molecules.

Besides the proton coupled transport of specific neurotransmitters by the vesicular neurotransmitter transporters, two main proton exchanger on SVs are known to contribute to proton efflux from the lumen, NHEs and CLCs.

1.5 NHE Exchangers as Transporters for Luminal Protons

The Na^+/H^+ exchangers NHE6 and NHE9 are proposed to transport cytosolic Na^+ and K^+ at the expense of luminal protons with a stoichiometry of 1:1 [40, 41]. However, recent work in isolated synaptic vesicles has shown that K^+/H^+ exchange was not blocked by the NHE specific inhibitor EIPA (5-(n-ethyl-n-isopropyl)amiloride), suggesting that the measured K^+ response is coming from VGLUT [19, 42] or another, unknown transporter.

With respect to $\Delta\mu_{H+}$ both Na^+/H^+ and K^+/H^+ exchange would result in a decrease of ΔpH while maintaining $\Delta\psi$, and thus by a decrease of the $\Delta\mu_{H+}$ accelerate V-ATPase activity. However, a study on NHE7, who shares similarity in the primary structure to that of NHE6, has shown that it can facilitate Na^+/H^+ exchange bi-directionally [43], and thus allowing it to acidify organellar lumen parallel or ahead of V-ATPase immediately after endocytosis, utilizing the large outwardly directed sodium gradient.

1.6 The Role of Chloride in Regulation of Synaptic Vesicle Acidification

Cl^- is the most abundant anion in the extra- and intracellular space with a $[Cl^-]_{cytosol}$ ranging from 6 - 80 mM in neurons [44, 45, 46, 47, 48, 49, 50],and has shown to play a key role in the regulation of the $\Delta\mu_{H+}$. In studies with synaptic vesicles isolated from mammalian brains, acidification measurements with the weakly-basic fluorescence dye, acridine orange (AO) have shown that Cl^- confers a shunting current for H^+ movement under normal conditions, which inhibits the formation of $\Delta\psi$, and in turn, promotes ΔpH [51, 52, 53]. In absence of exctravesicular Cl^-, however, movement of only a few protons already produces a large $\Delta\psi$, whereas high extravesicular Cl^- concentrations maximizes the ΔpH and stimulates uptake of cationic neurotransmitters, and, in contrast, low extravesicular Cl^- maximizes uptake of anionic transmitters, like glutamate, by promoting $\Delta\psi$ [22]. Therefore, the balance of ΔpH and $\Delta\psi$ is influenced by the permeability of the synaptic vesicle membrane to Cl^- with important physiological consequences. Namely,

the balance of $\Delta\mu_{H+}$ is a critical step for the regulation of neurotransmitter concentration and by this the quantal size of synaptic vesicles [54]. Furthermore, in clathrin-coated synaptic vesicles, one possible step of endocytosis, where V-ATPase activity is lacking, a Cl^- flux was observed supporting a Cl^- channel on the synaptic vesicle membrane [55]. Nevertheless, how Cl^- channels and/or transporters modify the pH in synaptic vesicles is still not fully understood. A prominent candidate is the Cl^- transporter ClC-3 [56, 57], however, VGLUT1 itself is also discussed as a candidate for $[Cl^-]_{SV}$ modulation [58, 59, 60].

1.7 CLCs as Regulator for $[Cl^-]_{SV}$

The chloride transporter ClC-3, which belongs to the CLC family [61], has been detected in early and late endosome as well as in synaptic vesicles [62, 63, 57]. The CLC-family consists of two sub-classes: Cl^--selective ion channels and transporters that catalyze the stoichiometric exchange of one H^+ for two Cl^-, and are expressed in most tissues fulfilling diverse functions [64]. CLCs are dimerized [65, 66, 67]. This dimerization can either be homologous or heterologous [68, 69]. ClC-3, which shares a high homology to ClC-4 and ClC-5 operates as a voltage-dependent Cl^-/H^+ exchanger in a 2:1 stoichiometry [70, 71]. It can build a heterodimer with ClC-4 and then guides ClC-4 to the endosomal pathway [69], but also its different splice variants result in different subcellular localization [68] including synaptic vesicles [62, 63, 57].

At low $[Cl^-]_{SV}$ the import of Cl^- into the SV lumen is activated by an inside positive membrane potential and an outwardly directed proton gradient once established by the proton pump. However, this process is highly electrically dissipative and should increase ΔpH by reducing $\Delta\psi$ as long as an active proton pump compensates for the loss of protons. ClC-5 and a prokaryotic homologue of CLC Cl^--channels are blocked at high luminal $[H^+]$ [72, 73]. ClC-3 shows close structural and functional homology to ClC-5, thus, it cannot be excluded that this H^+-dependent block also appears in ClC-3. It was also shown in several studies that ClC-3 facilitates acidification of lysosomes and endosomes by accumulation of luminal chloride [71, 74].

The $[Cl^-]_{SV}$ is around one magnitude higher than that of the cytoplasm. Under these conditions ClC-3 may operate in the reverse direction thus using the chloride gradient as a driving force to import cytoplasmic protons into the SV lumen as it has been shown for ClC-5 [75, 76] and by electrophysiological characterization [70]. However, application of the specific V-ATPase blocker Bafilomycin or Folimycin abolishes apparent acidification

in SV after endocytosis [18, 77, 78]. In a hypothesis developed by Farsi et al. [34] the pH change of ClC-3 mediated Cl^-/H^+ exchange may be small due to the 2:1 exchange ratio and the SV proton buffering capacity. However, a substantial membrane potential could be accumulated, and subsequently acidification of the synaptic vesicle by V-ATPase activity may switch the direction of ClC-mediated exchange, working to buffer $\Delta\mu_{H+}$ [34].

The importance of ClC-3 is supported by the finding that a loss of ClC-3 by genetic disruption in rodent models results in severe neurodegeneration represented by impairment of synaptic vesicle acidification and degeneration of the retina and hippocampus at early stages [79, 62, 80]. Although this phenotype suggests excessive glutamate release in the absence of ClC-3, excitatory synaptic transmission did not show any significant differences between *WT* and *Clcn3*$^{-/-}$ mice [62]. This finding can be explained by neurodegeneration and subsequent down regulation of vesicular glutamate transporters in *Clcn3*$^{-/-}$ mice. Using cultured hippocampal neurons to prevent potential interference of neurodegeneration in studying glutamatergic synaptic transmission in *Clcn3*$^{-/-}$ mice it was demonstrated that ClC-3 modulates the magnitude of synaptic events by altering the amount of glutamate release and SV size as well as the release probability of SV while leading the pool size of the readily releasable pool unaffected [57].

1.8 The Vesicular Glutamate Transporter Utilizes $\Delta\mu_{H+}$ for Neurotransmitter Transport into Synaptic Vesicles

The major excitatory neurotransmitter in the vertebrate central nervous system is glutamate. Recycled synaptic vesicles are refilled with glutamate by VGLUTs by use of a membrane potential gradient as driving force [51]. VGLUTs belong to the SLC17 family and so far, three distinct isoforms have been identified in mammals (VGLUT1, 2, and 3) which differ in their expression pattern and subcellular localization [81, 27, 28, 29, 82, 31, 83]. Loss of VGLUT is leading to severe cognitive malfunctions and lethality during postnatal neurogenesis due to abolished glutamatergic neurotransmission [84, 85, 86]. *Knock-out* mouse models of the different VGLUT isoforms exhibit a progressive phenotype including uncoordination, blindness and enhanced startle response [87, 86, 88].

It is widely accepted that glutamate transport is predominantly driven by $\Delta\psi$ [28, 30, 89, 27, 90, 91, 31, 33, 32], and some studies even propose no contribution

of ΔpH in formation of glutamate transport [92, 93, 94]. In contrast, an emerging number of studies show that VGLUT can also function as proton exchanger making its activity dependent on ΔpH [28, 33, 95]. Measurements on VGLUT reconstituted into liposomes have shown that it can function as a K^+/H^+ exchanger [42] which was recently supported by single-vesicle measurements in purified synaptic vesicles [19]. Moreover, it was reported by electrophysiological recordings that VGLUTs are allosterically stimulated upon acidification [58].

With Cl^- VGLUTs show at least two distinct interactions. Already early studies of VGLUT1 function have shown that this vesicular glutamate transporter isoform exhibits a conductance for chloride that is blocked by glutamate [28]. Accordingly, a biphasic chloride dependency of glutamate uptake characterized by a maximum glutamate uptake-rate at low mM extravesicular (cytosolic) Cl^- and subsequent decrease at higher Cl^- concentrations was observed [96, 33, 93, 97]. In addition, in absence of external Cl^-, glutamate uptake in isolated synaptic vesicles is very low. This observation led to the assumption that Cl^- allosterically modulates VGLUT in combination with a dissipation of $\Delta\psi$ as a result of Cl^- influx into synaptic vesicles [96, 33]. Electrophysiological studies, however, have recently directly confirmed an alternative but non contradictory explanation that luminal proton concentrations and Cl^- allosterically activate Cl^- conductance and glutamate transport [58] due to VGLUTs intrinsic Cl^- permeability [28].

However, it is still unclear if VGLUT in its native environment possesses a separate pH-dependent Cl^- channel, and/or if glutamate transport is mediated in a channel-like way coupled to the transport of H^+, and/or K^+ or not.

1.9 The pH of Synaptic Vesicles

The quantal size is related to the basal pH of synaptic vesicles. By selective dissipation of ΔpH in the presence of chloride a significant glutamate efflux and a decreased velocity of glutamate uptake was observed in isolated synaptic vesicles [33]. This finding was supported by the observation that the content of releasable small molecules on secretory vesicle of chromaffin cells is increased when the driving force for their uptake is enhanced, e.g. by increasing the pH gradients [98]. This dependency of ΔpH on neurotransmitter uptake can influence short-term synaptic plasticity by modulation of the function of vesicular neurotransmitter transporters. The time-constant for synaptic vesicle re-acidification measured with the fluorescent reporter protein pHluorin from single vesicle events, or newly endocytosed re-acidifying synaptic vesicles after repetitive stimulation,

revealed a relatively fast time constant of 3 – 5 s [99, 100, 101, 102]. Due to the very small response of pHluorin at the luminal pH 5.7 [17] caused by its high pK_a of 7.1 [103] the precision of pHluorin used as a reporter protein of the late, acidic phase of of re-acidification could thus lead to an underestimation of final pH_{SV} and apparent artificially shorter re-acidification kinetics. Indeed experiments with the fluorescent reporter protein mOrange2 whose response range ($pK_a = 6.5$) is more in the range of the luminal pH 5.7 compared to pHluorin has shown a substantially longer re-acidification of 15 s after electrical field stimulation. This time-constant is in the range of glutamate loading (15 s, [104]) and still faster then the time of vesicle reuse (30 s, [105]).

Early experiments reported an intravesicular pH of 5.7 of synaptic vesicles under resting conditions [17]. As a reporter protein pHluorin was linked to the synaptic vesicle membrane protein VAMP-2/synaptobrevin (SybII) facing the synaptic vesicle lumen and measured ratiometrically. This value was supported recently by independent measurements of luminal pH of synaptic vesicles with mOrange2 and pHluorin as reporter proteins. A resting pH of 5.80 was reported for glutamatergic synaptic vesicles [23]. However, in GABAergic synaptic vesicles the luminal resting pH of SVs was reported to be much higher (pH 6.44) [23]. However, a major drawback is still the lack of pH-sensitivity below pH 5.5 of the established pH-sensors in synaptic vesicles. Since a majority of synaptic vesicles at rest exhibit no or only weak fluorescence an optimal pH sensor would have a pK_a around the resting pH to allow precise pH determination. Furthermore, it cannot be excluded that the pH even acidifies to a much greater extent, but cannot be determined by common pH sensing fluorescent proteins.

1.10 How to Study Acidification of Synaptic Vesicles in Living Cells

1.10.1 The pH-sensitive Protein Cerulean

Monitoring pH of individual subcellular compartments in mammalian cells is an important step towards a better understanding of cellular processes and protein functions. Over the years a broad variety of pH-sensitive fluorescent reporter proteins have been found and genetically engineered, ranging from mildly alkaline to acidic pH, and covering the visible light spectrum from blue to red. The number of genetically encoded sensors suitable for acidic pH measures, e.g. in lysosomes, is rather small and mostly organic dyes have to be used. Albeit, genetically encoded bionsensors have the advantage that

their intracellular targeting is under control compared to organic dyes which distribute through the cell by diffusion. Due to the specific targeting to intracellular compartments genetically encoded biosensors enable to measure at the exact location. By the work of genetic engineering a number of promising candidates with sensitivity down to pH 5 and below have been found (e.g. E^2GFP, ECFP) [106, 107, 108, 109]. One of them, Cerulean, was developed by a triple mutation of the cyan fluorescent protein (S72A, Y145A and H148D). Ceruleans fluorescence properties were optimized to be a more promising FRET donor protein with improved quantum yield and higher extinction coefficient compared to ECFP [110]. Cerulean has already been used in a number of studies as a FRET sensor [111], but its pH-dependent absorption and fluorescence has not been exploited so far for pH-determination in *in vivo* experiments. The pKa of Cerulean is well below pH 6 and it has a still sizable fluorescence at pH 4, making it useful for measurements at extremely acidic environments. Most fluorescent sensors have in common that their fluorescence intensity is monitored by changes in dependency of the surrounding pH and most studies measure relative temporal variation rather than absolute numbers coming from calibrated levels of biosensor occupancy. Calibration of a pH sensors dose-response *in situ* is challenging to impossible because it is difficult to compare optical signals from tissue to those referring to the *in vitro* calibration since the fluorescence intensity is not only pH-dependent but also depends on other factors, including maturation, expression and photobleaching of the fluorescent protein based sensor. Ratiometric readout helps to overcome these problems partially but still is limited by the correct maturation of both proteins and the need of using two excitation wavelength and/or emission detection wavelength. Fluorescence lifetime imaging microscopy (FLIM), on the other hand, overcomes most of these limitations and provides a valuable alternative that gives well-calibrated measurements of absolute values. The distinct pH-sensitivity of Ceruleans fluorescence lifetime is used in this thesis as a genetically encoded fluorescent biosensor for determination of absolute pH in synaptic vesicles in primary hippocampal neurons.

1.10.2 Fluorescence Lifetime Imaging Microscopy

The fluorescence lifetime of a fluorophore is the average time a fluorophore stays in the excited state (S_1) before it returns to the ground state (S_0), and thus the subsequent emission of the fluorescence (Fig. 1.3 B). The emission of individual photons is a stochastic process and its temporal statistics and characteristic property of the fluorophore. The decay process of the fluorescence intensity can be quantified by the characteristic time

(often from assuming a sum of exponential functions). It describes the dwell time in the excited state which is determined by the total exit rate from the excited state. However, returning from the excited state can not only be by emission of a fluorescence photon, but also by non-radiative energy decay or energy transfer (e.g. Förster Resonance Energy Transfer, internal conversion, intrasystem crossing, quenching, radical formation). Calibration of the fluorescence lifetime within the biosensors environment in cells and e.g. brain tissue is relatively easy provided because the fluorescence lifetime is an intrinsic property of the fluorophore and thus does not vary with the expression level of the sensor and by this is independent of the fluorescence intensity.

1.10.3 Time-Correlated Single Photon Counting to Measure Fluorescence Lifetime

Using time-correlated single photon counting (TCSPC) the fluorophore is excited with a sequence of photon pulses (length: 50 fs – 200 ps) generated typically by pulsed lasers with defined wavelength, pulse length, and high (Mhz) pulse repetition frequency (Fig. 1.3B). The time between excitation pulse and the first detected emission photon at the emission wavelength is measured and registered in a histogram. This process is repeated 1,000 to 100,000 times, and the average fluorescence lifetime (τ_{mean}) is calculated (Fig. 1.3A and C and chapter 2.9.2). The plotted τ_{mean} is derived as the amplitude-weighted average fluorescence lifetime, when the time course of the fluorescence intensity decay is described by the best fit of a sum of exponential functions.

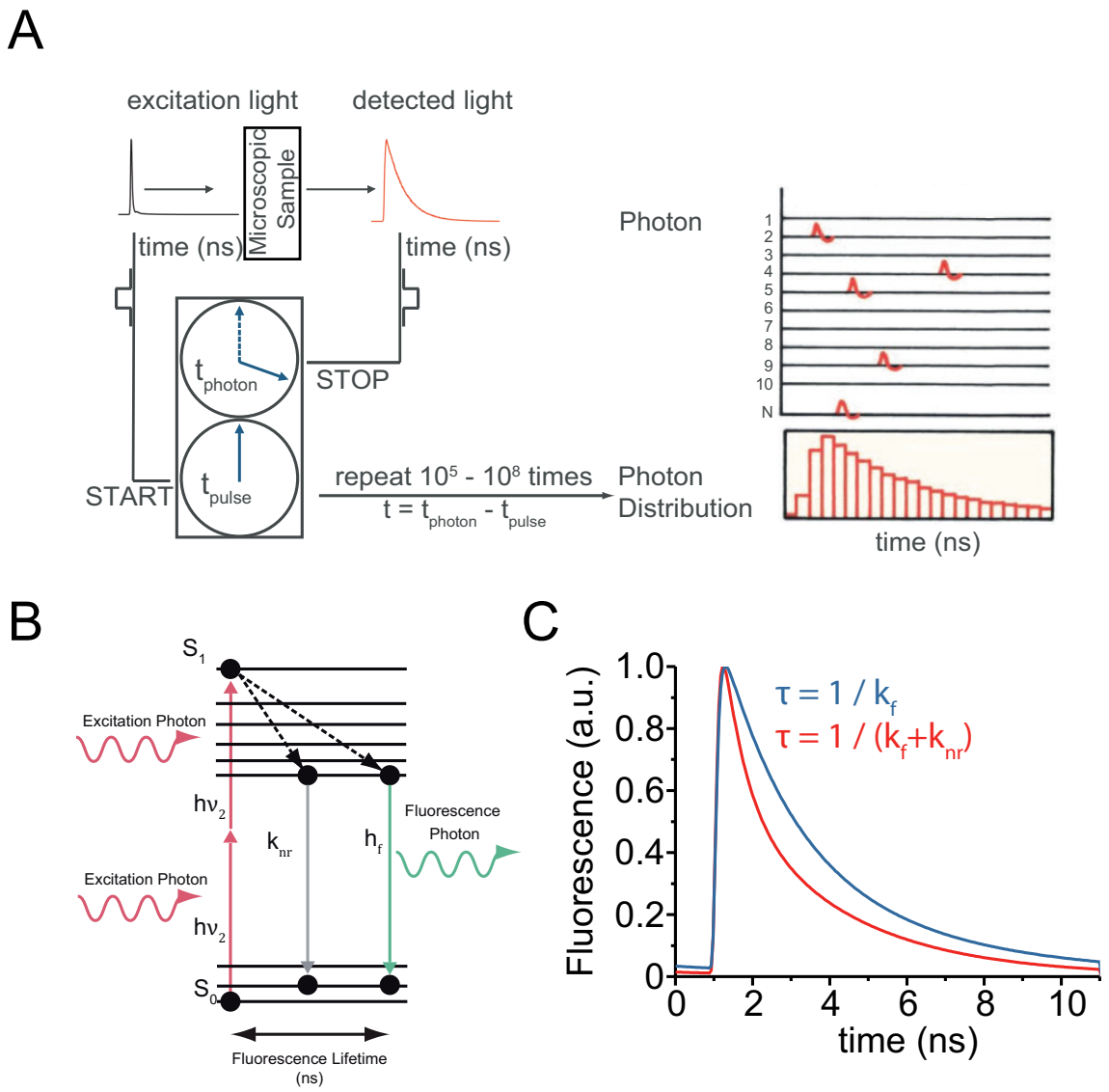

Figure 1.3: **Illustration of TCSPC and two-photon excitation** (**A**) In TCSPC τ_{mean} is measured by counting single photons. For this purpose the time it takes them between excitation of the fluorophore and detection of emitted photons is measured (scheme modified from [112]). (**B**) Illustration of two-photon excitation and emission. (**C**) Example of τ_{mean} as a function of the influences of radiative and non-radiative returnment to the ground state.

1.11 Aim of This Study

Efficient neurotransmitter uptake is one of the most crucial steps of synaptic vesicle cycle because it undoubtedly influences the quantal size of synaptic transmission. It is regulated by the complex interplay between vesicular neurotransmitter transporters, the ATP-driven proton pump, and luminal ion transporters. Despite of all the work compiled

during the last decades, the quantitative understanding of all ion fluxes regulating the electrochemical gradient and thus the neurotransmitter refilling is still lacking. Technical challenges limit the possibilities to monitor the physical state and ionic composition in synaptic vesicles. In this thesis, by the use of the pH sensor Cerulean and fluorescence lifetime imaging microscopy new insights into regulation of synaptic vesicle acidification could be unraveled. It is shown that the luminal chloride concentration modulates the extent of acidification. Furthermore, it is demonstrated that the chloride gradient is utilized by ClC-3 to acidify synaptic vesicles. In addition, it is demonstrated that synaptic vesicle acidification underlies a biphasic process with an initial acidification to pH 4.5 and a second step defined by a recovery phase to the resting pH of 5.7 by VGLUT mediated proton efflux.

Chapter 2

Material and Methods

2.1 Chemicals and Materials

All chemicals and regents with purity grade *pro analysi* (p.a.) were obtained from different companies listed in chapter 2.17. All solutions and buffer were prepared with bi-distilled water and filtered by a 0.22 μm pore size filter (Millipore) for sterilization when necessary.

2.2 Plasmid Construction

Cerulean was made by site-directed mutagenesis of ECFP inserting the following mutations S72A, Y145Y, H148D [110](courtesy of W. Bönigk, CAESAR, Bonn, Germany). For protein purification from *E. coli*, Cerulean was inserted into a pET vector equipped with a hexaHis-tag. SybII-Cerulean was made by fusing the cDNA encoding Cerulean to the C-terminus of the cDNA encoding Synaptobrevin-2/VAMP2 (SybII) in a FsY1.1 G.W. vector under control of a synapsin promoter (vector was kindly provided by Dr. M. Filippov, Nizhny Novgorod, Russia). SybII-pHluorin2 was made by substitution of Cerulean in SybII-Cerulean by pHluorin2 [113]. For ClC-5 knock-down experiments the shRNA (CCTATGATGATTTCAACACAA, Sigma) for ClC-5 was inserted into the FsY1.1 G.W. SybII-Cerulean plasmid and control of a H1 promoter. For non-targeted expression, Cerulean was inserted into a pcA vector. The final constructs were verified

by dideoxynucleotide sequencing (Eurofins Genomics).

2.3 Heterologous Expression and Purification of Cerulean in *E.coli*

Overexpression of Cerulean equipped with a hexaHis-tag was performed in *E. coli* strain BL21 (DE3) Codon Plus RIL that was transformed with the corresponding DNA. Starter cultures were grown in Luria-Bertani-Medium (bactotrypton 10 g/l, NaCl 10 g/l, yeast extract 5 g/l) with antibiotics (ampicillin 100 μg/ml, chloramphenicol 18 μg/ml), grown at 37 °C overnight and then transferred into 500 ml to reach an OD_{600} of $\sim$ 0.03. Bacteria were grown until they reached an OD_{600} of 0.4 - 0.6 and protein expression was then induced by addition of isopropyl-D-thiogalactopyranoside (IPTG, 1mM f.c.). Expression was further carried out at 20 °C overnight ($\sim$20 h). Cells were harvested and Cerulean was purified according to the semi-batch purification protocol of polyhistidine-tagged proteins under native conditions using Protino®Ni-NTA agarose (Macherey-Nagel). Subsequently the samples were concentrated by use of centrifuge filters. Simultaneously, buffer was exchanged to PBS with a centrifugal filter unit (Amicon Ultra 10K, Merck). The integrity and function of the proteins was judged by coomassie-blue stained SDS-PAGE gels and spectrometric analysis.

2.4 Cell Culture

tsA201 are transformed HEK293T cells (derived from human embryonic kidney, Sigma) and were cultured in Dulbecco's Modified Eagle Medium (DMEM, Invitrogen) supplemented with 10% FBS (Invitrogen) and 1 % Pen/Strep (100x, Invitrogen). Cells were incubated at 37°C and 5% CO2 until recording at room conditions (21 – 24 °C, air atmosphere). For FLIM experiments extracellular solution (ES) was used at pH 7.4 if not otherwise indicated.

2.5 Cell Transfection

tsA201 cells were transiently transfected overnight in 5 cm cell-culture dishes with 3ml medium using the Calcium-Phosphate Method [114] with 2.5 μg DNA. Briefly, 2.5 μg DNA dissolved in TE buffer was diluted in ddH_20 to a final volume of 124 μl. Then 41 μl 1 M $CaCl_2$ was added (124 mM final concentration) and mixed with 165 μl 2x

HEBS (in mM: 274 NaCl, 40 HEPES, 12 Glucose, 10 KCl, 1.4 $Na_2HPO_4 \cdot 2H20$, pH 7.05). The day after transfection, cells were washed with PBS/EDTA, splitted with 0.05 % Trypsin/EDTA (25300, Gibco, Life Technologies, Darmstadt, Germany) and seeded on 0.1 mg/ml poly-L-lysine (Sigma) coated glass coverslips. Image acquisition was performed 24 hours after splitting.

2.6 Lentivirus Production

Lentivirus particles were generated as described before [69, 115]. Using calcium-phosphate transfection method the transfer vector plasmid (FsY1.1 G.W., 75 μg) and the helper plasmids (pRSV-REV, pMDLg/pRRE, and the vesicular stomatitis virus G protein-expressing plasmid, kindly provided by Dr. Thomas Südhof, 30 μg each) were cotransfected into HEK293FT cells (Thermo).

For transfection of five 5-cm cell culture dishes DNA was diluted in 0.1 x TE and HEPES buffered H_2O (2.5 mM HEPES, pH 7.00) in a 2:1 relation. The solution was mixed with 2.5 M $CaCl_2$ to a final concentration of 125 mM. Under drop-wise agitation HeBS (2x: 0.28 M NaCl, 0.05 M HEPES, 1.5 mM Na_2HPO_4, pH 7.00) was added and incubated for at least 10 minutes. After 14 h, the transfection medium was replaced with fresh medium (DMEM, 10 % FCS and 100 mM sodium pyruvate, 100 mM non-essential amino acids and 100 mM glutaMAX). Lentiviral particles were harvested after 48 hours late, filtered (0.22 μm PVDF membrane, Millipore), concentrated by ultracentrifugation, The viral particles were resuspended in culture medium, aliquotted, flash-frozen in liquid nitrogen, and stored at -80 °C prior usage.

2.7 Animals

2.7.1 Mice Maintenance

According to institutional guidelines mice were housed under standard conditions in the animal facility of the Forschungszentrum Jülich and kept on a 12 h light/dark cycle. All experiments were approved and in compliance with the German Law for Protection of Animals, the Forschungszentrum Jülich, and the Landesamt für Natur, Umwelt und Verbraucherschutz (LANUV) of North-Rhine Westphalia (Reference number 84-02.04.2014.A334).

2.7.2 C57BL/6 *WT* Mouse Model

C57BL/6 were obtained from Jackson Laboratory (JAX).

2.7.3 ClC-3 *knock-out* (*Clcn3*$^{-/-}$) Mouse Model

Heterozygous *Clcn3*$^{+/-}$ were obtained from Dr. Thomas Jentsch (Department of Physiology and Pathology of Ion Transport, Max Delbrück Center, Berlin, Germany) and generated in a C57BL/6 background. Heterozygous animals were mated to breed homozygous *knock-out* animals. For genotyping, the primers ClC-3 WT R, F and KO F were used (Table 2.1).

2.7.4 ClC-3 E281Q *knock-in* (*Clcn3*^{E281Q}) Mouse Model

Heterozygous *Clcn3*^{E281Q} were obtained from Cyagen Biosciences Inc. and generated by XXXX knockin of E281Q mutation in a C57BL/6 background. Homozygous animals were mated.

2.7.5 VGLUT1 *knock-out* (*VGLUT1*$^{-/-}$) Mouse Model

VGLUT1$^{-/-}$ were obtained from Mutant Mouse Resource & Research Centers (RRID: MMRRC_011669-UNC) and back-crossed into a C57BL/6 background. Heterozygous animals were mated to breed homozygous *knock-out* animals. For genotyping, the primers VGLUT1 Neo3a, Com and WT were used (Table 2.1).

2.7.6 Genotyping

Genotypes were determined by polymerase chain reaction (PCR) from DNA obtained from tail biopsies after decapitation using the KAPA Mouse Genotyping hot start kit (Peqlab) and primers as referenced in table 2.1. Amplified PCR products were analyzed on a 1.5 % agarose gel, 25 min, 80 V, 200 mA and their size (compare to table XX) compared to a 100 bp gene ruler (Thermo Scientific, SM0241).

2.7.7 Animals Used for Primary Culture

Primary hippocampal cultures were prepared from mice of either sex. Exclusively homozygous *VGLUT1*$^{-/-}$, *Clcn3*$^{-/-}$, and wild-type animals were used for measurements. All cultures were prepared from animals at the postnatal (P) age of P0–P2.

Table 2.1: Primers Used for Genotyping

Primer	Sequence	Band Size
ClC-3 WT R	ACTCTGCCCATGTTTTCCACT	
ClC-3 WT F	GATCTAATTCTGCCTTCCTC	550 bp (WT)
ClC-3 KO F	GGAAGACAATAGCAGGCATGC	650 bp (KO)
VGLUT1 Com R	GAGAGACAGATCAAAGTGGG	
VGLUT1 Neo3a F	GCAGCGCATCGCCTTCTATC	594 bp (KO)
VGLUT1 WT F	CAGGAGGAGTTTCGGAAGC	509 bp (WT)

2.8 Primary Culture of Hippocampal Neurons

2.8.1 Preparation of Hippocampal Mass Culture

Dissociated mass culture from hippocampal neurons derived from *WT*, *Clcn3*$^{-/-}$, and *VGLUT1*$^{-/-}$ mice, respectively, at postnatal day 0 – 2 was prepared as described before [116]. Briefly, after decapitation hippocampi were dissected from brain and digested for 20 min at 37 °C with 10 units of papain (Worthington) followed by gentle mechanical trituration. Neurons diluted to a density of 350 cells/mm^2 were plated on 13 mm coverslips coated with 0.2 mg/ml poly-D-lysine (Sigma) solved in 0.1 M borate buffer saline (di-Sodium tetraborate, Merck) pH 8.0. Cultures were maintained at 37°C in an incubator, humidified with 95% air and 5% CO_2 in Neurobasal Medium A (NBA; Invitrogen), supplemented with 2% B-27 (Sigma), 1% Glutamaxx (Invitrogen) and 2% penicillin/streptomycin (Invitrogen). Two-thirds of culturing medium was renewed twice a week.

2.8.2 Lentiviral Transduction

Primary neuronal cultures were infected with lentivirus after two days *in vitro* (DIV). 25 – 75 μl viral solution was added to the cells and incubated over night at 5 % CO_2 and 37 °C. 14 – 16 hours after transduction, medium was completely replaced.

2.8.3 Imaging

Experiments were carried out between DIV 14 and 28 at room temperature (21 – 24 °C). Neurons were placed in a modified imaging chamber (RC-21BRFS, Warner Instruments) and, unless otherwise stated, kept in standard extracellular solution (ES). For electrical field stimulation neurons were exhibited to trains of action potentials (AP) at indicated

frequencies, pulses. Stimulation was carried out with the ML1001 Electronic Stimulator (ADInstruments). In acid quench experiments modified standard ES was used with 10 mM 2-(*N*-morpholino)ethane sulphonic acid (MES) replacing HEPES below pH 5.6. For experiments without or with reduced concentrations of chloride, chloride was substituted by equivalent amounts of Gluconate (see Chapter 2.16). Neurons were constantly held under presence of 25 μM D-APV (Sigma) to reduce recurrent activity from excitatory transmission. Usage of CNQX was not possible due to absorption and fluorescence properties of this blocker which interfere with Cerulean.

Different blocker compositions were applied when noted to emphasize the specific roles of different transporter types and ion channels on the pH_{SV} regulation in neurons. Neurons were exposed, if not otherwise stated, 5 minutes prior imaging to standard or modified ES plus blocker as indicated and recorded for not longer than 1 hour. The detailed concentration and dilution solutions are listed in table 2.3.

2.9 Fluorescence Lifetime Imaging Microscopy

2.9.1 Two-Photon Fluorescence Microscope

Data were acquired on an upright fluorescence microscope (A1 MP; Nikon) equipped with a 25 x water-immersion objective (NA 1.1; working distance 2.0 mm; Nikon) at room temperature. Fluorescence was excited by 100 fs light pulses (λ = 880 nm) by two-photon excitation. A mode-locked Titan-Sapphire laser (MaiTai DeepSee; output power X.X W at 880 nm; Newport Spectra Physics) generated laser pulses at a frequency of 80 Mhz. The laser light was directed onto cultured neurons through the lens with reduced power of around X mW. The focal spot was scanned over the sample with a scan size of 512 x 512 pixel (pixel size: 0.17 μm^2) and a frame-rate of 1/4 images*sec^{-1}. The emitted light of Cerulean (em: 475 nm) was separated from autofluorescence by a short pass filter (short pass filter, 500 nm, $\lambda_{obs} < 510$ nm; Omega Optical). FLIM data were recorded by a GaAsP hybrid photodetector (HPM-100-40; Becker & Hickl).

2.9.2 Time-Correlated Single Photon Counting

For fluorescence lifetime imaging microscopy (FLIM), time correlated single photon counting (TCSCP) technique was applied. Data were obtained using electronics for TCSPC (Simple-Tau 152; Becker & Hickl). The acquisition of Cerulean fluorescence was averaged over 80 seconds (20 frames in total) with a pixel dwell time of 12.1 μseconds

per pixel and frame. FLIM data were analyzed with SPCImage (Version 5.2, Becker & Hickl) by iterative re-convolution of the instrument response function, IRF(t), with an bi-exponential model function f(t) to the fluorescence decay in every pixel of the image applying equations 2.1 and 2.2.

$$I(t) = IRF(t) * f(t) \tag{2.1}$$

$$f(t) = \sum_{i=1}^{n} \left(a_i e^{\frac{-t}{\tau_i}} \right) \tag{2.2}$$

where τ_i is the characteristic lifetime and a_i is the respective fluorescence intensity of the ith component; n (=2) is the number of decay functions. Because the amount of photons collected per pixel was in most cases under the critical minimum of 1000 photons, for calculation a bin-factor (b) of 2 at a pixel size of 0.17^2 μm^2 was used. The bin-factor was calculated as follows (see equation 2.3):

$$b = (2n + 1) + (2n + 1) \tag{2.3}$$

Where n is the number of pixels. The (τ_{mean}) of every synaptic boutons is therefore represented by squared areas of 0.85^2 μm^2.

The amplitude-weighted average fluorescence lifetime (τ_{mean}) was used for further analysis and evaluation.

$$\tau_{mean} = \frac{\sum_{i=1}^{n} (a_i * \tau_i)}{\sum_{i=1}^{n} a_i}; n = 2 \tag{2.4}$$

Where a_i is the amplitude, τ_i is the fluorescence lifetime, and n is the number of decay functions.

2.10 pH Calibration in Synaptic Vesicles of Hippocampal Neurons

To determine absolute pH values τ has to be related to the specific pH_{SV} by calibration in living cells. To "clamp" the pH_{SV} to external pH (pH_e) high external [K^+] at a concentration of 122.4 mM was applied together with a variety of ionophores and blocking agents for transport and channel activity (Table 2.10). Under the assumption that, when internal and external potassium ion concentrations are equal, protons move freely, pH_{SV} should be equal to pH_e [117]. In order to dissipate proton gradients across the membranes

the K^+/H^+ exchanger Nigericin (Sigma), the uncoupler carbonyl cyanide *m*-chlorophenyl hydrazone (CCCP, Sigma), the potassium ionophore Valinomycin (Sigma), and the V-ATPase inhibitor Bafilomycin (Calbiotech) were added together with Triton X-100 (Sigma) to solubilize the plasma membrane [18] (see table 2.3). Five minutes before imaging neurons were incubated in standard ES and two to three FLIM images were recorded to verify cells integrity and expression of the biosensor. To equate pH_{SV} to pH_e, neurons were first incubated for 10 minutes with a mixture of ionophores composed of 20 μM CCCP, 10 μM Valinomycin, 10 μM Nigericin, 0.2 μM Bafilomycin and 0.02 % Triton X-100 in 122.4 mM K^+ calibration solution (CS) at a defined pH. To keep the buffering capacity of CS at the different pH values stable, PIPES or Potassium acetate buffer was used for solutions below pH 5.5, MES buffer was used for solutions set between pH 5.5 and 6.7, and HEPES buffer was used for solutions set above pH 6.7. Before recording the fluorescence lifetime image neurons were incubated for at least 10 minutes in CS to ensure adjustment of pH_{SV} to pH_e. After recording, the final pH of the solution was verified again with a pH meter and the measured value has been used as reference pH (Knick pH-Meter 766 Calimatic).

2.11 Data Analysis

2.11.1 Criteria for Data Selection and Analysis of FLIM Data

In order to avoid experimenter bias FLIM data were analyzed with a row of automated algorithms to identify synaptic boutons under strict criteria. The first selection to avoid false-identification of boutons from background or membrane staining in axons and dendrites was already made by calculation of the fluorescence lifetime in SPCImage. Here, the threshold of the minimum number of photons in the peak of a fluorescence curve was set to at least "30". Due to the higher concentration in a synaptic bouton the fluorescence is much brighter than in the plasma membrane of the axon between the boutons, thus a higher threshold excludes darker pixels from analysis.

To identify synaptic boutons and determine their τ_{mean} in an automated process, the data set for τ_{mean} and pixel intensities for a single image was exported as a matrix-text image file from SPCImage and further processed in Fiji by ImageJ [118]. In these text files for every pixel the absolute value of the number of photons and τ_{mean}, respectively, is stored and interpreted by Fiji as grey values which can be used for further evaluation (Figure 2.1). In a first step the fluorescence intensity image is used to identify synaptic boutons by application of a Gaussian blur filter with a radius of 1.0 to increase the

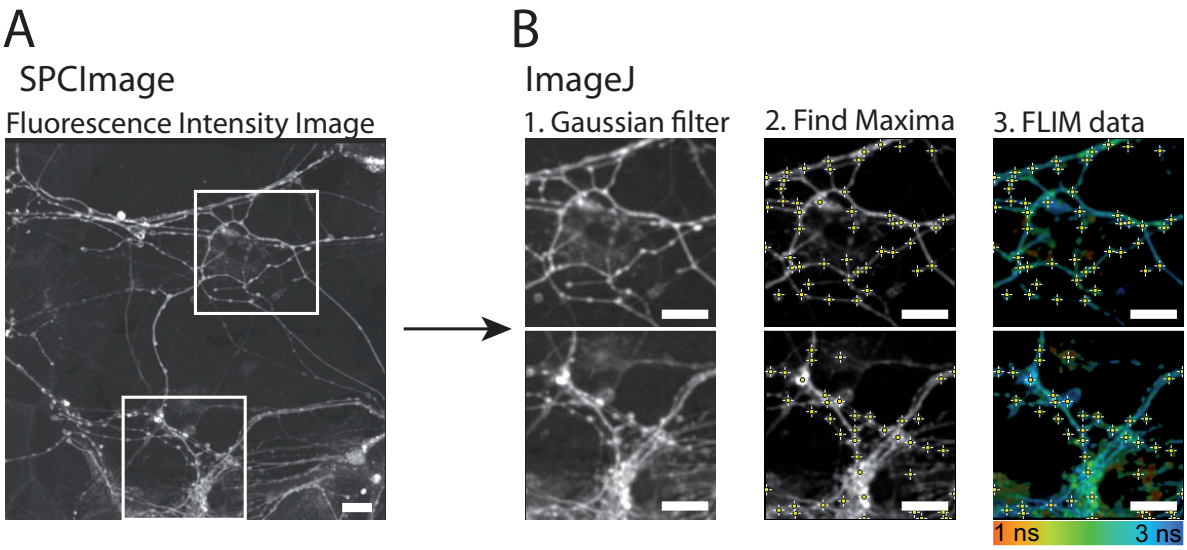

Figure 2.1: **Identification of synaptic boutons expressing SybII-Cerulean.** (A) Fluorescence intensity and fluorescence lifetime data are exported from SPCImage as text image. White squares indicate selected ROIs shown in (B). The upper panel demonstrates a position with clearly distinguishable synaptic boutons already in the FLIM image, wheres in the lower panel single boutons can only be identified by their local intensities. (B) Post-processing in ImageJ. Application of (1.) Gaussian filter and (2.) "Find maxima" plugin on the fluorescence intensity image to identify single synaptic boutons (yellow crosses in 2.) Identified ROIs in (2.) are used to determine their respective τ_{mean} in (3.).

difference between signal and background noise. In a second step, the "Find Maxima" plugin is used to identify single synaptic boutons. To verify that only maxima are selected which represent synaptic boutons, only spots with high fluorescence intensity compared to the background were selected by setting the minimal value for the noise tolerance value to "20". In any case the selection of the algorithm was verified by visual inspection and if necessary adjusted. However, this value strongly depends on the overall brightness of the fluorescence intensity image and has to be adjusted for every image again. The thus identified spots are defined as synaptic boutons when they fulfill the following criteria round-shaped, bright spots, and typically organized like pearls on a string with a diameter of 0.85 μm or 5 pixels (1 pixel = 0.17 μm). Due to the bin-factor set beforehand, this single pixel represents an area with an edge length of 0.85 μm (4x zoom). The volume of a typical synaptosome is 0.37 μm^3 [119] thus having a diameter of 0.89 μm assuming a spherical shape. Areas which are obviously representing vesicles in the soma of a neuron are excluded from the analysis by setting the gray value to "NaN". In the last step τ_{mean} of the identified synaptic boutons is determined by the gray value from the pixel representing the centre of the synaptic bouton in the text image containing

the fluorescence lifetime values per pixel. τ_{mean} data were further analyzed in OriginPro 2017 (OriginLab Corporation).

2.11.2 Fitting of pH Calibration Data

The correlation between the observed τ_{mean} and clamped pH was obtained by sigmoidal fitting of a DoseResponse curve with variable Hill slope in OriginPro 2017 with the following equation:

$$y = A1 + \frac{(A2 - A1)}{1 + 10^{(pK_a - pH)p}} \tag{2.5}$$

where y is the pH-dependent average fluorescence lifetime (τ_{mean}), pKa is the acid dissociation constant for protein binding, A1 and A2 represent the minimum and maximum asymptotic values of τ_{mean}, respectively, and p is the power value [120].

2.11.3 Time-Course Measurements by Fluorescence Intensity Changes

The time-course of the change in fluorescence intensity over time was analyzed in Fiji by ImageJ [118]. First a Gaussian blur filter with a radius of "1" was applied to all frames to increase signal-to-noise ratio. Second, the "Find Maxima" plugin of ImageJ was used to tag synaptic boutons. The noise tolerance value was set to a value were the thus identified synaptic boutons match with the following criteria: round-shaped, bright spots, and typically organized like pearls on a string with a diameter of 0.85 μm.

For neurons stained with SbyII-Cerulean the "Timer Series Analyzer V3" was used. Here oval regions of interests (ROIs) with a height and width of 5 pixels were set at the local maxima which were previously identified by the "Find Maxima" plugin. For SybII-pHluorin2 stained neurons the ROIs identified by the "Find Maxima" were used for the next step.

The average intensity for every ROI in every frames was determined and analyzed in OriginPro 2017G. Data traces from every bouton were normalized to the maximum intensity and all boutons were averaged for every frame. To calculate the decay of fluorescence intensity drop-down after stimulation traces were fitted to a bi-exponential decay function with time constant parameters (ExpDec2) in OriginPro 2017:

$$y = y_0 + A_1 e^{\frac{-x}{t_1}} + A_2 e^{\frac{-x}{t_2}} \tag{2.6}$$

where y_0 is the offset, A_1 and A_2 the amplitudes and t_1 and t_2 are the time constant for the fluorescence decay, respectively.

2.12 Statistical Analysis

For normally distributed values statistical analysis was performed by a two tailed student's t-test. When the values were not normally distributed the Mann-Whitney Rank Sum Test was used. The level of significance is indicated by asterisks (***, $p < 0.001$; **, $p < 0.01$; *, $p < 0.05$). Verification of normal distribution of data sets was carried out by Shapiro-Wilk tests. All determined values and test results are listed in the tables in chapter 3.9.

2.13 Confocal Imaging and Immunohistochemistry

2.13.1 Selective Labelling of GABA Release Sites

GABA release sites in primary hippocampal neurons were selectively labelled with α-VGAT-Oyster550 (Synaptic Systems) antibodies as described before [121, 122]. Briefly, primary hippocampal neurons were incubated with 5 μg/ml α-VGAT-Oyster550 in a 37°C incubator for 3 – 4 hrs in a carbonate buffer (in mM: 105 NaCl, 20 KCl, 2.5 $CaCl^2$, 1 D-glucose and 18 $NaHCO_3$. Before fixation, cells were washed three times with NBA and incubated again for 30 minutes.

2.13.2 Cell Fixation and Immunostaining

Neuronal cultures expressing SybII-Cerulean were fixed in PBS containing 4 % paraformaldehyde at room temperature. Primary antibody against VGLUT1 (guinea pig polyclonal, Chemicon) was diluted in CTA and then added to cells over night at room temperature. Subsequently, a secondary antibody linked to Dye649 (Dianova) was applied for 60 min. After washing in PBS, coverslips containing cells were mounted on a glass slide with a drop of Aqua-Poly/Mount (Polysciences).

Table 2.2: Primary and Secondary Antibodies

Primary Antibody			Secondary Antibody		
Name	Dilution	Company	Name	Dilution	Company
gp-α-VGLUT1	1:30000	Chemicon AB5905	d-α-gp-Dye649	1:500	Dianova 706-495-148
α-VGAT-Oyster550	5 μg/ml	SYSY 131 103C3			

2.13.3 Confocal Imaging and Data Analysis of Fixed Samples

Images were acquired using a Leica TCS SP5 II inverted microscope equipped with a 63x oil immersion objective at room temperature. Cerulean was excited with a 488 nm Argon laser, Oyser550 (Invitrogen) with a 543 nm He-Ne laser, and Dye649 with an 633 nm He-Ne laser. Emission signals were detected after filtering at 465 – 510 nm, 556 – 588, and 651 – 800 nm bandpass filters, respectively. Confocal images were assembled in Fiji for ImageJ [118] and analyzed for colocalization by Pearson's correlation coefficient with the JACoP plugin [123].

2.14 FM1-43 Measurement

Analysis of synaptic vesicle recycling of synaptic vesicles was carried out in untransfected hippocampal neurons loaded with 5 μM FM1-43 (Invitrogen) by exposition to 600 AP at 10 Hz via field electrode stimulation (see chapter 2.8.3). Neurons were exposed to ES containing 148.4, 75, 18.9, 13 and 0 mM Cl^-, respectively, supplemented with 20 μm CNQX and 25 μm D-APV (see section 2.16 for buffer composition). One minute after stimulation medium was changed to Ca^{2+}-free ES containing 2 μm TTX, 25 μm Bicuculline, 20 μm CNQX, and 25 μm D-APV. After 5 minutes neurons were exposed to ES supplemented with 20 μm CNQX and 25 μm D-APV and recorded for 60 seconds.

Images were recorded on an Olympus IX 73 fluorescence microscope equipped with a 40x air immersion objective (NA = 0.6, LUCPlanFLN, Olympus), an emission filterset for GFP (49002 – ET – EGFP (FITC/Cy2), Chroma) and an Andor Neo sCMOS (Andor). Images (1280 x 1080 pixel, pixel size = 0.1 μM/pixel) were acquired at a frame rate of 0.5 s and an illumination time of 0.09 s. FM1-43 fluorescence was activated by LED Illumination ($pE300^{white}$, CoolLED). LED illumination intensity was set to a low level to reduce bleaching of the dye.

Time-series were analyzed in Fiji by ImageJ [118]. By use of the "Timer Series Analyzer V3" synaptic boutons were selected which match with the following criteria: round-shaped, bright spots, and typically organized like pearls on a string with a diameter of 0.85 μm. Here oval ROIs with a height and width of 5 pixels were set at the local

maxima which were previously identified by the "Find Maxima" plugin. Then the average intensity for every ROI in every frame was determined and analyzed in OriginPro 2017G. Data traces from every bouton were averaged for 30 frames.

2.15 Blocker and ionophores

Table 2.3: Blocker and ionophore compositions

Blocker	Concentration	Stock	Manufacturer
Bafilomycin A1	1 μM	200 μM in DMSO	Calbiotech
Bicuculline	50 μM	10 mM in ES	Sigma
CCCP	20 μM	50 mM in EtOH	Sigma
CNQX	20 μM	8 mM in ES	Sigma
D-APV	25 μM	10 mM in ES	Sigma
DL-Histidine	10 mM	1 M in ddH_2O	Sigma
EIPA	10 μM	5 mM in DMSO	Sigma
Nigericin	10 μM	10 mM in EtOH	Sigma
Rose Bengal	100 nM	50 μM in DMSO	Sigma
TTX	2 μM	10 mM in ES	Sigma
Triton X-100	0.02 %	2 % v/v in ES	Sigma
Valinomycin	10 μM	10 mM in EtOH	Sigma

2.16 Buffers

Table 2.4: Extracellular Solution – ES, 148.4 mM Cl^-

Concentration	Substance
140 mM	NaCl
2.4 mM	KCl
10 mM	HEPES
10 mM	D-Glucose
2 mM	$CaCl_2$
1 mM	$MgCl_2$
0.025 mM	D-APV
pH adjusted to 7.4 with NaOH.	

Table 2.5: Extracellular Solution – ES, 75 mM Cl^-

Concentration	Substance
66.6 mM	NaCl
73.4 mM	NaGlu
2.4 mM	KCl
10 mM	HEPES
10 mM	D-Glucose
2 mM	$CaCl_2$
1 mM	$MgCl_2$
0.025 mM	D-APV
pH adjusted to 7.4 with NaOH.	

Table 2.6: Extracellular Solution – ES, 18.9 mM Cl^-

Concentration	Substance
10.5 mM	NaCl
129.5 mM	NaGlu
2.4 mM	KCl
10 mM	HEPES
10 mM	D-Glucose
2 mM	$CaCl_2$
1 mM	$MgCl_2$
0.025 mM	D-APV
pH adjusted to 7.4 with NaOH.	

Table 2.7: Extracellular Solution – ES, 13 mM Cl^-

Concentration	Substance
4.6 mM	NaCl
135.4 mM	NaGlu
2.4 mM	KCl
10 mM	HEPES
10 mM	D-Glucose
2 mM	CaCl
1 mM	MgCl
0.025 mM	D-APV
pH adjusted to 7.4 with NaOH.	

Table 2.8: Extracellular Solution – ES, chloride free

Concentration	Substance
140 mM	NaGlu
2.4 mM	KGlu
10 mM	HEPES
10 mM	D-Glucose
2 mM	CaGlu
1 mM	MgGlu
0.025 mM	D-APV

pH adjusted to 7.4 with NaOH.

Table 2.9: Acid Quench

Concentration	Substance
140 mM	NaCl
2.4 mM	KCl
10 mM	HEPES (pH 6.5), MES (<pH 6.5)
10 mM	D-Glucose
2 mM	$CaCl_2$
1 mM	$MgCl_2$
0.025 mM	D-APV

pH adjusted with NaOH.

Table 2.10: Calibration Solution – CS

Concentration	Substance
20 mM	NaCl
122.4 mM	KCl
10 mM	HEPES (> pH 6.7)
	MES (pH 5.5 – pH 6.7)
	PIPES or Potassium acetate (< pH 5.5)
10 mM	D-Glucose
2 mM	CaCl
1 mM	MgCl
0.025 mM	D-APV
0.02 mM	CCCP
0.01 mM	Valinomycin
0.01 mM	Nigericin
0.2 μM	Bafilomycin A1
0.02 %	Triton X-100

pH adjusted with NaOH and HCl, respectively.

2.17 Manufacturers

Abcam, Cambridge UK
ADInstruments, Oxford, UK
Andor, Belfast, Northern Ireland
Becker & Hickl, Berlin, Germany
Calimatic, Berlin, Germany
Chemicon, Temecula, CA, USA
Chroma, Bellows Falls, VT, USA
CoolLED, Andover, UK
Eurofins Genomics, Ebersberg, Germany
Invitrogen JAX, Bar Harbor, ME, USA
Leica, Mannheim, Germany
Macherey-Nagel, Düren, Germany
Merck, Darmstadt, Germany
Mutant Mouse Resource & Research Centers USA
Newport Spectra Physics, Irvine, CA, USA
Nikon Instruments Europe, Amsterdam, Netherlands
Omega Optical, Brattleboro, VT, USA
OriginLab Corporation, MA, USA
Peqlab, Erlangen, Germany
Polysciences Inc., Worrington, PA, USA
Sigma-Aldrich, Munich, Germany
Synaptic Systems, Göttingen, Germany
Thermo Fischer, Darmstadt, Germany
Thermo Scientific, Braunschweig, Germany
Worthington, Lakewood, NJ, USA

Chapter 3

Results

3.1 pH Imaging in Synaptic Vesicles of Cultured Hippocampal Neurons

To determine the pH in synaptic vesicles, Cerulean was fused to the amino terminus of the SNARE protein synaptobrevin-2 (SybII) (Fig. 3.1A) and expressed in cultured hippocampal neurons via lentiviral transduction. A punctured distribution of the sensor resembles SybII expression in neurons [124] and mostly overlaps with antibody labelling of VGLUT1 (Pearson's coefficient = 0.39 ± 0.04, Mean ± SD) but not VGAT (Pearson's coefficient = 0.24 ± 0.04, Mean ± SD) which indicates predominant expression in glutamatergic nerve terminals (Fig. 3.1B). Furthermore, about 90% of synaptic boutons on a single cover-slip were marked by VGLUT1 antibody, whereas only about 10% were marked as VGAT positive synaptic boutons. The Pearson's coefficient was calculated on spots were all three proteins were expressed as shown in the representative images in figure 3.1C. A representative FLIM measurement of SybII-Cerulean is shown in figure 3.2A providing mean fluorescence lifetimes (τ_{mean}) for every pixel color-coded according to the look-up table from red (1 ns) to blue (3 ns). Cerulean's fluorescence decay was best described by a bi-exponential decay function which led to better fitting results than a mono-exponential fit (Figure 3.2B). In figure 3.2C the fitted decays of selected synaptic boutons from A are shown with a τ_{mean} of 2.1 ± 0.3 ns (SD, n = 58). The τ_{mean}

were calibrated according to the high K^+/Nigericin-method [117] measuring synaptic boutons from around 5 - 10 spots for each preset pH. Nigericin is a K^+/H^+ exchanger which equilibrates pH_{ex} and pH_{SV} when extracellular K^+ is the same as intracellular K^+. The punctuate distribution permits identification and evaluation of individual synaptic boutons by automated analysis in Fiji (see chapter 2.11.1). During calibration the fluorescence lifetimes change from 0.7 to 2.8 ns at preset pH between pH 3.9 and pH 8.0. Calibration is used to calculate pH from τ by sigmoidal fitting with a DoseResponse model (Fig. 3.2D, see chapter 2.11.2) which was generated by plotting τ_{mean} against the pH (see table 3.1 and 3.2 for data and parameter). The resulting pK_a (the pH value were τ_{mean} is 50% of maximal) is pH 5.3 and thus, in the optimal range for the expected resting pH_{SV} of pH 5.7 as determined before with synaptopHluorin [17].

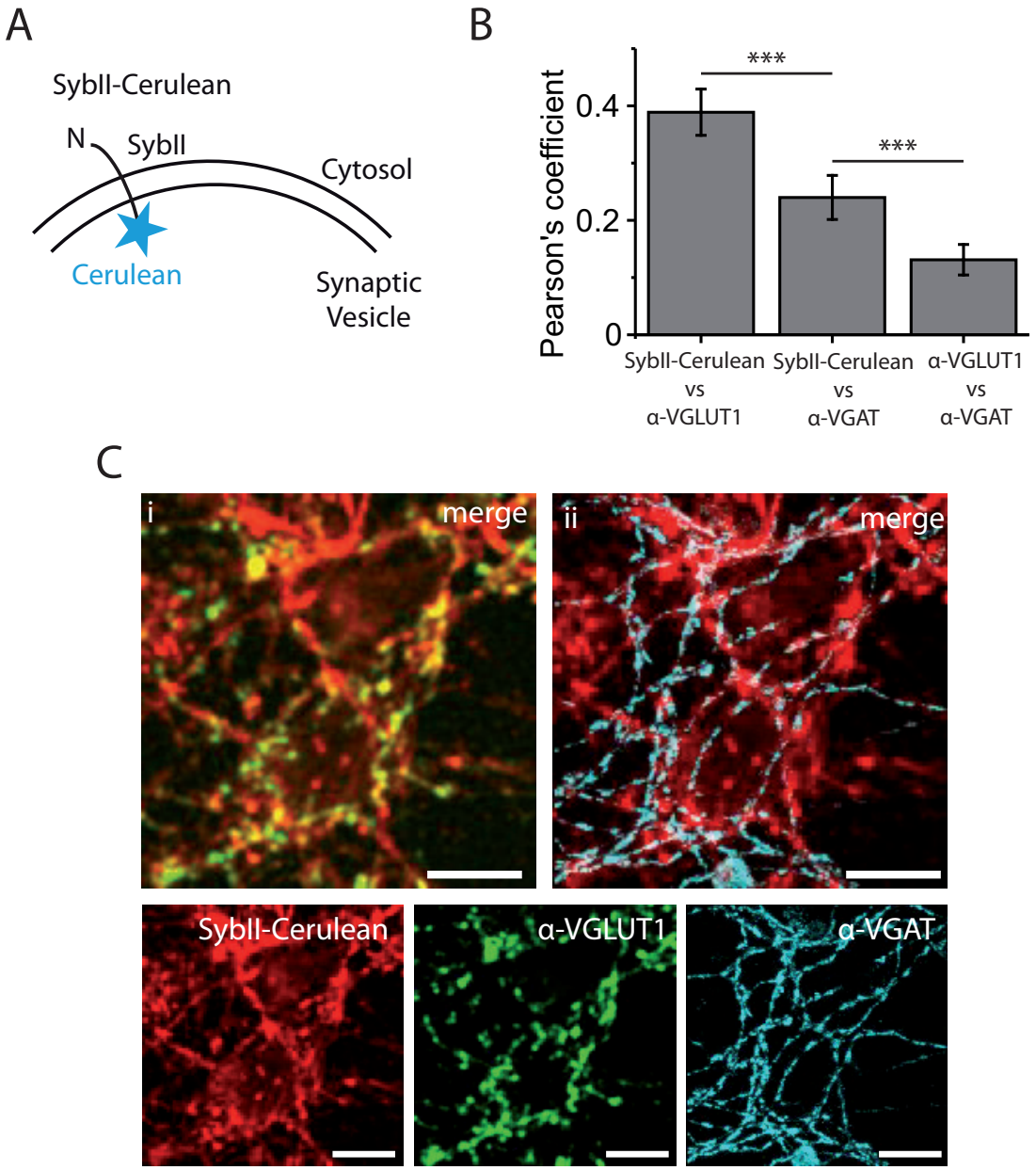

Figure 3.1: **SybII-Cerulean is predominantly overlapping with glutamatergic synaptic boutons.** (A) Schematic of the SybII-Cerulean fusion protein, with Cerulean fused to the C-terminus of synaptobrevin-2 (SybII) thus facing the synaptic vesicle lumen after endocytosis. (B) Bar plot representing the colocalization of SybII-Cerulean with glutamatergic and GABAergic synaptic boutons, respectively, by Pearson's coefficient (n = 2 independent preparations). All data are mean ± SD. (C) SybII-Cerulean (Red) transfected hippocampal neurons stained with an antibody against the GABAergic marker protein VGAT (Magenta). VGLUT1 (Green) was marked by antibody staining after fixation. Scale bar: 10 μm.

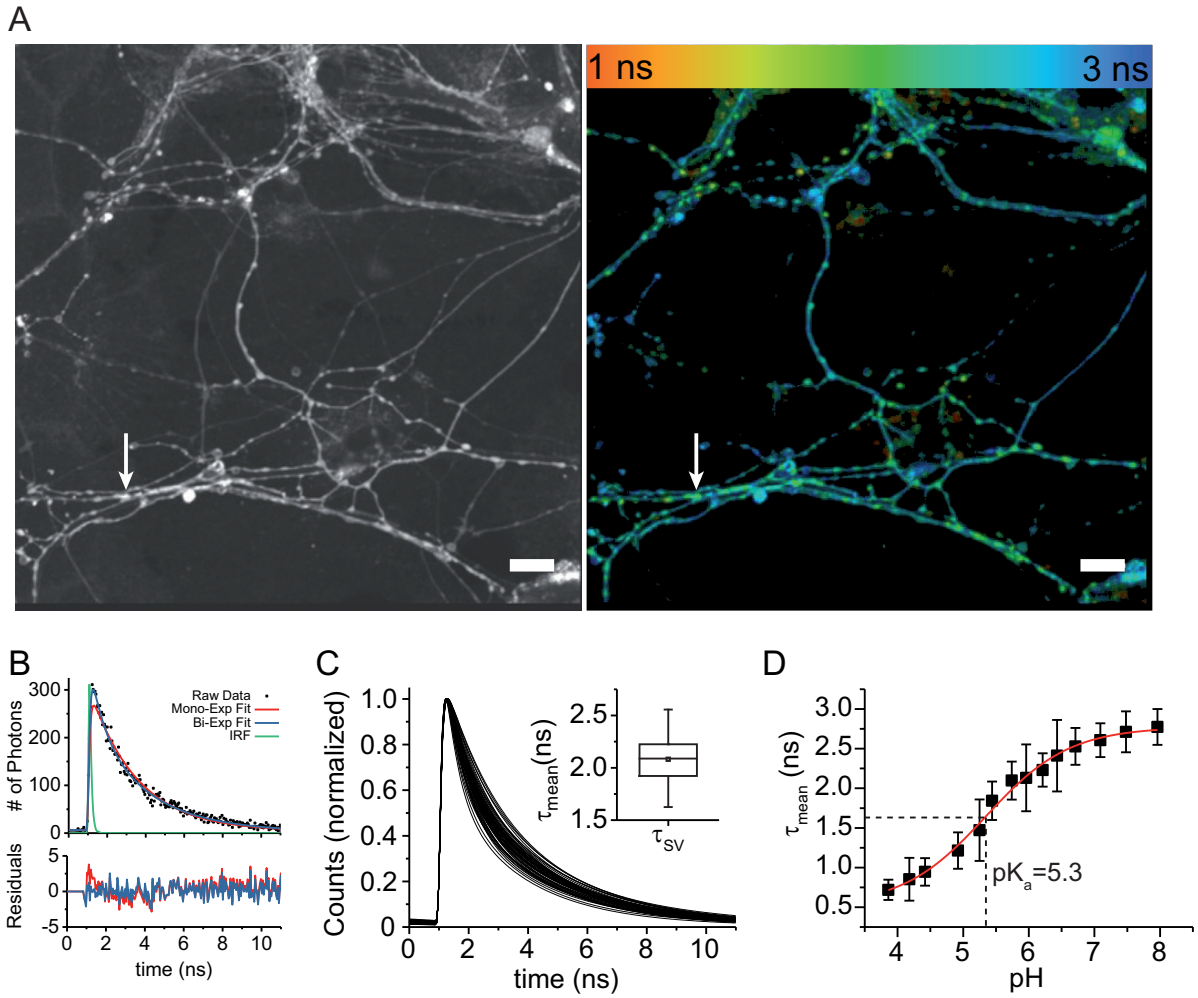

Figure 3.2: **pH measurement in synaptic vesicles of cultured hippocampal neurons.** (A) Left: Fluorescence intensity image of primary hippocampal neurons at DIV 15, thirteen days after transfection with lentivirus containing the DNA of SybII-Cerulean. Right: Corresponding fluorescence intensity image showing τ_{mean}, color-coded accordingly the look-up table (red 1 ns to blue 3 ns). In both images, the punctuate distribution represents single synaptic boutons. Scale bar: 10 μm (B) Comparison of mono- and bi-exponential fits of selected single bouton (white arrow in A). Mono-exponential fit: $\tau_{mean} = 2.4ns$, $\chi^2 = 1.42$. Bi-exponential fit: $\tau_{mean} = 2.1ns$ with $a1 = 35.1\%$, $\tau_1 = 0.7ns$, $a2 = 64.9\%$, $\tau_2 = 2.9ns$, $\chi^2 = 1.03$. Bi-exponential fitting leads to a better description of the fluorescence decay than mono-exponential fitting. (C) τ_{mean} of 58 representative synaptic boutons from A. Insert shows the corresponding distribution of τ_{mean} with a mean of 2.1 $\pm$ 0.3 ns (SD, n = 58). The errors denote the 1.5 IQR, the boxes represent the 25th to 75th percentiles. (D) Using the high-K^+ method the pH dependence of SybII-Cerulean was calibrated at different pH values and fitted to a DoseResponse model (red line). For fitting parameters and data see tables 3.1 and 3.2. All data are mean $\pm$ SD.

3.2 Determination of the Resting pH of Synaptic Vesicles

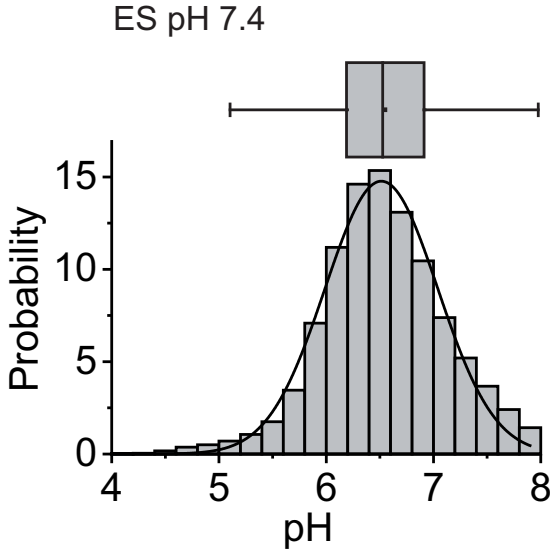

Figure 3.3: **pH distribution in synaptic vesicles** Distribution of pH_{SV} of 20722 boutons measured in 37 cover-slips from 11 mice (DIV 14 – P21). The mean value is pH 6.54 ± 0.58 (SD). The error bars denote the 1.5 IQR, the boxes represent the 25^{th} to 75^{th} percentiles. The horizontal line represents the median, whereas the square symbol denotes the respective mean values. Gaussian distribution shown by black line in lower panels. Dataset and N listed in table 3.3.

Under resting conditions pH_{SV} was heterogeneously distributed with a mean of 6.54 ± 0.58 (SD), which is considerably higher than published data [17, 23] (Fig. 3.3A). It has been reported that transient over-expression of SybII leads up to 30 % protein within the bouton plasma membrane [125, 126]. The deviation of the results measured with SybII-Cerulean from published synaptic vesicle pH might thus be due to a fraction of sensors facing the extracellular environment and reporting the higher pH in the external medium (as indicated in the inserts in figure 3.4A – D). In experiments with SybII-pHluorin as pH-sensor the acid quench method was developed to only visualize the fluorescence of the luminal population. For this, acidic ES with a pH of 5.0 is applied to the cells and the remaining fluorescence is immediately determined [99]. Due to the low pH, the surface population of pHluorin is quenched and only fluorescence from luminal proteins remain. A pH of 5.7 was determined for synaptic vesicles at rest with this method [17, 23]. Cerulean, however, still exhibits a considerable fluorescence intensity at pH 5, therefore, this method is not useful to completely quench the surface pool of sensor proteins, but

can be used in an adapted manner.

Under the assumption that the measured pH of 6.5 under resting conditions is a mixture of two pH populations, the known pH 7.4 from the surface population, and the unknown lower pH_{SV}. Then, pH_{SV} can be estimated by the variation of the measured fluorescence lifetime to the expected fluorescence lifetime at set external pH which is known from the calibration curve. If $pH_{surface}$ equals pH_{SV}, then the difference of the measured fluorescence lifetime to the expected fluorescence lifetime of $pH_{surface}$ would be zero, and thus on the calibration curve (Fig. 3.4E). To give an estimation of the resting pH_{SV} SybII-Cerulean fluorescence lifetimes were determined at various extracellular pH.

Perfusion of extracellular solution with pH 7.4 gives a $\tau_{mean} = 2.40 \pm 0.27$, and an apparent pH of 6.57 ± 0.58 (Fig. 3.4A). Whereas perfusion of acidic solution with pH 5.2 reduces $\tau_{mean} = 1.78 \pm 0.24$, resulting in an apparent pH of 5.51 ± 0.29 (SD) (Fig. 3.4B). External pH 6.5 results in an apparent pH of 6.19 ± 0.51 (SD) ($\tau_{mean} = 2.24 \pm 0.29$, Fig. 3.4C), whereas an apparent pH of 5.58 ± 0.30 (SD) is observed at external pH 5.5 ($\tau_{mean} = 1.84 \pm 0.24$, Fig. 3.4D). Because the difference between the measured τ at pH 5.5 and the expected τ was substantially small it can be concluded that the resting pH of synaptic vesicles is around pH 5.5 – 5.6 considering the graph in figure 3.4E where the variation of $\tau_{measured}$ to the calibration curve is plotted. These data are in full agreement with the notion that surface membrane and synaptic vesicle Cerulean both contribute to the measured fluorescence lifetime.

In such system with two populations with distinct τ at a synaptic bouton, contributions by Cerulean in the surface membrane can also be corrected by calculation of τ_{mean} without the contribution of the lifetime value (τ_{ex}) obtained from the calibration curve at the superfused pH. To achieve this, the fluorescence lifetime decay was fitted by a tri-exponential fit with a fixed value for the known fluorescence lifetime of τ_{ex} from the pH calibration (see equation 2.2, with n = 3). The τ_{SV} was then calculated from the amplitude-weighted fluorescence lifetime τ_1 and τ_2 without contributions of τ_3 (see equation 2.4). Figure 3.4F provides τ_{SV} for three different external pH and *WT*. At external pH 5.5, when no pH gradient between surface population and synaptic vesicle population exists (τ_{ex} equals τ_{SV}) this method fails and results in underestimated values for pH_{SV}, because the fixed τ_{ex} which is excluded from the calculation by this method resembles also τ_{SV}. With this method a mean resting pH_{SV} of 5.5 was obtained, when the corrected value for acidic solution pH 5.5 is excluded (Fig. 3.4F).

In conclusion it could have shown that the synaptic vesicles at rest have a pH between 5.5 and 5.7 which is line with previously published data for glutamatergic synaptic vesicles [17, 18, 23].

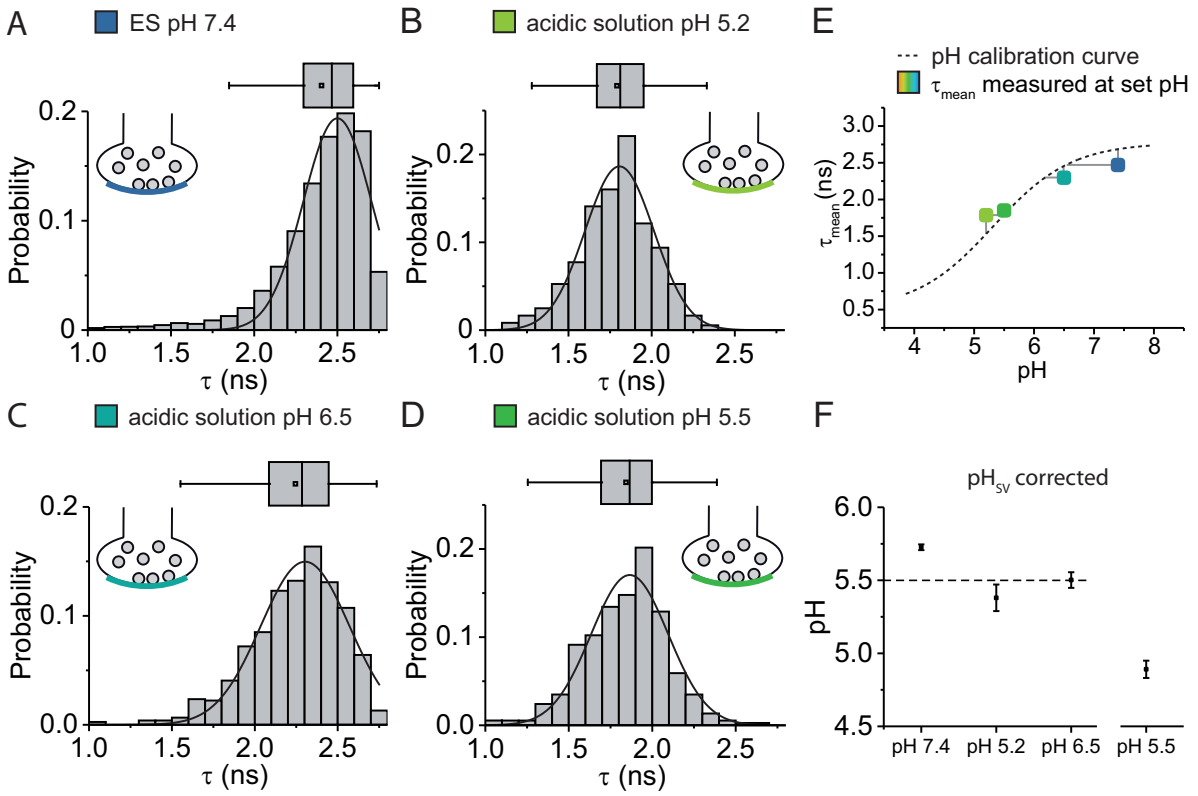

Figure 3.4: **The resting pH in synaptic vesicles** (A) Distribution of τ_{mean} of 20722 boutons measured in 37 cover-slips from 11 mice (DIV 14 – P21) exposed to ES pH 7.4. $\tau_{mean} = 2.40 \pm 0.27$ (SD). (B) Distribution of τ_{mean} of 362 boutons measured in 1 cover-slip from 1 mouse superfused with acidic solution of pH 5.2. $\tau_{mean} = 1.78 \pm 0.24$ (SD). (C) Distribution of τ_{mean} of 764 boutons measured in 1 cover-slip from 1 mouse superfused with acidic solution of pH 6.5. $\tau_{mean} = 2.24 \pm 0.29$ (SD). (D) Distribution of τ_{mean} of 372 boutons measured in 1 cover-slip from 1 mouse superfused with acidic solution of pH 5.5. $\tau_{mean} = 1.84 \pm 0.24$ (SD). The error bars denote the 1.5 IQR, the boxes represent the 25th to 75th percentiles. The horizontal line represents the median, whereas the square symbol denotes the respective mean values. Gaussian distribution shown by black line in lower panels. (E) τ_{mean} values from experiments A-D in relation to the calibration curve (from Fig. 3.1D). The solid lines indicate the deviation from the calibration curve. The vertical line indicates the deviation from the expected τ_{mean} when pH_{ex} would equal pH_{SV}. The horizontal line indicates the deviation of τ_{mean} as a result of the mix between pH_{ex} and pH_{SV}. The smaller the deviations the smaller the difference between pH_{ex} and pH_{SV}. (F) Mean pH values from experiments A-D corrected by consideration of fluorescence lifetime of surface population in the fitting function. The dashed line indicates the mean pH_{SV} of 5.5 determined from the calculated pH_{SV} from pH 7.4, pH 5.2, and pH 6.5. Mean ± 95% Confidence Interval (CI). Dataset and N for (A-E) listed in table 3.4, and for (F) in table 3.5.

3.3 Biphasic Acidification of Synaptic Vesicles after Endocytosis

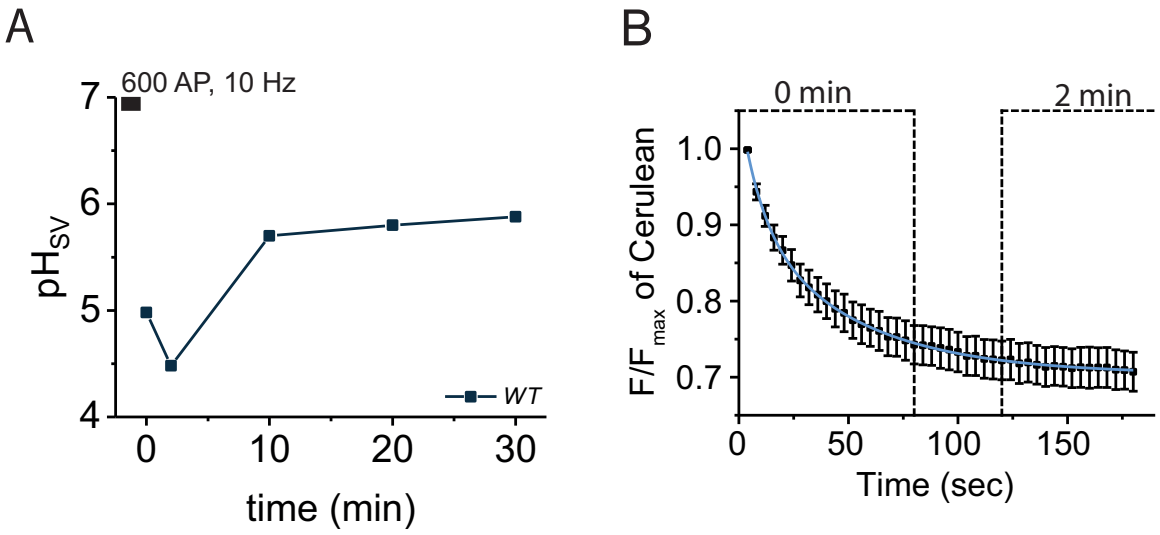

Figure 3.5: **Synaptic vesicles over-acidify to pH 4.5 after endocytosis** (A) The effect of electrical whole field stimulation on pH_{SV} over time after stimulation with trains of 600 APs at a frequency of 10 Hz in *WT* neurons. All data are mean ± 95%CI. Dataset listed in table 3.6 (B) Time-course of synaptic vesicle acidification monitored by change in fluorescence amplitude of Cerulean after stimulation with 600 AP at 10 Hz. Intensity of every bouton (n = 58) is normalized to its maximum. The dashed boxes indicate the time window for FLIM measurements. Blue line is the fitted decay in fluorescence intensity represented by a bi-exponential time-course with a fast component of 10.02 ± 0.86 seconds and and a slower rate of 49.49 ± 2.29 seconds. All data are mean ± 95%CI. Fitting parameter are listed in 3.7.

Three classes of synaptic vesicles can be distinguished with distinct roles in synaptic transmission: the readily releasable pool, the recycling pool, and the reserve pool (Fig. 1.1B) [4]. These pools differ in number and in the stimulus required for their exocytosis and subsequent recycling. The reserve pool encompasses the vast majority of vesicles and only recycles upon strong stimulations. The large dynamic range of Cerulean permits insights into pH regulation of this vesicle pool. Reserve pool exocytosis was evoked by repetitive electrical stimulation with trains of 600 AP at 10 Hz [127] and the post-stimulus endocytosis rate and acidification using Cerulean was measured. For this purpose directly after the end of stimulation, and after 2, 10, 20, and 30 min FLIM data were recorded (Fig 3.5 A). For Time Correlated Single Photon Counting (TCSPC) FLIM measurements the number of photon counts collected for every pixel is limiting the minimal acquisition time for one frame. To collect sufficient photons in decays representing single synaptic

boutons FLIM measurements last about 80 seconds and thus dynamic changes in time periods shorter than 80 seconds are not resolved and averaged. During collection of FLIM data 20 consecutive single frames at a frame rate of 0.25 Hz were recorded including the fluorescence intensity information for every pixel (Fig 3.5 B). This allows the analysis of pH-dependent fluorescence intensity changes upon stimulation with higher temporal resolution. The fluorescence intensity does not only reflect the time course of vesicle acidification, but also of endocytosis, however, permitted identification of time periods in which fluorescence signal are stable enough for FLIM measurements (figure 3.5B, dashed box). In the first 80 seconds after the stimulation protocol ends pH_{SV} drops to pH 4.98 $\pm$ 0.02 (mean $\pm$ 95 % CI) and further decreases after 2 minutes to pH 4.48 $\pm$ 0.03 (120 – 200 seconds after stimulation)(Fig 3.5 A). Within 10 minutes after stimulation pH_{SV} recovered to pH 5.7 $\pm$ 0.02 (Fig 3.5 A). Even 30 minutes after stimulation pH_{SV} was not back to baseline (pH 5.88 $\pm$ 0.02) compared to the initial pH 6.54 (see figure 3.4A) confirming that the high pH measured before stimulation is influenced by the surface population of the sensor (Fig 3.5 A). The change of fluorescence intensity which was collected in parallel to FLIM recording shows an bi-exponential decrease with a fast rate of 10.02 $\pm$ 0.86 seconds and and a slower rate of 49.49 $\pm$ 2.29 seconds, reflecting the rate of endocytosis and acidification (Fig 3.5 B) which is substantially longer than estimated previously with pHluorin ($\tau =\sim 17s$) [128, 129, 102, 130, 131].

It was shown that during compensatory endocytosis caused by long-term stimulation, the surface population participates in the recycling of SV proteins [126, 125]. The thus obtained steady-state pH_{SV} is in perfect agreement with the values obtained in figure 3.4 and further supports the notion that SybII-Cerulean permits accurate quantification of steady-state synaptic vesicle pH.

Furthermore, this over-acidification after endocytosis and re-alkalization process of pH_{SV} has not been seen before. One the one hand, common pH-sensors compared to Cerulean do not even permit pH sensing at this low pH and, on the other hand, re-alkalization is an indicator for a H^+ efflux.

3.4 V-ATPase Independent Acidification of Synaptic Vesicles

Previous studies demonstrated that the V-ATPase is crucial for acidification of synaptic vesicles [15, 132]. Since V-ATPase mediated proton pumping is electrogenic, it is normally assumed that ion channels or transporters are required to mediate counter-ion

fluxes/transport to prevent switch off of the pump caused by electrical repulsion of $[H^+]_{SV}$. The anion-proton exchanger ClC-3 [57, 68, 62], as well as anion channels associated with VGLUT [95] have been proposed to serve this purpose, but so far, no agreement has been reached about the role of these proteins.

Therefore, pharmacological tools together with *knock-out* animals were used to test the role of the V-ATPase, ClC-3, and VGLUT for acidification of reserve pool vesicles after endocytosis. Figure 3.6A depicts acidification time courses obtained by FLIM for control as well as for neurons pretreated with 1 μM Bafilomycin a specific V-ATPase inhibitor. Bafilomycin only slightly decreased peak acidification of synaptic vesicles 2 minutes after stimulation and even slightly decreased steady-state values. Different concentrations from 1 μM to 5 μM were tested, and incubation times from 5 minutes to 4 hours prior imaging as well as compounds from three companies were tested. There was never any significant reduction in synaptic vesicle acidification observed after this stimulus protocol and by the use of Cerulean as a pH-sensor (Figure 3.6 B) in contrast to other studies [133, 134]. In neurons expressing SybII-pHluorin2, Bafilomycin delayed the pH-dependent decrease in fluorescence intensity after stimulation about 40 seconds but did not prevent it (Figure 3.6 C). Besides the V-ATPase thus further transporter were tested which may lead to synaptic vesicle acidification by accumulation of luminal H^+ utilizing the ionic concentration gradient build up after endocytosis.

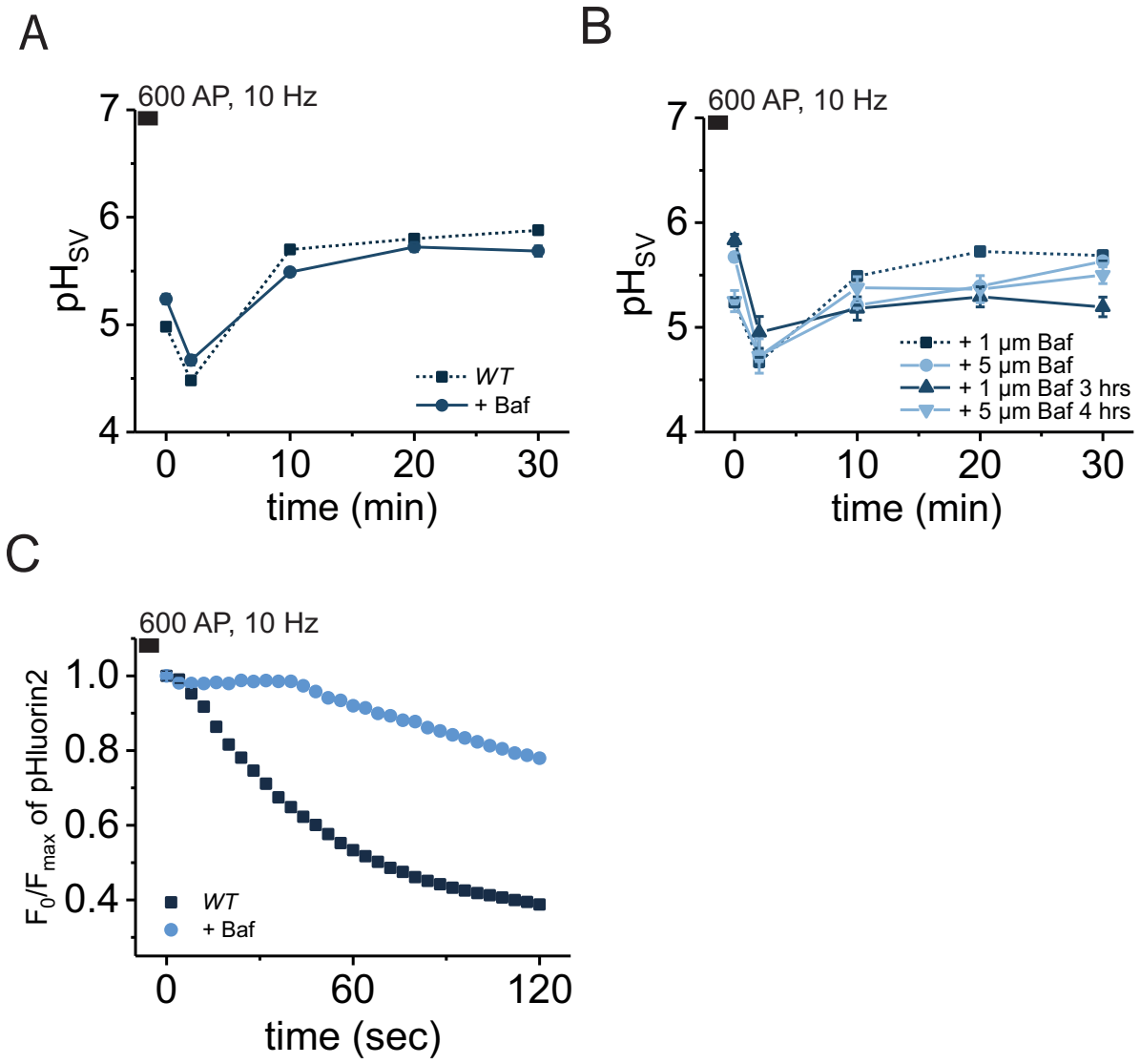

Figure 3.6: **pH_{SV} drops to pH 4.5 after electrical stimulation** (A) Time-course of pH_{SV} in endocytosis after stimulation with trains of 600 APs at a frequency of 10 Hz in *WT* neurons in control (squares) and Bafilomycin (circles) treated conditions. (B) Time-course of pH_{SV} after stimulation in *WT* neurons treated with different concentrations and incubation times of Bafilomycin. (C) Time-course of synaptic vesicle acidification monitored by change in fluorescence intensity of SybII-pHluorin2 in *WT* neurons (squares, n = 3 cover-slips and 795 synaptic boutons) and treated with 1 μM Bafilomycin (squares, n = 3 cover-slips and 1173 synaptic boutons). Intensity of every bouton is normalized to its maximum. All data are mean ± 95%CI. Dataset for A and B listed in table 3.8.

3.5 NHE Exchanger Do Not Contribute to Synaptic Vesicle Acidification

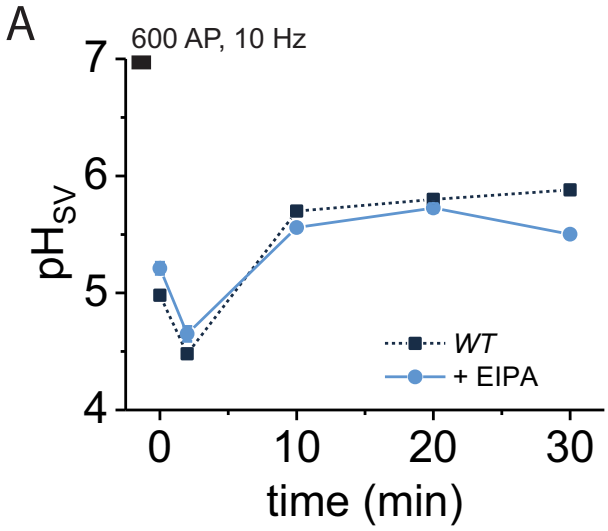

Figure 3.7: **Acidification is unaffected from NHE activity** (A) The effect of electrical whole field stimulation on pH_{SV} over time after stimulation with trains of 600 APs at a frequency of 10 Hz in *WT* (squares) and EIPA treated neurons (circles). All data are mean ± 95%CI. Dataset listed in table 3.9.

The N^+/H^+ exchanger NHE6 has shown to be expressed in synaptic vesicle membrane and could, in theory, utilize the large inward directed sodium gradient after endocytosis to acidify synaptic vesicle lumen [19]. *WT* neurons exposed to the NHE-specific blocker ethyl-isopropyl amiloride (EIPA) showed no difference in peak acidification acidification after endocytosis compared to untreated neurons (Fig. 3.7A). Thus ruling out that N^+/H^+ exchange is responsible for the V-ATPase independent acidification observed before.

3.6 *Clcn3*$^{-/-}$ and *VGLUT1*$^{-/-}$ Independent Synaptic Vesicle Acidification

ClC-3 is a Cl^-/H^+ antiporter with a 2:1 transport stoichiometry that might acidify synaptic vesicles after endocytosis utilizing the outwardly directed chloride gradient. In freshly endocytosed synaptic vesicles extracellular electrolytes are taken up leading to an $[Cl^-]_{SV}$ which is around one magnitude higher than that of the cytoplasm. However,

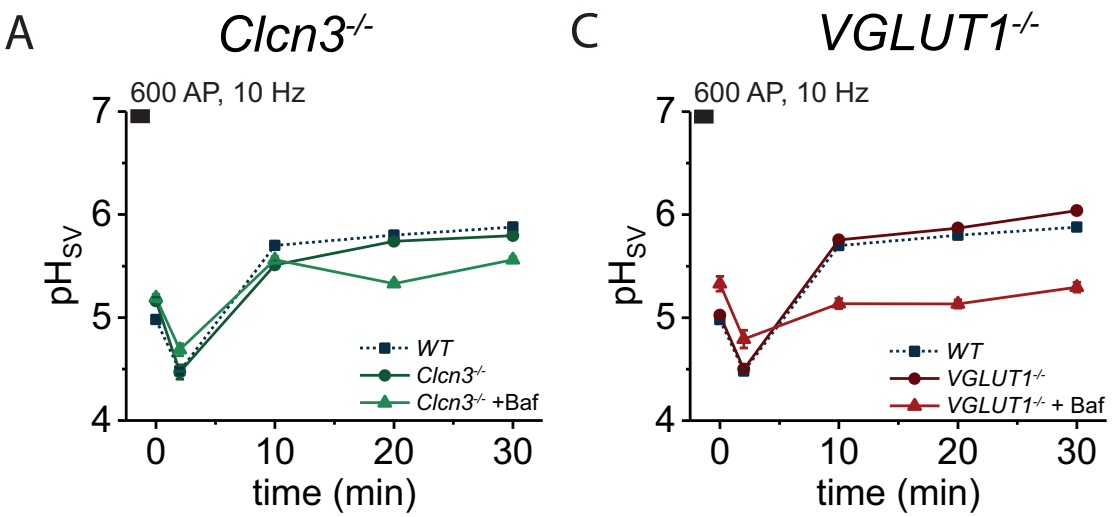

Figure 3.8: **Acidification is unaffected in KO mouse models of VGLUT1 and ClC-3.** (A) The effect of of pH_{SV} after endocytosis over time after in *Clcn3*$_{-/-}$ neurons stimulated with trains of 600 APs at a frequency of 10 Hz. Squares indicate control conditions and circles Bafilomycin treated neurons. (B) The effect of of pH_{SV} after endocytosis over time in *VGLUT1*$^{-/-}$ neurons stimulated with trains of 600 APs at a frequency of 10 Hz. Squares indicate control conditions and circles Bafilomycin treated neurons. All data are mean ± 95%CI. Dataset listed in table 3.10.

in *Clcn3*$^{-/-}$ neurons no change in the pH_{SV} after endocytosis was observed and also no changes in the effect of Bafilomycin (Figure 3.8A). The vesicular glutamate transporter VGLUT1 also can function as an chloride channel [58, 59, 95] and thus might support acidification by electrogenic proton co- or antiporter. In *VGLUT1*$^{-/-}$ neurons no change in pH_{SV} was observed compared to *WT*. Bafilomycin, however, decreased the maximum acidification and reduced the recovery to the resting pH (Figure 3.8C). In conclusion, neither the V-ATPase, nor ClC-3 nor VGLUT1 are indispensable for synaptic vesicle acidification after endocytosis, but VGLUT1 has a remarkable influence on synaptic vesicle re-alkalization.

3.7 Anion Transport is Critical Determinant of Synaptic Vesicle Acidification

To assess whether anion transporters/channels might play an important role in synaptic vesicle acidification the experiments were repeated in external solutions with reduced [Cl^-]. After endocytosis, synaptic vesicles initially contain a luminal solution that resembles the external solution, and modification of the external medium is therefore an easy

approach to change the driving force for transporters/channels involved in synaptic vesicle acidification. The standard external solution contains 148.4 mM Cl^-. With *WT* neurons perfused with external medium containing 75 mM, 18.9, 13 mM or no Cl^- the peak acidification and recovery considerably changed (Figure 3.9A). When 13 mM $[Cl^-]_{ex}$ was applied, acidification was completely abolished (pH_{SV} = 6.54 ± 0.04), whereas without $[Cl^-]_{ex}$ a small change was observed (pH_{SV} = 6.33 ± 0.04). The remaining acidification in neurons exposed to no $[Cl^-]_{ex}$ might be explained by an import of luminal Cl^- by ClC-3 utilizing the remaining concentration gradient which is abolished when neurons are exposed to 10 mM $[Cl^-]_{ex}$. This would already support the V-ATPase driven acidification by decreasing $\Delta\mu$.

To exclude that the reduced acidification in absence of chloride might be a side effect of reduced endocytosis, neurons were loaded with FM1-43 at different external Cl^- concentrations and the change in intensity after washout of the dye in ES was analyzed (Fig. 3.9B). Here, no $[Cl^-]$-dependent change in the endocytosis was observed. And, it could further be shown that the reduced acidification is not biased by an increased surface population of the biosensor. FM1-43 is a fluorescent styryle dye which only exhibits as long as it is inserted into membranes and can be washed out. Thus the amount of intensity after internalization at different $[Cl^-]$ reflects the relative amount of endocytosed synaptic vesicles after stimulation. If endocytosis would have been inhibited by reduced $[Cl^-]$, remaining FM1-43 would have been washed out and the fluorescence intensity would be lower compared to *WT*.

To analyze if ClC-3 might be responsible for inducing acidification of synaptic vesicles by utilization of the Cl-gradient $[Cl^-]_{ex}$ was reduced in *Clcn3*$^{-/-}$ neurons. Whereas at 148.4 mM $[Cl^-]_{ex}$ acidification of *Clcn3*$^{-/-}$ resembled *WT* data (Figure 3.8C, pH_{SV} = 4.47 ± 0.07), reduced peak acidification and steady state pH_{SV} were observed at 20 mM luminal chloride (Figure 3.9C, squares, pH_{SV} = 6.14 ± 0.04). This effect was further enhanced when the V-ATPase activity was blocked by additional treatment with 1 μM Bafilomycin (Figure 3.9C, triangles, pH_{SV} = 6.53 ± 0.04). Analysis of *knock-out* animals is often complicated by up-regulation of related isoforms that compensate for the genetic ablation of individual proteins. Therefore, the gain-of-function mutation E281Q of ClC-3 which lacks chloride conductance [70] was expressed in *Clcn3*$^{-/-}$ mice. *Clcn3*^{E281Q} neurons acidify in a similar $[Cl^-]_{SV}$-dependent manner than *Clcn3*$^{-/-}$ neurons (Fig. 3.8D). However, recently it has been shown that ClC-3 permits sorting of ClC-4 into endosomal compartments [69]. Thus, it cannot be excluded that in *Clcn3*^{E281Q} neurons ClC-4 rescues the loss of ClC-3 function in synaptic vesicles. But the same study [69] also shows that in absence of ClC-3, ClC-4 retains in the ER. Therefore, in *Clcn3*$^{-/-}$

neurons another transporter might overcome the loss of ClC-3.

The ClC-3 and ClC-4 related exchanger ClC-5 is absent in adult mouse brain [62], but not in juvenile animals. In *Clcn3*$^{-/-}$ hippocampal cultures ClC-5 expression was significantly up-regulated (determined by qPCR, R. Guzman, SUPPLEMENTS). Therefore, the expression of ClC-5 in *Clcn3*$^{-/-}$ was suppressed and the acidification of pH_{SV} determined. In *WT-Clcn5*^{KD} neurons peak acidification was slightly increased (pH_{SV} = 4.08 ± 0.16) and recovery decreased (pH_{SV} = 5.00 ± 0.25) (Figure 3.10A). In contrast, *Clcn3*$^{-/-}$*-Clcn5*^{KD} neurons show a significantly decreased acidification at 148.4 mM luminal Cl^- (pH_{SV} = 5.45 ± 0.09) that resembles *WT* data at 18.9 mM external Cl^- (Figure 3.10B, pH_{SV} = 5.33 ± 0.04). When V-ATPase activity was blocked by addition of Bafilomycin (Figure 3.10B) acidification was abolished (pH_{SV} = 6.67 ± 0.05). Stimulation in *Clcn3*$^{-/-}$*-Clcn5*^{KD} neurons exposed to 18.9 mM luminal Cl^- acidified below pH 6 (pH_{SV} = 5.85 ± 0.05), but above the resting pH_{SV}, with steady-state values similar to *WT* synaptic vesicles exposed to the same $[Cl^-]_{ex}$ (Figure 3.9A and Figure 3.10A).

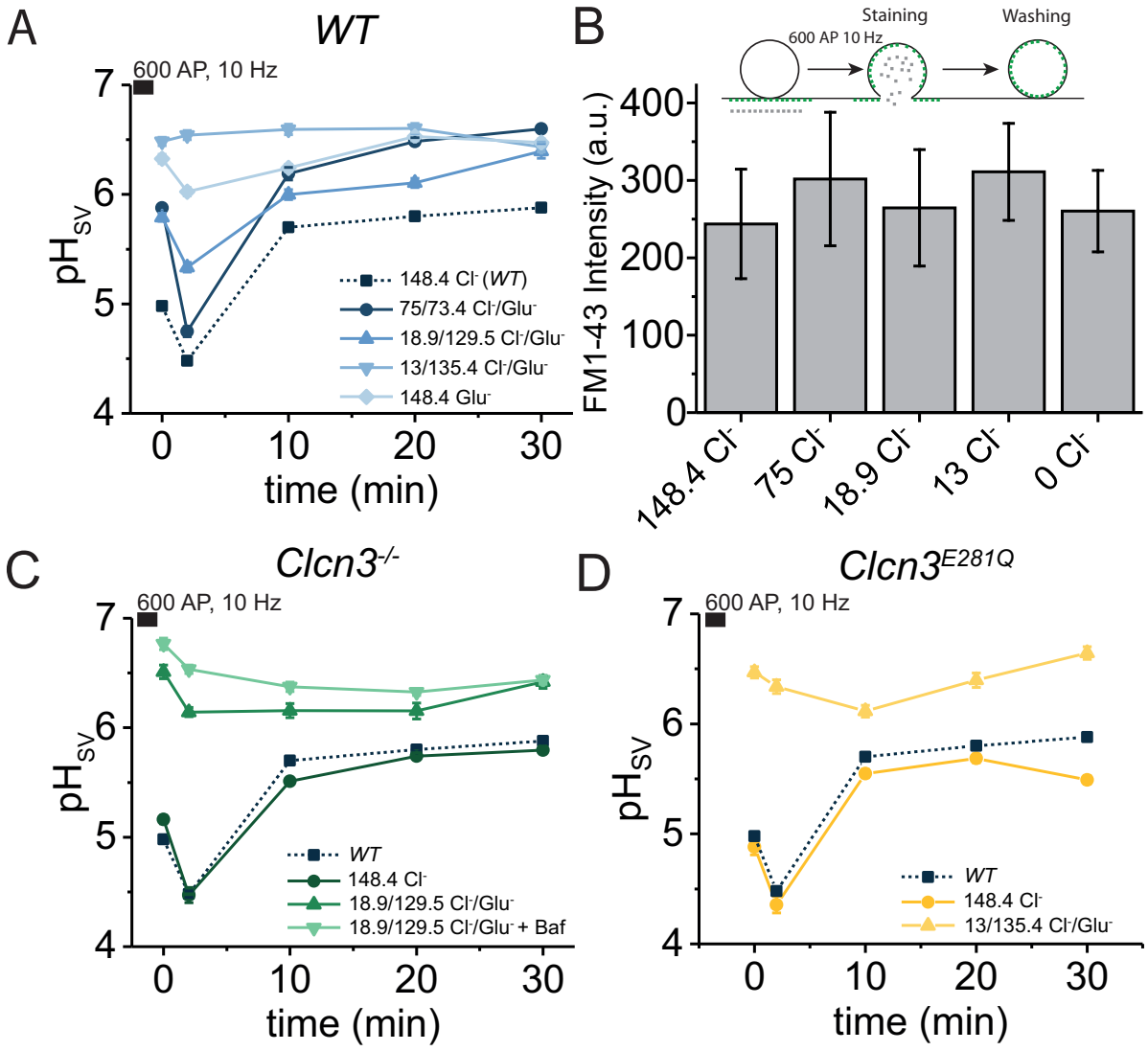

Figure 3.9: **Chloride dependent acidification of synaptic vesicles** (A) Time-course of pH_{SV} after stimulation with trains of 600 APs at a frequency of 10 Hz in *WT* neurons exposed to different $[Cl^-]_{ex}$ before stimulation. (B) FM1-43 fluorescence intensity which remains after washout in synaptic vesicles after electrical stimulation at different cytosolic $[Cl^-]$ does not differ between $[Cl^-]$. (C) Acidification after endocytosis in *Clcn3*$^{-/-}$ neurons exposed to 20 mM $[Cl^-]_{ex}$ (circles) and additionally treated with 1 μM Bafilomycin (triangles) compared to standard ES (squares, dashed line). (D) Acidification after endocytosis in *Clcn3*^{E281Q} neurons exposed to 150 mM (circles) and 13 mM (triangles) $[Cl^-]_{ex}$. All data are mean ± 95%CI. Dataset listed in table 3.11.

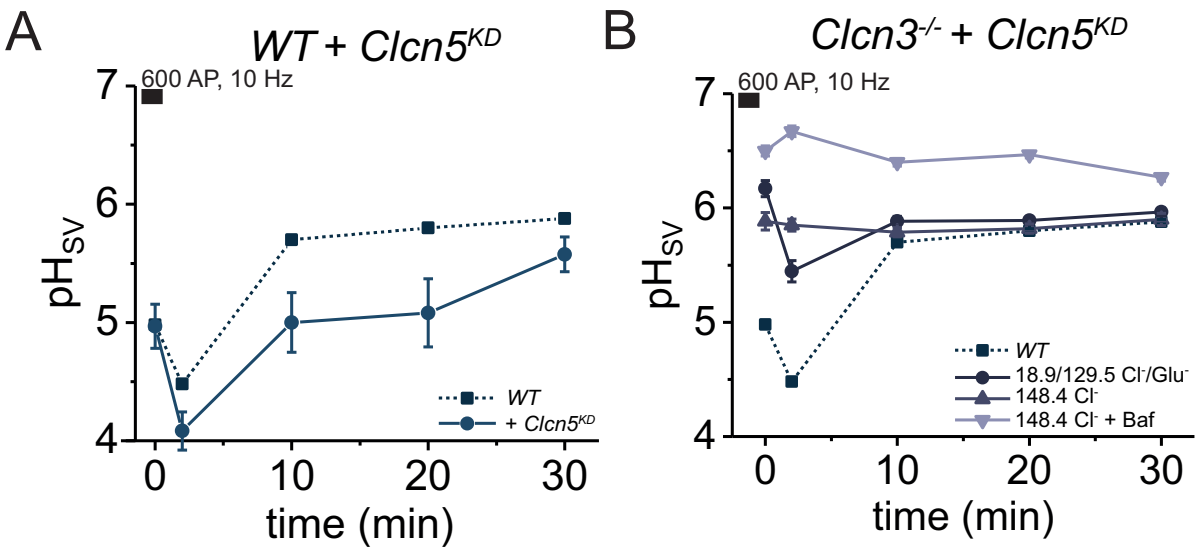

Figure 3.10: **ClC-3 dependent acidification of synaptic vesicles** (A) Effect of ClC-5 *knock-down* on acidification after endocytosis in *WT* neurons (circles) compared to *WT* (squares, dashed line). (B) Effect of ClC-5 *knock-down* on acidification after endocytosis in *Clcn3*$^{-/-}$ neurons at different $[Cl^-]_{ex}$. 148.4 mM $[Cl^-]_{ex}$ (circles), 20 mM $[Cl^-]_{ex}$ (squares), and 20 mM $[Cl^-]_{ex}$ plus 1 μM Bafilomycin (triangles). All data are mean ± 95%CI. Dataset listed in table 3.12.

3.8 VGLUTs Alkalize Synaptic Vesicle Lumen

Previous findings have raised the implication that glutamate import into synaptic vesicles might be coupled to H^+ translocation [42, 59]. Furthermore, it is proposed that VGLUT exhibits a pH-dependent Cl^- conductance which could modulate $[Cl^-]_{SV}$ [58, 59]. To investigate the effect of VGLUT1 on pH_{SV}, acidification in *VGLUT1*$^{-/-}$ neurons was measured (Fig. 3.11A). Compared to *WT* neurons no difference in peak acidification and recovery of the pH was measured. For investigation of *VGLUT1*$^{-/-}$ neurons cultures not younger than DIV 21 have been used because in juvenile brain VGLUT2 is highly expressed with low expression of VGLUT1 [135]. During maturation the expression of VGLUT1 and VGLUT2 switches and three weeks after birth VGLUT1 is the predominant vesicular glutamate transporter in synaptic vesicles in the hippocampus [135]. However, the related transporter VGLUT2 is still expressed in cultured neurons compensating the knock-out of VGLUT1 in *VGLUT1*$^{-/-}$ neurons [86]. To overcome possible side-effects in *VGLUT1*$^{-/-}$ neurons by upregulation of VGLUT2 the VGLUT-specific blocker Rose Bengal (RB) was applied to neurons [136, 59, 137]. In presence of the scavenger histidine to protect neurons from single oxygen production during illumination [138] RB left peak pH_{SV} in *WT*, *VGLUT1*$^{-/-}$, and *Clcn3*$^{-/-}$ neurons unaffected, but decelerated recovery and reduced steady state pH (Fig. 3.11A, B, and C). Additional block of V-ATPase activity with Bafilomycin in *WT*, *VGLUT1*$^{-/-}$, and *Clcn3*$^{-/-}$ neurons keeps peak acidification unaffected (Fig. 3.11A, B, and C), thus supporting the previous results of ClC-3 mediated acidification in synaptic vesicles. Furthermore, reduction of $[Cl^-]_{SV}$ in *WT* and *VGLUT1*$^{-/-}$ neurons treated with RB together with Bafilomycin only reduced recovery but peak acidification was similar to *WT* and *VGLUT1*$^{-/-}$ neurons exposed to decreased $[Cl^-]_{SV}$ (Figure 3.11D). These findings support the hypothesis that activity of VGLUT1 is coupled to efflux of $[H^+]_{SV}$ re-alkalizing pH_{SV}, and that a reduction of ΔCl^- does not affect the pH_{SV} when VGLUT1 is absent.

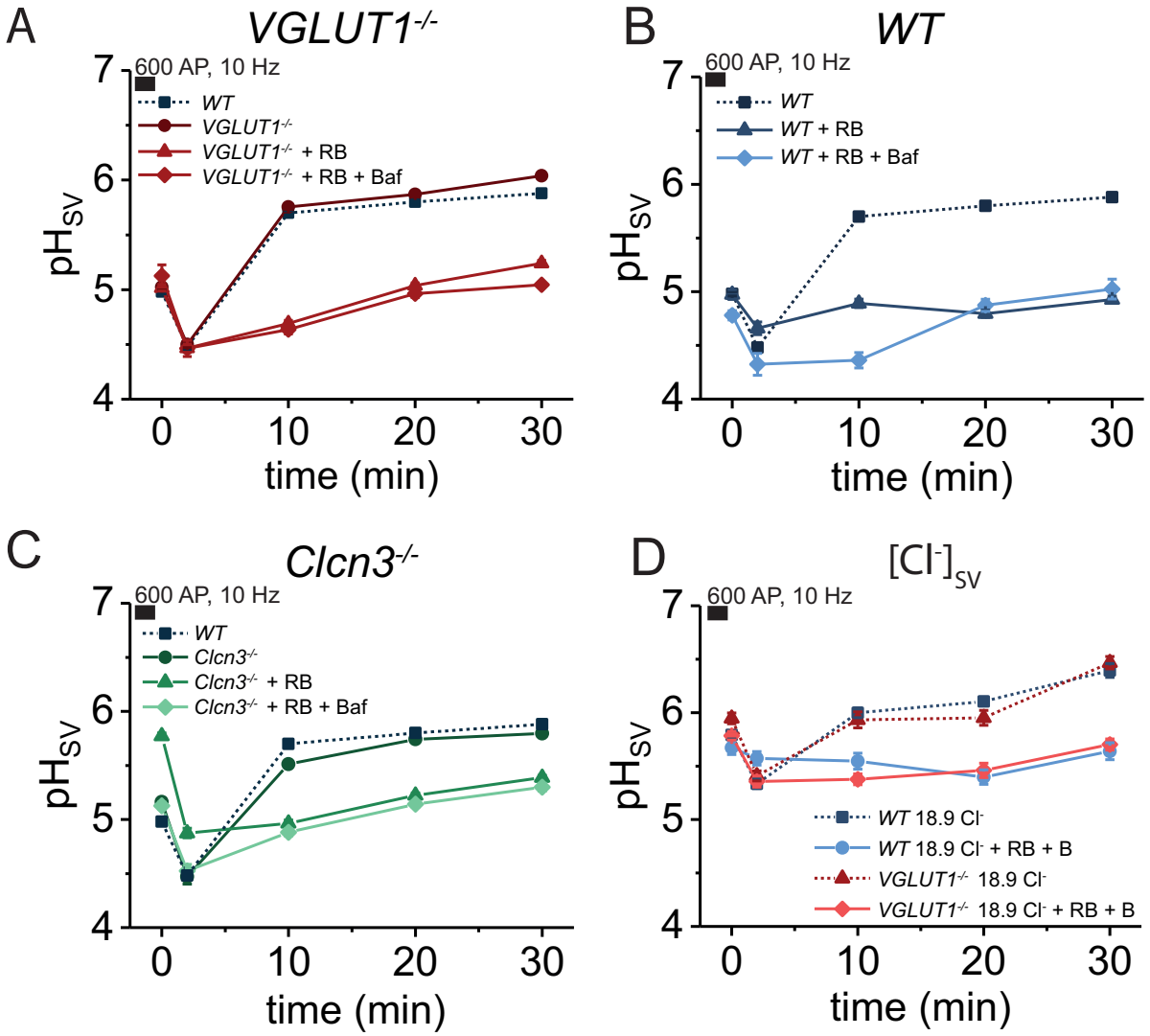

Figure 3.11: **VGLUTs alkalize synaptic vesicles after peak acidification** (A) Time-course of pH_{SV} after stimulation with trains of 600 APs at a frequency of 10 Hz in *VGLUT1*$^{-/-}$ neurons (squares) treated with RB (upward triangles) and RB + Bafilomycin (diamonds). (B) Acidification after endocytosis in *WT* neurons (squares, dashed line) treated with the VGLUT-specific blocker RB (upward triangles) and RB + Bafilomycin (diamonds). (C) Acidification after endocytosis in *Clcn3*$^{-/-}$ neurons (squares) treated with RB (upward triangles) and RB + Bafilomycin (diamonds). (D) Acidification after endocytosis in *VGLUT1*$^{-/-}$ and *WT* neurons exposed 18.9 mM Cl^- (squares and upward triangles for *WT* and *VGLUT1*$^{-/-}$, respectively) and additionally treated with RB and Bafilomycin (circles and diamonds for *WT* and *VGLUT1*$^{-/-}$, respectively). All data are mean ± 95%CI. Dataset listed in table 3.13.

3.9 Data

Table 3.1: Fitting data for pH calibration of SybII-Cerulean in hippocampal neurons

pH	No boutons	τ_{mean}	±SD
3.86	46	0.72	0.13
4.18	197	0.854	0.27
4.42	624	0.95	0.17
4.92	1310	1.22	0.23
5.25	374	1.47	0.39
5.44	1408	1.84	0.24
5.74	1857	2.10	0.24
5.96	442	2.13	0.42
6.21	629	2.23	0.21
6.43	2084	2.41	0.45
6.71	2034	2.53	0.23
7.09	1038	2.61	0.21
7.48	1783	2.71	0.26
7.96	2863	2.77	0.23

Table 3.2: Fitting parameter for pH calibration of SybII-Cerulean in hippocampal neurons

Model	DoseResp
Equation	$y = A1 + \frac{(A2-A1)}{1+10^{(pKa-pH)p}}$
A1	0.50 ± 0.15 ns
A2	2.77 ± 0.67 ns
pK_a	5.33 ± 0.1
p	0.68 ± 0.1
Reduced χ^2	5.29
R-Square	0.99
Adj. R-Square	0.99

Table 3.3: Dataset for figure 3.3 "pH distribution in synaptic vesicles"

Mouseline & Time-point	Treatment	pH	±SD	Median	Boutons	Cover-slips	Mice
WT		6.54	0.58	6.52	20722	37	11

Table 3.4: Dataset for figure 3.4A-E "The resting pH in synaptic vesicles"

Mouseline & Time-point	Treatment	τ_{mean}	±SD	Median	Boutons	Cover-slips	Mice
WT		2.40	0.27	2.47	20722	37	11
WT pH 6.5		2.24	0.29	2.28	764	1	1
WT pH 5.2		1.78	0.24	1.80	362	1	1
WT pH 5.5		1.84	0.24	1.86	372	1	1

Table 3.5: Dataset for figure 3.4F "The resting pH in synaptic vesicles"

Mouseline & Time-point	Treatment	pH	±SD	Median	Boutons	Cover-slips	Mice
WT 3exp		5.73	0.7	5.7	4844	10	5
WT pH 6.5 3exp		5.5	0.71	5.44	672	1	1
WT pH 5.2 3exp		5.38	0.69	5.33	226	1	1
WT pH 5.5 3exp		4.89	0.53	4.87	304	1	1

Table 3.6: Dataset for figure 3.5A "Synaptic vesicles over-acidify to pH 4.5 after endocytosis"

Mouseline & Time-point	Treatment	pH	±95 % CI	Median	Boutons	Cover-slips	Mice
WT 0 min		4.98	0.02	5.02	1992	15	8
WT 2 min		4.48	0.03	4.44	648	7	4
WT 10 min		5.70	0.02	5.68	1514	9	5
WT 20 min		5.80	0.02	5.83	1197	5	5
WT 30 min		5.88	0.02	5.88	901	6	5

Table 3.7: Dataset for figure 3.5B "Synaptic vesicles over-acidify to pH 4.5 after endocytosis"

Model	ExpDec2
Equation	$y = y_0 + A_1 e^{\frac{-x}{t_1}} + A_2 e^{\frac{-x}{t_2}}$
y0	0.7 ± 0
A1	0.15 ± 0.01
t1	10.02 ± 0.86 sec
A2	0.21 ± 0.01
t2	49.49 ± 2.29
Reduced χ^2	3.47E-6
R-Square	1
Adj. R-Square	1

Table 3.8: Dataset for figure 3.6 "V-ATPase independent acidification of synaptic vesicles"

Mouseline & Time-point	Treatment	pH	±95 % CI	Median	Boutons	Cover-slips	Mice
WT 0 min	1 μM Baf	5.24	0.04	5.24	246	2	2
WT 2 min	1 μM Baf	4.67	0.05	4.66	236	2	2
WT 10 min	1 μM Baf	5.49	0.03	5.54	333	2	2
WT 20 min	1 μM Baf	5.72	0.04	5.76	304	2	2
WT 30 min	1 μM Baf	5.69	0.05	5.69	218	2	2
WT 0 min	1 μM Baf 3hrs	5.83	0.06	5.86	255	1	1
WT 2 min	1 μM Baf 3hrs	4.95	0.15	4.98	69	1	1
WT 10 min	1 μM Baf 3hrs	5.18	0.11	5.35	56	1	1
WT 20 min	1 μM Baf 3hrs	5.29	0.1	5.43	68	1	1
WT 30 min	1 μM Baf 3hrs	5.2	0.09	5.35	68	1	1
WT 0 min	5 μM Baf	5.67	0.04	5.69	203	1	1
WT 2 min	5 μM Baf	4.73	0.06	4.76	149	1	1
WT 10 min	5 μM Baf	5.21	0.03	5.25	281	1	1
WT 20 min	5 μM Baf	5.39	0.03	5.39	262	1	1
WT 30 min	5 μM Baf	5.63	0.03	5.6	239	1	1
WT 0 min	5 μM Baf 4hrs	5.25	0.1	5.37	108	1	1
WT 2 min	5 μM Baf 4hrs	4.73	0.16	4.6	48	1	1
WT 10 min	5 μM Baf 4hrs	5.38	0.11	5.51	90	1	1
WT 20 min	5 μM Baf 4hrs	5.36	0.13	5.53	80	1	1
WT 30 min	5 μM Baf 4hrs	5.5	0.08	5.55	106	1	1

Table 3.9: Dataset for fig 3.7 "Acidification is unaffected from NHE activity"

Mouseline & Time-point	Treatment	pH	±95 % CI	Median	Boutons	Cover-slips	Mice
WT 0 min	10 μM EIPA	5.21	0.05	5.25	228	1	1
WT 2 min	10 μM EIPA	4.65	0.06	4.64	156	1	1
WT 10 min	10 μM EIPA	5.56	0.03	5.53	304	1	1
WT 20 min	10 μM EIPA	5.73	0.04	5.69	260	1	1
WT 30 min	10 μM EIPA	5.5	0.03	5.46	299	1	1

Table 3.10: Dataset for figure 3.8 "Acidification is unaffected in KO mouse models of VGLUT1 and ClC-3"

Mouseline & Time-point	Treatment	pH	±95 % CI	Median	Boutons	Cover-slips	Mice
Clcn3$^{-/-}$ 0 min	ctrl	5.16	0.04	5.22	337	3	2
Clcn3$^{-/-}$ 2 min	ctrl	4.47	0.07	4.46	120	2	2
Clcn3$^{-/-}$ 10 min	ctrl	5.51	0.03	5.51	603	4	3
Clcn3$^{-/-}$ 20 min	ctrl	5.74	0.03	5.75	571	4	3
Clcn3$^{-/-}$ 30 min	ctrl	5.8	0.03	5.77	957	4	3
Clcn3$^{-/-}$ 0 min	1 μM Baf	5.19	0.04	5.19	291	1	1
Clcn3$^{-/-}$ 2 min	1 μM Baf	4.69	0.06	4.71	168	1	1
Clcn3$^{-/-}$ 10 min	1 μM Baf	5.56	0.03	5.56	344	1	1
Clcn3$^{-/-}$ 20 min	1 μM Baf	5.33	0.03	5.3	345	1	1
Clcn3$^{-/-}$ 30 min	1 μM Baf	5.56	0.03	5.57	286	1	1
VGLUT1$^{-/-}$ 0 min	ctrl	5.02	0.02	5.02	858	5	1
VGLUT1$^{-/-}$ 2 min	ctrl	4.5	0.03	4.51	636	5	1
VGLUT1$^{-/-}$ 10 min	ctrl	5.75	0.02	5.77	1488	5	1
VGLUT1$^{-/-}$ 20 min	ctrl	5.87	0.02	5.88	1193	4	1
VGLUT1$^{-/-}$ 30 min	ctrl	6.04	0.02	6.03	1180	4	1
VGLUT1$^{-/-}$ 0 min	1 μM Baf	5.33	0.07	5.29	90	1	1
VGLUT1$^{-/-}$ 2 min	1 μM Baf	4.79	0.09	4.79	92	1	1
VGLUT1$^{-/-}$ 10 min	1 μM Baf	5.14	0.05	5.14	137	1	1
VGLUT1$^{-/-}$ 20 min	1 μM Baf	5.13	0.04	5.14	214	1	1
VGLUT1$^{-/-}$ 30 min	1 μM Baf	5.3	0.05	5.26	139	1	1

Table 3.11: Dataset for figure 3.9 "Chloride dependent acidification of synaptic vesicles"

Mouseline & Time-point	Treatment	pH	±95 % CI	Median	Boutons	Cover-slips	Mice
WT 0 min	75 mM Cl^-	5.88	0.03	5.92	552	1	1
WT 2 min	75 mM Cl^-	4.75	0.05	4.72	292	1	1
WT 10 min	75 mM Cl^-	6.19	0.06	6.34	477	1	1
WT 20 min	75 mM Cl^-	6.48	0.03	6.51	728	1	1
WT 30 min	75 mM Cl^-	6.6	0.03	6.61	555	1	1
WT 0 min	18.9 mM Cl^-	5.79	0.04	5.80	261	1	1
WT 2 min	18.9 mM Cl^-	5.33	0.04	5.35	159	1	1
WT 10 min	18.9 mM Cl^-	6.00	0.05	5.98	216	1	1
WT 20 min	18.9 mM Cl^-	6.11	0.04	6.12	265	1	1
WT 30 min	18.9 mM Cl^-	6.39	0.06	6.38	229	1	1
WT 0 min	13 mM Cl^-	6.48	0.04	6.52	635	1	1
WT 2 min	13 mM Cl^-	6.54	0.04	6.54	480	1	1
WT 10 min	13 mM Cl^-	6.59	0.05	6.62	439	1	1
WT 20 min	13 mM Cl^-	6.60	0.05	6.61	515	1	1
WT 30 min	13 mM Cl^-	6.43	0.04	6.43	538	1	1
WT 0 min	148.4 mM Glu^-	6.33	0.04	6.32	535	2	2
WT 2 min	148.4 mM Glu^-	6.03	0.04	6.09	507	2	2
WT 10 min	148.4 mM Glu^-	6.24	0.03	6.24	616	2	2
WT 20 min	148.4 mM Glu^-	6.53	0.04	6.52	778	2	2
WT 30 min	148.4 mM Glu^-	6.47	0.04	6.45	591	2	2
$Clcn3^{-/-}$ 0 min	18.9 mM Cl^- + 1 μM Baf	6.77	0.05	6.75	334	1	1
$Clcn3^{-/-}$ 2 min	18.9 mM Cl^- + 1 μM Baf	6.53	0.04	6.49	308	1	1
$Clcn3^{-/-}$ 10 min	18.9 mM Cl^- + 1 μM Baf	6.37	0.04	6.38	342	1	1
$Clcn3^{-/-}$ 20 min	18.9 mM Cl^- + 1 μM Baf	6.33	0.03	6.33	425	1	1
$Clcn3^{-/-}$ 30 min	18.9 mM Cl^- + 1 μM Baf	6.44	0.04	6.44	373	1	1
$Clcn3^{-/-}$ 0 min	18.9 mM Cl^-	6.51	0.06	6.48	257	1	1
$Clcn3^{-/-}$ 2 min	18.9 mM Cl^-	6.14	0.04	6.12	215	1	1
$Clcn3^{-/-}$ 10 min	18.9 mM Cl^-	6.16	0.06	6.16	203	1	1
$Clcn3^{-/-}$ 20 min	18.9 mM Cl^-	6.15	0.07	6.15	205	1	1
$Clcn3^{-/-}$ 30 min	18.9 mM Cl^-	6.42	0.06	6.41	242	1	1
$Clcn3^{E281Q}$ 0 min	ctrl	4.88	0.07	4.81	138	1	1
$Clcn3^{E281Q}$ 2 min	ctrl	4.36	0.08	4.23	97	1	1
$Clcn3^{E281Q}$ 10 min	ctrl	5.55	0.04	5.53	248	1	1
$Clcn3^{E281Q}$ 20 min	ctrl	5.69	0.04	5.69	296	1	1
$Clcn3^{E281Q}$ 30 min	ctrl	5.49	0.04	5.5	333	1	1
$Clcn3^{E281Q}$ 0 min	13 mM Cl^-	6.47	0.05	6.5	361	1	1
$Clcn3^{E281Q}$ 2 min	13 mM Cl^-	6.34	0.06	6.34	319	1	1
$Clcn3^{E281Q}$ 10 min	13 mM Cl^-	6.12	0.05	6.15	265	1	1
$Clcn3^{E281Q}$ 20 min	13 mM Cl^-	6.4	0.07	6.43	308	1	1
$Clcn3^{E281Q}$ 30 min	13 mM Cl^-	6.64	0.06	6.61	237	1	1

Table 3.12: Dataset for figure 3.10 "ClC-3 dependent acidification of synaptic vesicles"

Mouseline & Time-point	Treatment	pH	±95 % CI	Median	Boutons	Cover-slips	Mice
WT-Clcn5^{KD} 0 min	148.4 mM Cl^-	4.97	0.19	5.02	10	2	1
WT-Clcn5^{KD} 2 min	148.4 mM Cl^-	4.08	0.16	4.11	4	1	1
WT-Clcn5^{KD} 10 min	148.4 mM Cl^-	5.00	0.25	5.17	19	2	1
WT-Clcn5^{KD} 20 min	148.4 mM Cl^-	5.08	0.29	5.22	13	2	1
WT-Clcn5^{KD} 30 min	148.4 mM Cl^-	5.58	0.15	5.58	30	2	1
Clcn3$^{-/-}$*-Clcn5*^{KD} 0 min	148.4 mM Cl^-	6.17	0.07	6.11	256	2	1
Clcn3$^{-/-}$*-Clcn5*^{KD} 2 min	148.4 mM Cl^-	5.45	0.09	5.39	262	1	1
Clcn3$^{-/-}$*-Clcn5*^{KD} 10 min	148.4 mM Cl^-	5.88	0.04	5.86	411	2	1
Clcn3$^{-/-}$*-Clcn5*^{KD} 20 min	148.4 mM Cl^-	5.89	0.03	5.91	546	2	1
Clcn3$^{-/-}$*-Clcn5*^{KD} 30 min	148.4 mM Cl^-	5.97	0.03	5.93	522	2	1
Clcn3$^{-/-}$*-Clcn5*^{KD} 0 min	148.4 mM Cl^- + 1 μM Baf	6.5	0.04	6.53	517	1	1
Clcn3$^{-/-}$*-Clcn5*^{KD} 2 min	148.4 mM Cl^- + 1 μM Baf	6.67	0.05	6.67	510	1	1
Clcn3$^{-/-}$*-Clcn5*^{KD} 10 min	148.4 mM Cl^- + 1 μM Baf	6.4	0.03	6.38	570	1	1
Clcn3$^{-/-}$*-Clcn5*^{KD} 20 min	148.4 mM Cl^- + 1 μM Baf	6.47	0.03	6.44	703	1	1
Clcn3$^{-/-}$*-Clcn5*^{KD} 30 min	148.4 mM Cl^- + 1 μM Baf	6.27	0.03	6.26	588	1	1
Clcn3$^{-/-}$*-Clcn5*^{KD} 0 min	18.9 mM Cl^-	5.88	0.08	5.92	205	1	1
Clcn3$^{-/-}$*-Clcn5*^{KD} 2 min	18.9 mM Cl^-	5.85	0.05	5.86	293	1	1
Clcn3$^{-/-}$*-Clcn5*^{KD} 10 min	18.9 mM Cl^-	5.79	0.04	5.79	428	1	1
Clcn3$^{-/-}$*-Clcn5*^{KD} 20 min	18.9 mM Cl^-	5.82	0.04	5.78	346	1	1
Clcn3$^{-/-}$*-Clcn5*^{KD} 30 min	18.9 mM Cl^-	5.9	0.05	5.87	408	1	1

Table 3.13: Dataset for fig 3.11 "VGLUTs alkalize synaptic vesicles after peak acidification"

Mouseline & Time-point	Treatment	pH	±95 % CI	Median	Boutons	Cover-slips	Mice
WT 0 min	100 nM RB	4.97	0.05	4.99	180	1	1
WT 2 min	100 nM RB	4.66	0.06	4.63	166	1	1
WT 10 min	100 nM RB	4.89	0.04	4.90	160	1	1
WT 20 min	100 nM RB	4.80	0.03	4.81	207	1	1
WT 30 min	100 nM RB	4.93	0.03	4.92	219	1	1
WT 0 min	100 nM RB + 1 μM Baf	4.78	0.04	4.79	247	1	1
WT 2 min	100 nM RB + 1 μM Baf	4.32	0.10	4.27	43	1	1
WT 10 min	100 nM RB + 1 μM Baf	4.36	0.07	4.30	81	1	1
WT 20 min	100 nM RB + 1 μM Baf	4.87	0.06	4.93	122	1	1
WT 30 min	100 nM RB + 1 μM Baf	5.02	0.09	5.09	79	1	1
WT 0 min	18.9 mM Cl^- + 100 nM RB + 1 μM Baf	5.67	0.06	5.67	168	1	1
WT 2 min	18.9 mM Cl^- + 100 nM RB + 1 μM Baf	5.57	0.06	5.58	100	1	1
WT 10 min	18.9 mM Cl^- + 100 nM RB + 1 μM Baf	5.55	0.07	5.54	94	1	1
WT 20 min	18.9 mM Cl^- + 100 nM RB + 1 μM Baf	5.40	0.07	5.46	88	1	1
WT 30 min	18.9 mM Cl^- + 100 nM RB + 1 μM Baf	5.64	0.08	5.58	76	1	1
VGLUT1$^{-/-}$ 0 min	100 nM RB	5.02	0.03	5.08	407	1	1
VGLUT1$^{-/-}$ 2 min	100 nM RB	4.47	0.04	4.45	281	1	1
VGLUT1$^{-/-}$ 10 min	100 nM RB	4.69	0.03	4.73	582	1	1
VGLUT1$^{-/-}$ 20 min	100 nM RB	5.04	0.02	5.08	605	1	1
VGLUT1$^{-/-}$ 30 min	100 nM RB	5.24	0.03	5.27	320	1	1
VGLUT1$^{-/-}$ 0 min	100 nM RB + 1 μM Baf	5.12	0.01	5.14	63	1	1
VGLUT1$^{-/-}$ 2 min	100 nM RB + 1 μM Baf	4.46	0.08	4.42	113	1	1
VGLUT1$^{-/-}$ 10 min	100 nM RB + 1 μM Baf	4.64	0.04	4.65	203	1	1
VGLUT1$^{-/-}$ 20 min	100 nM RB + 1 μM Baf	4.96	0.04	4.99	184	1	1
VGLUT1$^{-/-}$ 30 min	1100 nM RB + 1 μM Baf	5.05	0.02	5.06	425	1	1
VGLUT1$^{-/-}$ 0 min	18.9 mM Cl^- + 100 nM RB + 1 μM Baf	5.78	0.04	5.77	264	1	1
VGLUT1$^{-/-}$ 2 min	18.9 mM Cl^- + 100 nM RB + 1 μM Baf	5.36	0.05	5.40	144	1	1
VGLUT1$^{-/-}$ 10 min	18.9 mM Cl^- + 100 nM RB + 1 μM Baf	5.38	0.05	5.43	226	1	1
VGLUT1$^{-/-}$ 20 min	18.9 mM Cl^- + 100 nM RB + 1 μM Baf	5.46	0.07	5.44	152	1	1
VGLUT1$^{-/-}$ 30 min	18.9 mM Cl^- + 100 nM RB + 1 μM Baf	5.70	0.05	5.68	162	1	1
Clcn3$^{-/-}$ 0 min	100 nM RB	5.77	0.03	5.78	491	1	1
Clcn3$^{-/-}$ 2 min	100 nM RB	4.87	0.04	4.9	291	1	1
Clcn3$^{-/-}$ 10 min	100 nM RB	4.96	0.03	4.98	321	1	1
Clcn3$^{-/-}$ 20 min	100 nM RB	5.22	0.02	5.23	444	1	1
Clcn3$^{-/-}$ 30 min	100 nM RB	5.39	0.02	5.38	517	1	1
Clcn3$^{-/-}$ 0 min	100 nM RB + 1 μM Baf	5.13	0.03	5.18	299	1	1
Clcn3$^{-/-}$ 2 min	100 nM RB + 1 μM Baf	4.52	0.06	4.52	152	1	1
Clcn3$^{-/-}$ 10 min	100 nM RB + 1 μM Baf	4.88	0.03	4.95	333	1	1
Clcn3$^{-/-}$ 20 min	100 nM RB + 1 μM Baf	5.14	0.03	5.18	294	1	1
Clcn3$^{-/-}$ 30 min	100 nM RB + 1 μM Baf	5.30	0.04	5.32	180	1	1

Table 3.14: Statistical Analysis 2min

Mouseline	Treatment	W	p-value	Normality	Significance
WT	148.4 mM Cl^-	0.97	8.48E-10	failed	
WT	+ Baf	0.99	0.07	passed	p<0.001
WT	+ EIPA	0.98	9.53E-04	failed	p<0.001
WT	75 mM Cl^-	0.94	7.54E-08	failed	p<0.001
WT	18.9 mM Cl^-	0.96	2.52E-04	failed	p<0.001
WT	13 mM Cl^-	0.99	0	failed	p<0.001
WT	0 mM Cl^-	0.96	4.13E-10	failed	p<0.001
WT	100 nM RB	0.99	0.14	passed	p<0.001
WT	100 nM RB + 1 μM Baf	0.93	0.01	failed	p<0.001
WT	20 mM Cl^- 100 nM RB + 1 μM Baf	0.92	1.78E-05	failed	p<0.001
WT - Clcn5^{KD}	148.4 mM Cl	0.9	0.45	passed	p<0.001
Clcn3$^{-/-}$	148.4 mM Cl^-	0.97	0.01	failed	-
Clcn3$^{-/-}$	1 μM Baf	0.99	0.23	passed	p<0.001
Clcn3$^{-/-}$	18.9 mM Cl^-	0.96	4.85E-06	failed	p<0.001
Clcn3$^{-/-}$	18.9 mM Cl^- +1 μM Baf	0.91	8.44E-13	failed	p<0.001
Clcn3$^{-/-}$	100 nM RB	0.99	0.15	passed	p<0.001
Clcn3$^{-/-}$	100 nM RB + 1 μM Baf	0.98	0.01	failed	-
Clcn3$^{-/-}$-Clcn5^{KD}	148.4 mM Cl^-	0.97	9.80E-06	failed	p<0.001
Clcn3$^{-/-}$-Clcn5^{KD}	148.4 mM Cl^- + 1 μM Baf	0.92	1.94E-15	failed	p<0.001
Clcn3$^{-/-}$-Clcn5^{KD}	18.9 mM Cl^-	0.94	9.97E-10	failed	p<0.001
Clcn3^{E281Q}	148.4 mM Cl^-	0.91	4.87E-06	failed	p<0.001
Clcn3^{E281Q}	18.9 mM Cl^-	0.97	5.38E-06	failed	p<0.001
VGLUT1$^{-/-}$	148.4 mM Cl^-	0.97	4.73E-09	failed	-
VGLUT1$^{-/-}$	1 μM Baf	0.96	0.01	failed	p<0.001
VGLUT1$^{-/-}$	100 nM RB	0.99	0.01	failed	-
VGLUT1$^{-/-}$	100 nM RB + 1 μM Baf	0.96	0	failed	-
VGLUT1$^{-/-}$	18.9 mM Cl^- + 100 nM RB + 1 μM Baf	0.93	1.28E-06	failed	p<0.001

Table 3.15: Statistical Analysis 10 min

Mouseline	Treatment	W	p-value	Normality	Significance
WT	148.4 mM Cl^-	0.98	5.45E-14	failed	
WT	+ Baf	0.91	2.26E-13	failed	p<0.001
WT	+ EIPA	0.99	3.86E-05	failed	p<0.001
WT	75 mM Cl^-	0.95	1.24E-05	failed	p<0.001
WT	18.9 mM Cl^-	0.97	2.48E-04	failed	p<0.001
WT	13 mM Cl^-	0.94	1.05E-11	failed	p<0.001
WT	0 mM Cl^-	0.97	8.69E-09	failed	p<0.001
WT	100 nM RB	0.97	0	failed	p<0.001
WT	100 nM RB + 1 μM Baf	0.94	4.79E-04	failed	p<0.001
WT	20 mM Cl^- 100 nM RB + 1 μM Baf	0.92	2.05E-05	failed	p<0.001
WT - Clcn5^{KD}	148.4 mM Cl	0.86	0.01	failed	p<0.001
Clcn3$^{-/-}$	148.4 mM Cl^-	0.96	2.38E-11	failed	p<0.001
Clcn3$^{-/-}$	1 μM Baf	0.98	6.12E-05	failed	p<0.001
Clcn3$^{-/-}$	18.9 mM Cl^-	0.99	0.07	passed	p<0.001
Clcn3$^{-/-}$	18.9 mM Cl^- +1 μM Baf	0.89	1.08E-14	failed	p<0.001
Clcn3$^{-/-}$	100 nM RB	0.97	1.74E-06	failed	p<0.001
Clcn3$^{-/-}$	100 nM RB + 1 μM Baf	0.97	2.61E-06	failed	p<0.001
Clcn3$^{-/-}$-Clcn5^{KD}	148.4 mM Cl^-	0.98	9.21E-05	failed	p<0.001
Clcn3$^{-/-}$-Clcn5^{KD}	148.4 mM Cl^- + 1 μM Baf	0.98	2.76E-07	failed	p<0.001
Clcn3$^{-/-}$-Clcn5^{KD}	18.9 mM Cl^-	0.93	1.20E-13	failed	p<0.001
Clcn3^{E281Q}	148.4 mM Cl^-	0.99	0.03	failed	p<0.001
Clcn3^{E281Q}	18.9 mM Cl^-	0.97	4.98E-06	failed	p<0.001
VGLUT1$^{-/-}$	148.4 mM Cl^-	0.98	5.03E-13	failed	p<0.001
VGLUT1$^{-/-}$	1 μM Baf	0.98	0.05	failed	p<0.001
VGLUT1$^{-/-}$	100 nM RB	0.98	9.26E-08	failed	p<0.001
VGLUT1$^{-/-}$	100 nM RB + 1 μM Baf	0.99	0.14	passed	p<0.001
VGLUT1$^{-/-}$	18.9 mM Cl^- + 100 nM RB + 1 μM Baf	0.97	2.98E-05	failed	p<0.001

Table 3.16: Dataset for FM1-43 measurements in figure 3.9

$[Cl^-]_{extern}$	Fluorescence (a.u.)	±SD	Median	Boutons	Cultures	Mice	Significance
148.4 mM Cl^-	242	71	231	287	2	1	
75 mM Cl^-	302	86	290	309	3	1	$p<0.001$
18.9 mM Cl^-	265	75	243	318	2	1	$p<0.001$
13 mM Cl^-	312	63	315	228	2	1	$p<0.001$
0 mM Cl^-	260	53	255	361	3	1	$p<0.001$

Chapter 4

Discussion

4.1 Resting pH in Synaptic Vesicles

The resting pH of synaptic vesicle was determined in several studies. Using the pH-dependent change in the fluorescence amplitude of pHluorin a pH_{SV} of 5.67 ± 0.71 was determined in synaptic vesicles in cultured hippocampal neurons [17]. In accordance with this, experiments using mOrange2 reported a pH_{SV} of 5.80 ± 0.04 for glutamatergic and a remarkably higher pH_{SV} of 6.44 ± 0.03 for GABAergic synaptic vesicles [23]. In purified synaptic vesicles, however, a luminal pH between 6.4 – 7.0 and 6.6 – 7.2 for glutamatergic and GABAergic synaptic vesicles, respectively, was measured by the use of pHluorin [19]. This discrepancy from purified synaptic vesicles compared to living cells may be explained by differences in luminal ionic and anionic composition which affect acidification.

What all common sensors are missing is an adequate sensitivity at low pH. The determined resting pH_{SV} are at the lower range of the sensitivity of pHluorin and mOrange2. Compared to pHluorin and mOrange2, Cerulean more accurately covers the pH range in the lumen of synaptic vesicles. pHluorin for example has a high pK_a of 7.1, and is lacking sensitivity below pH 6 considering that a difference between pH 5.7 (the resting pH) and 6.0 corresponds to the difference of $[H^+]$ equivalent to that between pH 7.4 and 6.0 [18]. The use of mOrange2 as a pH probe enhances the sensitivity below pH 6.0, however, considerable sensitivity below pH 5.6 is still not achieved [18]. Furthermore,

pHluorins, but not Cerulean, sense the surrounding pH by protonation directly at the chromophore [17], thus lowering the total $[H^+]$ of their environment they are measuring in.

Using fluorescence intensity to determine absolute and relative changes in the pH with pHluorin and mOrange2 faces a major problem which can influence the luminal pH during measurement and might leading to a false-interpretation of pH_{SV}. The typical fluorescent proteins used for determination of luminal pH have their optimal pH-sensitivity in the physiological range (pH 5.5 – 8) with a pK_a around 7 and are nearly non-fluorescent at pH 5.5. For quantification it is therefore necessary to artificially neutralize all intracellular membrane compartments in order to visualize all fluorescence proteins expressed. Typically the addition of 50 mM NH_4Cl is used to achieve this. The weak base $NH_4{}^+$ dissociates into H^+ and the cell permeable NH_3 in neutral pH. Once diffused into acidic organelles, intracellular H^+ is sequestered turning NH_3 into NH_4, thus causing de-acidification [139]. This conversion is reversible, therefore, it is generally accepted that also cellular impacts, if any, are reversible and transient. Thus, it is practice to apply high concentrations of NH_4Cl prior recording of fluorescence images to select suitable spots in the sample for imaging [140]. Especially in studies of synaptic vesicle dynamics this is a common procedure when using fluorescence-intensity based fluorescent proteins [17, 141, 142, 143, 144, 145, 146, 147, 148, 149, 150, 103, 151]. By using synaptic vesicle-specific proteins like synaptophysin or SybII, the fluorescent protein tag is almost completely quenched and thus non-fluorescent at pH 5.5 [129, 99, 100, 152]. In a recent study the effect of NH_4Cl on neurons was tested with the result that 50 mM NH_4Cl depolarizes the membrane, leads to $[Ca^{2+}]_{cytosol}$ increase and synaptic vesicle release, the latter two effects persisted even after thorough washout [153]. These problems even persist at low 5 – 10 mM application of NH_4Cl. In experiments with Cerulean and FLIM, treatment of neurons with NH_4Cl is not necessary to quantify the pH-dependent fluorescence properties because the fluorescence lifetime of Cerulean is concentration independent and Cerulean still exhibits sufficient fluorescence at the lowest pH measured in synaptic vesicles.

In this study Cerulean has been used to determine absolute pH values with FLIM in synaptic vesicles in cultured hippocampal neurons. A dynamic range of Cerulean's fluorescence lifetime from pH 3.9 to 8.0 was determined with a pK_a of 5.3. However, it has to be considered that the sensor has limited sensitivity between pH 6.5 and pH 8, due to the small change in τ_{mean} in this pH-range. Thus, a significant difference at pH values above 6.5 cannot be made by the use of Cerulean.

In the hippocampus the majority of neurons are glutamatergic. Co-localization

analysis of SybII-Cerulean with immunohistochemically stained VGLUT1 and VGAT shows that Cerulean predominantly expresses at VGLUT1-positive synaptic boutons (Fig. 1.2B and C), and thus the dynamics described here should be interpreted preferentially for glutamate accumulation. However, the small Pearson's coefficient for co-localization with VGLUT might be due to the different staining techniques. In this experiment SybII-Cerulean was expressed by lentiviral expression which leads to overexpression and a substantial localization at other membranes than the synaptic vesicles. Whereas VGLUT1 was stained by antibody labelling of PFA-fixed neurons and VGAT in living cells by a fluorescent-labelled fist antibody. VGLUT1 and VGAT have a more distinct localization in the synaptic vesicle membrane.

Besides SybII, synaptophysin [129] and VGLUT1 [78] are possible fusion proteins to target Cerulean to synaptic vesicle membrane. As an advantage, both proteins show a more exclusive localization pattern to the synaptic vesicle membrane with less background. However, because the calculation of τ_{mean} needs a minimal number of photons the use of synaptophysin as well as VGLUT1 is a drawback. SybII is the most abundant protein in the synaptic vesicle membrane with a copy number of about 70 proteins per vesicle whereas synaptophysin (30 proteins/vesicle) and VGLUT1 (9 proteins/vesicle) are less present [154]. Because the number of these proteins in the synaptic vesicle would directly determine the number of fluorescent proteins and thus the fluorescence intensity. Use of synaptophysin and VGLUT1 would further elongate the recording time per image and reduce the possibility to record dynamic events. This furthermore would increase illumination-induced phototoxicity.

With the use of SybII-Cerulean a pH_{SV} of 6.54 is determined at rest. This value is, however, in alignment with the pH measured with SynaptopHluorin at the onset of application of acidic solution (pH 6.67, [18]) but still widely above the proposed resting pH of 5.7. To determine the resting pH of synaptic vesicles several approaches have been used. Due to the transient over-expression of SybII-Cerulean by lentiviral transduction, up to 30% of the sensor accumulates at the plasma membrane [126, 125]. When exposed to extracellular solution with a pH of 7.4, the determined pH value of a synaptic bouton is thus shifted to a more alkaline level compared to the average pH_{SV} of all synaptic vesicles in the synaptic bouton. In experiments where pHluorin is used as a pH probe this surface population can be quenched by application of acidic solution with a pH of 5.0 because pHluorin does not exhibit any fluorescence emission at pH below 5.5 and thus only fluorescence from the synaptic vesicles remains [99]. This method is not directly applicable for Cerulean because it still exhibits considerable fluorescence at values below pH 4. Although, short perfusion with acidic solutions, e.g. pH 5.8, does

not change the intracellular pH (Fig. A.1), it is questionable how stable neurons are when perfused with acidic solutions at a pH of 3.0 for a few minutes. Another way to reduce the surface population is to cleave the sensor from the membrane tag by inserting a TEV-protease cleaving site between the fluorescence protein and the membrane protein. Upon incubation with TEV protease the excess of sensor at the surface membrane will be cleaved and washed out afterwards [121, 155]. However, this method failed with a modified version of SybII-Cerulean, where a TEV-protease cleavage site has been inserted into the linker-region between SybII and Cerulean, for unknown reasons (data not shown). Therefore, the resting pH of synaptic vesicles has been determined by using the following approaches:

(1) In a first experiment the pH of the surface population has been adjusted with acidic solutions of different pH until the measured τ_{mean} as a combination of the $\tau_{surface}$ representing $pH_{surface}$ and τ_{SV} representing pH_{SV}, is equal to the expected τ known from the calibration data at the specific pH. With this method a resting pH of around 5.5 has been determined (Fig. 3.4 E). (2) Second, a mathematical approach has been employed were the assumed $\tau_{surface}$ is excluded from the calculation of the amplitude weighted average fluorescence lifetime. Thus, a resting pH of 5.5 is obtained (Fig 3.4 F). (3) In a third step the resting pH has been determined after long-term stimulation. It was earlier reported that during compensatory endocytosis the surface population participated in the recycling of synaptic vesicle proteins [126, 125]. Ten minutes after electrical field stimulation the pH in synaptic vesicles was reduced from the initial high pH 6.5 (Fig. 3.4 A) to 5.7 where it increased slowly the next 20 minutes but did not reach initial pH (Fig. 3.5). Furthermore, a possible mislocalization of the sensor to non-synaptic vesicle organelles, such as the endosome which have a luminal pH of 6 – 6.5 [156], can be ruled out by these results. However, in case of metabolic stress, where endocytosis is reduced or inhibited this method would not work properly because the surface fraction of sensor would not be reduced. Thus, to determine the resting pH_{SV} after stimulation, it has to be clear that endocytosis is not affected by the experiment.

The three different approaches resulted in a similar value for pH_{SV} at rest in a range from pH 5.5 to 5.7 which is also in alignment with published values [17, 23]. Thus, it can be concluded that the method of FLIM and Cerulean to determine pH in synaptic vesicles is a useful and convincing method yielding results in accordance with published results.

4.2 Time-Course of Synaptic Vesicle Acidification After Endocytosis

Under high frequency-stimulation three pools of synaptic vesicles in a synapse have been identified (see reviews [4, 5]): (1) the ready releasable pool (RRP) (2), the recycling pool, and the reserve pool. Vesicles from the RRP and recycling pool can be easily mobilized upon stimulation, whereas the large reserve pool is only slowly utilized upon ongoing stimulation when the RRP is depleted. In a synapse of a typical hippocampal neuron the RRP includes about 5% of the total amount of synaptic vesicles, whereas recycling pool and resting pool include 10% and 85%, respectively [4]. To analyze the acidification of synaptic vesicles after endocytosis with Cerulean as a pH probe the following problem occurs. Because of relatively high fluorescence signal even at low pH, all synaptic vesicles, regardless to which pool they belong, are fluorescent. This means that, upon electrical stimulation, when the RRP is released and subsequently retrieved by compensatory endocytosis, the signal-to-noise-ratio (SNR) between the active synaptic vesicles from the RRP and the inactive vesicles from the reserve pool is too low to be detected by changes in the fluorescence lifetime of Cerulean. Unlike to pHluorin experiments, the majority of synaptic vesicles, thus, have to be forced to undergo synchronous exocytosis followed by endocytosis to map the course of synaptic vesicle acidification. To achieve this, an electrical stimulation protocol of 600 action potentials at a rate of 10 Hz has been applied [127] and the change of fluorescence intensity and lifetime has been recorded simultaneously. This allows to monitor the endocytosis rate and to give absolute pH values at distinct time points after endocytosis.

The kinetics of compensatory endocytosis of synaptic vesicles was reported to be between 15 and 20 seconds [157, 158, 100, 129, 128, 130, 102, 131]. After stimulation, the fluorescence intensity of Cerulean drops down in a bi-exponential manner with a fast rate of 10 seconds and a slower rate of 49 seconds which is substantially longer compared to pHluorin measurements but can be explained by the increased sensitivity at acidic pH (Fig. 3.5B). In addition, the measurement revealed that synaptic vesicles acidify to a much greater extent than the resting pH. By comparison of the absolute pH values from the first 80 s after stimulation and from 120 – 200 s, when intensity change was stable, pH_{SV} decreased to pH 4.5 in *WT* neurons, while it was already in the first 80 seconds with pH 5 considerably below the resting pH of 5.7 (Fig. 3.5A). This acidic pH could have been measured for the first time by the high dynamic range of Cerulean because commonly used pH-probes are completely dark at this acidic pH.

Assuming that $pH_{cytosol}$ is around pH 7.2 then a maximum acidification upon pH 4.5 would result in a ΔpH of 2.7 units. However, upon prolonged low-frequency stimulation, the cytosolic pH decreases to pH 6.6 during the first 50 seconds after stimulation and stabilizes at pH 6.8 after 150 seconds (unpublished data by M. Kahms, University of Münster, Germany). This results in a ΔpH of 2.3 units and not 2.7. Nevertheless, this is still substantially higher, compared to the ΔpH of 1.8 measured before [17, 18] and might have a substantial influence on $\Delta\psi$. However, since the sensor used in this study (YFP) is also strongly Cl^--dependent in its sensitivity [159], it cannot be excluded that also $[Cl^-]_{cytosol}$ is changing.

To sum up, it could be demonstrated that synaptic vesicles after endocytosis over-acidify to a level which could not have been measured with common pH-sensors like pHluorin and mOrange2, respectively. Acidification after endocytosis further underlies a biphasic process with a re-alkalization after peak acidification. This supports the notion that to establish the resting pH_{SV} a H^+-efflux from the synaptic vesicle takes place. To further analyze the proton fluxes in synaptic vesicles after endocytosis the different transporters and channels identified in synaptic vesicles were pharmacologically or genetically blocked.

4.3 Synaptic Vesicles Can Acidify Without V-ATPase Activity

Early experiments investigating glutamate uptake into purified synaptic vesicles have shown that ATP is required to drive the V-ATPase generating an electrochemical gradient [160, 132]. This gradient builds up the driving force for the uptake of neurotransmitters [161, 51, 22, 52]. This uptake was inhibited by molecules that dissipate the electrochemical proton gradient like FCCP, CCCP, and the V-ATPase specific inhibitor Bafilomycin. Also in cultured hippocampal neurons with the fluorescence reporter protein pHluorin acidification was impaired when V-ATPase was blocked [23, 162]. In the prevalent model of synaptic vesicle acidification the V-ATPase starts to acidify as soon as endocytosis is complete.

Synaptic vesicles are formed and recycled locally at presynaptic terminal [163, 164] but the precise mechanisms of synaptic vesicle recycling remain still unclear [165, 166, 167]. The well-defined protein composition and homogeneous size of synaptic vesicles requires a high grade of control over this process. To date, five mechanisms for synaptic vesicle endocytosis have been discussed. Clathrin-mediated endocytosis, which is a type of

endocytosis that capitalizes the formation of a clathrin coat including a number of adaptor and accessory proteins, and the GTPase dynamin [164, 168, 169], as well as clathrin-independent, fast endocytosis [170, 171, 172], kiss-and-run [173, 174], bulk endocytosis [175, 176, 177] and ultra-fast endocytosis [178, 179] are known and still being investigated.

The formation of the different endocytosis pathways strongly depends on the temperature and stimulation paradigm applied (summarized in [180]). After low-frequency stimulation (< 20 Hz) at room temperature inherent formation of clathrin-coated vesicles (CCVs) from the plasma membrane has been detected [129] whereas higher frequency protocols lead to budding of CCVs from endosomal like structures, or favor the other pathways of endocytosis (see review [166]).

The use of pHluorin and mOrange2, respectively, as pH-reporter allows to stimulate only a small number of synaptic vesicles to investigate endocytosis followed endocytosis because of their high signal-to-background ratio. Because the majority of synaptic vesicles exhibit only weak fluorescence at rest recycling of a single synaptic vesicle can be detected. This allows to stimulate with short pulses at high frequencies which typically activates synaptic vesicles from the RRP and include only a minority of the whole subset of synaptic vesicles in a bouton. The use of Cerulean, however, cannot resolve single events, because of the remarkable high fluorescence from synaptic vesicles at rest. Thus it is necessary to synchronously stimulate and recycle all synaptic vesicles in a synaptic bouton by the application of prolonged low-frequency stimulation. Therefore, it can be assumed that by the use of Cerulean and FLIM, as described in this thesis, synaptic vesicles are preferentially endocytosed as CCVs. The pathway of clathrin-coated endocytosis is further characterized by a slow time constant of 10 – 20 seconds [170, 181]. The pH-dependency of pHluorin and mOrange2 is typically monitored by their change in fluorescence intensity which allows recording with high temporal resolution. In contrast, FLIM measurements are relatively slow, since emitted fluorescence is accumulated over 80 seconds, thus dynamic changes at lower time-scales cannot be resolved.

In contrast to previous findings where acidification was prevented [23, 162], pharmacological blocking of V-ATPase with Bafilomycin did not disrupt the acidification of synaptic vesicles, regardless of incubation time and concentration applied (Fig. 3.6). Only in absence of ΔCl or of the Cl^-/H^+ exchanger ClC-3 a substantial Bafilomycin-induced effect could be seen (Fig. 3.9 and 3.10).

The contradictory results between Cerulean and pHluorin measurements are not easy to explain. Differences in the stimulation protocol which would lead to different endocytosis pathways, however, do not explain this difference. With pHluorin as fluorescent reporter protein, in neurons exposed to low frequency stimulation the application of

Bafilomycin also inhibited the formation of a ΔpH [100, 23, 182]. The block of acidification was also monitored for several minutes [182]. Thus the difference in the temporal resolution between fluorescence intensity and FLIM is also no explanation for this phenomenon observed. A possible explanation might be the high signal-to-background ratio of pHluorin. Assuming that after endocytosis only a small number of synaptic vesicles treated with Bafilomycin fail to acidify the synaptic bouton, this would still exhibit a substantial amplitude in fluorescence intensity. Furthermore, in case of bulk endocytosis, these large structures might as well be less acidic than synaptic vesicles at rest, because endosomes typically acidify between pH 6.0 and 6.5 [156].

Recently it was shown that in CCVs V-ATPase activity is inhibited, because the torsion of the head unit is blocked by the clathrin-coat [183]. This is in prevalence with previous observations that pHluorin quenching showed delayed kinetics during post-stimulus recovery at living synapses where uncoating was delayed due to genetic modification [130, 184, 185]. The same behavior was observed in this thesis when neurons were exposed to Bafilomycin and the change of pHluorin2 was measured after stimulation. Here, the kinetics of pHluorin2 quenching were delayed as well (see figure 3.6C). The stimulation protocol in this case was the same for experiments using pHluorin2 and Cerulean.

An alternative pathway of acidification, as it was observed here, could be provided by activating exchanger proteins which utilize preexisting ionic gradients like Cl^- or Na^+ to accumulate H^+. Compared to the cytosol $[Cl^-]_{SV}$ and $[Na^+]_{SV}$ in freshly endocytosed synaptic vesicles are around one magnitude higher. Utilization of the ΔNa^+ was excluded because pharmacological blocking of the Na^+/H^+-exchanger NHE did not prevent synaptic vesicle acidification (Figure 3.7).

4.4 CLC Cl^-/H^+ Exchange Regulates Luminal pH

The luminal $[Cl^-]$ in freshly endocytosed synaptic vesicles is around one magnitude higher than that of the cytoplasm. This Cl^--gradient can in principle be used as a driving force for luminal acidification by transport activity of the Cl^-/H^+-antiporter ClC-3 as it has been shown for ClC-5 recently [76]. Electrophysiological recordings of ClC-3 show a voltage-dependent transport of protons against their diffusion gradient and an activation of ClC-3 by high luminal $[Cl^-]$ [70]. This demonstrates that ClC-3 can exchange cytosolic H^+ against luminal Cl^- in freshly endocytosed synaptic vesicles. A gradual decrease of $[Cl^-]_{SV}$ by application of external solution at different relations of Cl^- and gluconate

indeed reduced synaptic vesicle acidification and could even prevent it in *WT* neurons (Fig. 3.9A and B). An influence of Cl^- on Cerulean's τ_{mean} could be excluded, because there was no difference in the τ_{mean} of purified Cerulean in presence and absence of 140 mM Cl^- measured from pH 4 – 7 (Figure A.4, together with T. Gensch, ICS-4, Forschungszentrum Jülich).

Clcn3$^{-/-}$ deficient neurons, however, still exhibit a similar acidification than *WT* neurons (Fig 3.8A) and treatment with Bafilomycin did not prevent acidification (Fig 3.8A). To exclude a side-effect by compensatory up-regulation of related Cl^-/H^+ exchanger of the CLC family a gain of function mutant of ClC-3 was investigated. The ClC-3 mutant E281Q lacks Cl^- conductance [70] but did not prevent synaptic vesicle acidification (Fig. 3.9C). However, in a recent study it was demonstrated that ClC-3 promotes sorting of ClC-4 by exhibiting heterodimers [69]. If this ClC-3-ClC-4 heterodimer is also localized to the membrane of synaptic vesicles is not investigated yet. But the result that *Clcn3*^{E281Q} neurons still acidify can either be explained by compensation by ClC-4 or by a yet unidentified Cl^-/H^+ exchanger. The same study also demonstrated that in absence of ClC-3 sorting of ClC-4 into the endosomal membrane is inhibited and ClC-4 retains in the ER membrane [69]. Thus, it is unlikely that in *Clcn3*$^{-/-}$ neurons ClC-4 compensates for the loss of ClC-3 but in *Clcn3*^{E281Q}.

ClC-5 shares similar transport properties with ClC-3 and ClC-4 and is expressed in the juvenile brain [62]. QPCR experiments (R. Guzman, ICS-4, Forschungszentrum Jülich) further indicate that ClC-5 expression is up-regulated in juvenile *Clcn3*$^{-/-}$ neurons (see Fig A.3). Therefore, ClC-5 was down-regulated in *Clcn3*$^{-/-}$ neurons by expression of shRNA together with the pH-sensor and acidification after endocytosis was measured. In *Clcn3*$^{-/-}$-*Clcn5*^{KD} neurons synaptic vesicle acidification is reduced to pH 5.45 at persisting high ΔCl^- (Fig. 3.10B). In *WT*-*Clcn5*^{KD} neurons synaptic vesicles acidify to pH 4.08, and fail to recover to the resting pH (Fig. 3.10A). Without further investigation a concrete explanation for the observed over-expression cannot be given. A loss of ClC-5 may have an influence in ClC-3 trafficking thus increasing the amount of ClC-3 in the synaptic vesicle membrane or further changes the function of the endosomal system.

The remaining acidification in *Clcn3*$^{-/-}$-*Clcn5*^{KD} neurons might be due to V-ATPase activity. Additional Bafilomycin treatment decreased acidification of the synaptic vesicle lumen in *Clcn3*$^{-/-}$-*Clcn5*^{KD} neurons to pH 6.67 (Fig 3.9 E). The remaining difference between the initial pH of 7.4 and the measured pH can be explained by the Cerulean's lack of sensitivity above pH 6.5. In *Clcn3*$^{-/-}$ and *WT* neurons the additional Bafilomycin induced effect was only visible when $[Cl^-]_{SV}$ was reduced to 18.9 mM. In *WT* neurons peak acidification was reduced from pH 5.33 to 5.63 when Bafilomycin was additionally

applied. This can be explained by a lack of ΔCl when $[Cl^-]_{SV}$ was reduced to 18.9 mM and thus the Cl^-/H^+ exchanger fails to acidify synaptic vesicles.

These experiments demonstrate that ClC-3 (and ClC-4) mediated H^+/Cl^- exchange is necessary for regulation of synaptic vesicle acidification, and that up-regulation of ClC-5 in *Clcn3*$^{-/-}$ neurons and can partially compensate for the loss. The latter one might further explain why *Clcn3*$^{-/-}$ animals exhibit severe neurodegeneration starting two weeks after birth [79, 62, 80], that is correlated with down-regulation of ClC-5 expression in the brain during maturation [62].

Bafilomycin treatment in *Clcn3*$^{-/-}$-*Clcn5*^{KD} further demonstrates that acidification of synaptic vesicles is a combined process of V-ATPase activity and utilization of the ΔCl^- as a driving force for Cl^-/H^+ exchange mediated by ClC-3 and ClC-4. Given the rather contradictory data already published in different independent *Clcn3*$^{-/-}$ mouse lines these data may help to clarify the role of ClC-3 in synaptic vesicle acidification. It was previously shown that *in vitro* acidification of synaptic vesicles in ClC-3 abundant mice is reduced [62]. In this study, purified synaptic vesicles from *Clcn3*$^{-/-}$ neurons have shown a decreased ATP-induced $[Cl^-]_{ex}$-dependent acidification together with a reduced glutamate uptake. Furthermore, the amount of VGLUT1 was drastically reduced to 50% in *Clcn3*$^{-/-}$. This, however, could explain the reduced glutamate uptake in the *knock-out* synaptic vesicles. It should also be considered that the authors have used adult mice for their preparations, whereas in this study hippocampal neurons were prepared from newborn mice which do not show morphological changes in the hippocampus as it was demonstrated for adult brain [62]. The importance of the luminal ionic composition in regulation of acidification is demonstrated by measurements from Farsi et al. (2016) [19]. The authors used isolated glutamatergic and GABAergic synaptic vesicles and determined a resting pH between pH 6.4 and 7.2 which is substantially higher than determined in cultured hippocampal neurons, where the ionic composition resembles the *in vivo* conditions. During the isolation process the ionic composition of the synaptic vesicle lumen might change and cannot be changed or controlled afterwards, unlike in cultured neurons where the ionic composition of the synaptic vesicle lumen can be changed by perfusing the cells with different media.

Since it has been shown in this thesis that the accumulation of protons in the synaptic vesicle depends on ClC-3 activity, the role of Cl^- as a regulator of the acidification emerges. In the classical model of synaptic vesicle acidification a ΔpH is build up by the ATP-consuming activity of the V-ATPase which needs Cl^- import into the vesicle lumen to regulate the $\Delta\psi$ by decreasing the charge imbalance between luminal and cytosolic site of the synaptic vesicle membrane, and thus keeping the V-ATPase running. This raises and

supports the question why synaptic vesicles should not utilize the energy derived from the already existing Cl^- gradient to accumulate H^+ without the consumption of ATP and thus saving energy. And indeed, reduction of the Cl^- gradient after endocytosis subsequently decreased the ΔpH in *WT* neurons (Fig. 3.9 A and B). The remaining acidification is due to V-ATPase activity as additional Bafilomycin treatment in *Clcn3*$^{-/-}$-*Clcn5*^{KD} neurons inhibited exhibition of a ΔpH. In addition, in absence of ΔCl^- Bafilomycin treated neurons did not establish a ΔpH as well. Glutamate import into synaptic vesicles relies to a greater extent on $\Delta\psi$ than on ΔpH. Import of one positive charge in form of H^+ and export of two negative charged Cl^- would result in a net accumulation of positive charge in the synaptic vesicle lumen, which is also supported by V-ATPase activity, thus increasing $\Delta\psi$. However, both transport processes can only work until a certain point is reached. Too much positive charge in the vesicle lumen will block the V-ATPase activity, and Cl^-/H^+ exchange by ClC-3 is only working unless a substantial ΔCl^- is existing. Therefore, it cannot be excluded that the transport direction of Cl^-/H^+ exchange by ClC-3 switches once the reversal potential of the transporter is reached. This will support the V-ATPase activity by providing a counter-ion for regulation of charge-imbalance. However, also the import of negative charged Glutamate would compensate for the charge-imbalance but reduce $\Delta\psi$. In conclusion, the combined transport processes of V-ATPase, ClC-3 and VGLUTs have to be balanced to provide optimal conditions for glutamate loading while $\Delta\psi$, ΔpH, and ΔCl^- vary.

4.5 VGLUT1 Regulates Synaptic Vesicle Acidification by Providing a H^+-Efflux From Synaptic Vesicle Lumen

In the history of VGLUT research several models of ion and anion transport were discussed. In early experiments it was shown that glutamate uptake is activated by low $[Cl^-]_{cytosol}$ and inhibited gradually by increasing $[Cl^-]_{cytosol}$ [161, 97, 93]. This effect is attributed to an allosteric binding site on the cytoplasm site [94, 33, 91]. It was further described that VGLUTs operate as solute-chloride exchanger [95] and that the transport cycle may be associated with a net Cl^- flux [94, 59] which was recently supported by the finding that increasing $[H^+]_{SV}$ and $[Cl^-]_{SV}$ allosterically activate Cl^- conductance and glutamate transport [58]. In a current model VGLUT1 is described as a voltage- and H^+-dependent antiporter which is activated either by positive voltage or by a ΔpH at lower voltage [59].

The authors further propose that glutamate import by VGLUT is first driven by the the $\Delta\psi Cl$ which impedes V-ATPase activity due to the high voltage. Once the $\Delta\psi Cl$ is decreased by Cl^--efflux through the anion-channel of VGLUT1 $\Delta\psi Cl$ vanishes and V-ATPase activity can further acidify the synaptic vesicle lumen. Nevertheless, they assume that in the beginning, when $\Delta\psi Cl$ is high, luminal protons are still imported by the V-ATPase delivering the H^+ for glutamate exchange by VGLUT1. At this point the model is somehow contradictory if it is assumed that the high voltage inhibits V-ATPase activity. Even when V-ATPase activity is slow, glutamate loading by VGLUT would also be very small.

The results of this thesis have shown that initial acidification of recycled synaptic vesicles is dependent on ClC-3 activity. Considering that the rate limiting process of glutamate uptake according to the prevalent view of VGLUT1 activity is the availability of luminal H^+ and considering that V-ATPase activity is inhibited by $\Delta\psi Cl$ Cl^-/H^+ exchange by ClC-3 might explain the availability of luminal protons for glutamate exchange as well as speed up glutamate loading.

To investigate the role of VGLUT1 in regulation of pH_{SV} a *knock-out* model has been used. *VGLUT1*$^{-/-}$ neurons did not show any difference in pH_{SV} after endocytosis compared to *WT* (Fig. 3.8 C and D), but additional treatment with the VGLUT blocker Rose Bengal reduced the recovery after maximum acidification in *WT* and *VGLUT1*$^{-/-}$ neurons (Fig. 3.11 A,B and C,D). In *Clcn3*$^{-/-}$ neurons acidification was also reduced (Fig. 3.11 E and F). The additional effect of RB treatment can be explained by a block of the remaining fraction of VGLUT2 in *VGLUT1*$^{-/-}$ neurons even after DIV 21 when these neurons were measured [86]. Together with Bafilomycin treatment pH_{SV} in *VGLUT1*$^{-/-}$ neurons fails to recover, too (Figure 3.8 C and D). Both results indicate a VGLUT-mediated H^+ efflux from the vesicle lumen. If H^+ is coupled to glutamate loading, according to previous results [59, 95, 42, 60] cannot be determined by this method, but also not excluded. However, when buffering capacity of synaptic vesicles is exhausted, VGLUTs can exhibit a second transport mode which involves the exchange of luminal H^+ with cytosolic K^+, that ensures charge-neutral proton exit, promoting alkalization of the vesicle and keeping $\Delta\psi$ high while accumulating glutamate [13, 42].

When $[Cl^-]_{SV}$ is reduced to 18.9 mM RB treated synaptic vesicles acidify to a similar extent than *WT* neurons. This experiment indicates that the putative Cl^--conductance of VGLUT1 does not regulate synaptic vesicle acidification. Assuming that a $[H^+]$-dependent Cl^- channel would lead to an efflux of luminal Cl^- the initial ΔCl would be rapidly vanished and a block of this channel would support ClC-3 mediated Cl^-/H^+ exchange thus supporting acidification of the vesicular lumen. In *Clcn3*$^{-/-}$ neurons peak

acidification is actually slightly reduced. This is further supported by the notion that in Bafilomycin treated *VGLUT1*$^{-/-}$ neurons peak acidification is also slightly reduced.

4.6 A Proposed Model of Synaptic Vesicle Acidification

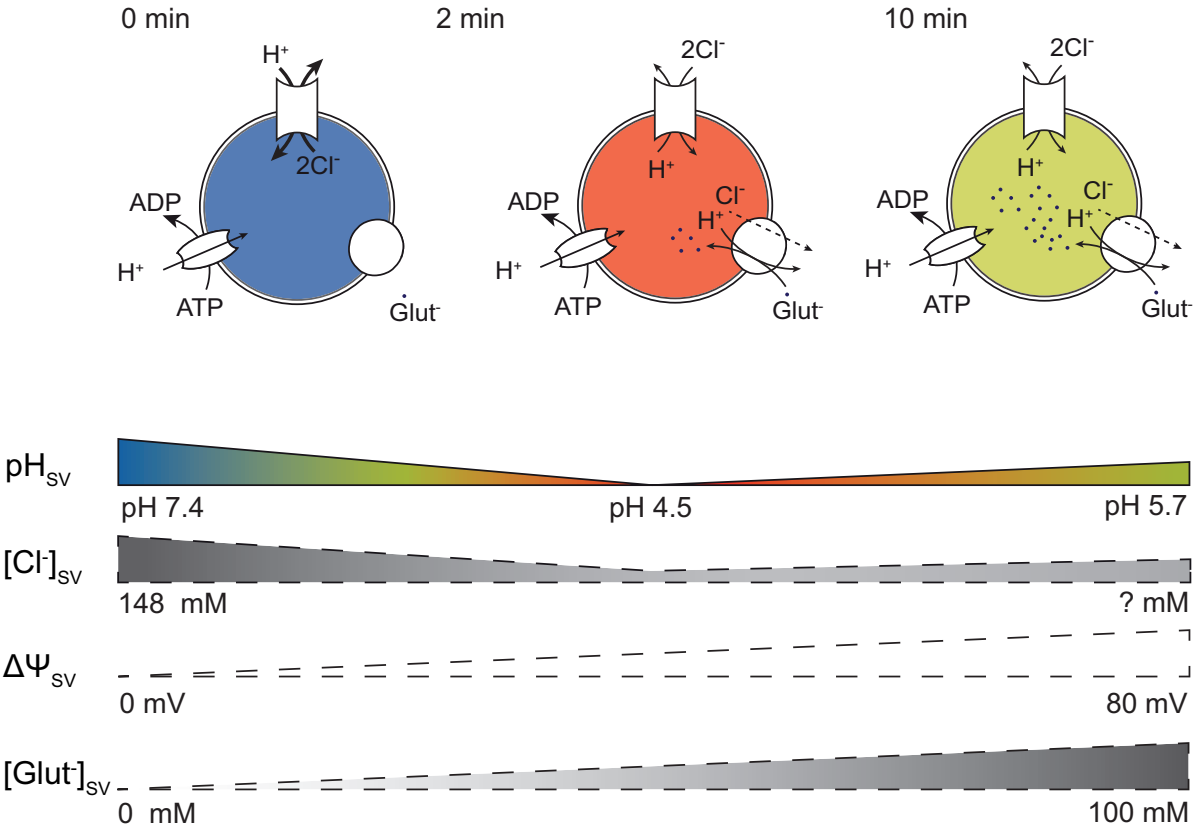

Figure 4.1: **Model of synaptic vesicle acidification.** Luminal pH is indicated by a blue over green to red scale. Glutamate neurotransmitter molecules are symbolized by small dots. (0 min) In presence of high $[Cl^-]_{SV}$, efflux of Cl^- facilitates acidification by exchange to cytosolic H^+ mediated by ClC-3. The thus generated $\Delta\psi$ promotes glutamate loading by activation of the acid-dependent VGLUT. (2 min) As $[Cl^-]_{SV}$ gradually decreases, glutamate import is driven by $\Delta\psi$ generated by the V-ATPase. (10 min) The synaptic vesicle is fully loaded with glutamate and V-ATPase, ClC-3 and VGLUT1 transport activity is in a steady state. Time-course of pH_{SV}, $[Cl^-]_{SV}$, $\Delta\psi$, and $[Glut^-]_{SV}$. A dotted border indicates assumptions based on literature.

Based on the results of this thesis a model for the regulation of synaptic vesicle acidification after stimulated endocytosis is proposed (Figure 4.1). Utilizing the ΔCl^- in freshly endocytosed synaptic vesicles ClC-3 quickly acidifies the synaptic vesicle lumen

together with the ATP-driven H^+-transport by the V-ATPase. A ClC-3-supported acidification reduces the ATP-consumption needed to fully acidify the synaptic vesicle lumen. Once peak acidification is reached 2 minutes after endocytosis, pH_{SV} slowly increases up to the resting pH of 5.7 the next 8 minutes. This increase in the pH_{SV} is probably coupled to VGLUT activity, because it is disrupted when VGLUT activity is blocked. Due to the $2Cl^-/H^+$ exchange by ClC-3, $[Cl^-]_{SV}$ is rapidly decreased. Considering that at one point the reversal potential of ClC-3 is reached, $[Cl^-]_{SV}$ will either kept at a stable level or – if transport direction of ClC-3 switches – Cl^- is imported to support the electrogenic transport of H^+ by the V-ATPase. During this process $\Delta\psi$ is formed and glutamate is imported by VGLUT1. However, it is still unclear to which extent and at which time-scale maximum $[Glut^-]_{SV}$ is reached. In clathrin-coated synaptic vesicles, when the V-ATPase is blocked [183], this model still allows a fast acidification and formation of $\Delta\psi$ allowing fast glutamate loading into freshly endocytosed synaptic vesicles.

These findings and the proposed mechanism are in contradiction with the prevalent view that ClC-3 supports efficient acidification of synaptic vesicles by providing a Cl^- conductance to counterbalance the accumulation of positive charged H^+ by the V-ATPase [34]. For ClC-5 it already has been shown that it can directly acidify endosomes [76], but for ClC-3 it only has been postulated theoretically [34, 59]. The data presented here are the first to directly demonstrate the ability of ClC-3 to acidify the synaptic vesicle lumen independently of V-ATPase activity by utilization of ΔCl. This would provide a fast and ATP-independent pathway of synaptic vesicle acidification. Together with the recent identification of a H^+-dependent Cl^- conductance in VGLUT1 [58, 59], which could overtake the shunt-function for regulation of V-ATPase activity, a comprehensive insight into pH_{SV} regulation is given confirming the importance of $[Cl^-]_{SV}$.

Chapter 5

Conclusion

5.1 Importance of Luminal [Cl^-]

The importance of the luminal Cl^- concentration, as a modulator of synaptic vesicle acidification, was identified in this thesis. It raises the question, how variations in extra- and intracellular [Cl^-] impact the glutamatergic quantal size and thus synaptic plasticity. The intracellular Cl^- was thought to be passively distributed or distributed according to its electrochemical potential equilibrium [186, 187], across the membrane as a side-effect of the regulation of intracellular Na^+, K^+. In neurons $[Cl^-]_{cytosol}$ was measured in a wide range from from 6 - 80 mM [44, 45, 46, 47, 48, 49, 50]. In a theoretical analysis from Delpire and Staley [188] an explanation for the disparate distribution of $[Cl^-]_{cytosol}$ has been delivered. They propose that the formation of the transmembrane Cl^- gradient is influenced by the fixed 'Donnan' charges inside and outside the cell, free and unbound water, and the water transport through the co-transporters. These factors greatly affect the reversal potential for Cl^-.

In inhibitory neurotransmission ligand-gated Cl^- channels, such as GABA receptor-type A ($GABA_A$ receptor) are activated to counteract the action of glutamate receptors thus suppressing excitatory neurotransmission. Hereby, it was found out that Cl^- must be actively accumulated because peripheral neurons and immature CNS neurons accumulate Cl^- above the equilibrium potentials, while in mature CNS neurons the Cl^- concentration is below the thermodynamic equilibrium potential [189, 190, 191]. Cytosolic [Cl^-] may be

regulated by the Na^+-K^+-$2Cl^-$ cotransporter NKCC1 [192, 46, 47], the contribution of KCC2 as an export pathway for Cl^- is unclear [188]. It is known that during maturation $[Cl^-]_{cytosol}$ in neurons decreases to facilitate inhibitory synaptic transmission [193, 50].

Furthermore, for regulation of synaptic vesicle acidification the luminal concentration of Cl^- is also crucial. Because the ionic composition of synaptic vesicles after endocytosis resembles the composition of the extracellular space modulations in this area could have tremendous effects on the quantal size of synaptic transmission. It was recently shown that glial cells actively accumulate Cl^- [194] but if the Cl^- concentration in the synaptic cleft is stable or underlying fluctuations is not investigated yet. It is known that due to synaptic activity $[K^+]$ and $[Cl^-]$ in the synaptic cleft increases about 7 mM measured in the sensorimotor cortex of cats [195]. However, from these data the authors proposed an increase in the osmolarity up to 30 mM which could indeed change the reversal potential for Cl^- as described before, thus leading to a concentration change of Cl^- in the cytosol. Thus, it is now important to adequately determine the cytosolic and extracellular Cl^- concentration during physiological relevant activity.

5.2 Determination of Luminal $[Cl^-]$

To further investigate the role of luminal Cl^- it is first necessary to determine the luminal $[Cl^-]_{SV}$. It is further important to determine $[Cl^-]_{SV}$ in living neurons, because, as already described before, the use of purified synaptic vesicles might change the luminal $[Cl^-]$. Second, the correct targeting of the fluorescence bio-sensor is important to reduce recordings from non-synaptic vesicles. For this, genetically-encoded fluorescent chloride sensors can be used which are fused to a synaptic-vesicle membrane protein e.g. SybII and synaptophysin, respectively. As an alternative, organic dyes are useful candidates, too. However, these dyes have the disadvantage that their subcellular localization is diffusion dependent and not limited to specific cellular compartments. One possibility here is to use membrane-impermeable chloride sensitive quinolinium dyes (MEQ) which can be loaded via endocytosis of recycled synaptic vesicles. Both sensor types have been extensively used in intensity-based fluorescent chloride imaging, whereas the fluorescence intensity decay is almost solely used with organic fluorescent dyes [196]. The currently available fluorescent protein based chloride sensors are not suitable for absolute or relative concentration measurements based on FLIM and the FRET-based sensors have limited dynamic range. Furthermore, all Cl-sensitive fluorescent proteins have in common that their Cl^- affinity is highly pH dependent. Quinolinium dyes [197], whose pH-sensitivity is

based on collisional quenching are well suited Cl-sensors, especially when used for FLIM. When collided with Cl^- the excited fluorophore returns back to the S_0 state without emission of light, thus the lifetime of MEQ is inversely proportional to the chloride concentration. Due to this property, they further have a much higher dynamic range compared to fluorescent protein based Cl^--sensors. Several variants of quinolinium dyes exist, the membrane permeable MQAE has already been used in FLIM experiments [194, 48, 196] but not the membrane-impermeable variant MEQ. The unique properties of MEQ, will allow precise determination of $[Cl^-]_{SV}$.

Once $[Cl^-]_{SV}$ is known at different stages of synaptic vesicle cycling, the corresponding $[Cl^-]_{cytosol}$ is important. Most measurements of $[Cl^-]_{cytosol}$ focused on the soma, because they are easier to record, especially when organic dyes are used. Together with reference staining of synaptic boutons, MQAE loaded hippocampal neurons would allow to record $[Cl^-]_{cytosol}$ of the synaptic bouton.

5.3 A Quantitative Model of Synaptic Vesicle Acidification

The experimental results in this thesis demonstrate a possible regulation of synaptic vesicle acidification rather by the utilization of the ΔCl^- then by V-ATPase activity. The transport direction of ClC-3 and the H^+-transport by V-ATPase activity strongly depends on the $\Delta\psi$. Currently, simultaneous measurements of both pH_{SV} and $\Delta\psi$ are very challenging and thus the model of synaptic vesicle ion regulation has unknown quantities taken into account. Therefore, on the basis of a mathematical model of lysosomal pH regulation from Ishida et al., 2013 ([198]) a quantitative model describing the synaptic vesicle ion regulation would enlighten the acidification and glutamate loading of synaptic vesicles. The model has to be modified by incorporating a description of the VGLUT1 transporter, and tuning other synaptic-vesicle specific parameters. The description of the VGLTU1 transporter, however, is complicated by the diversity of ionic and anionic interactions of this transporter as well as the lack of a sufficient transport model. Whether glutamate loading is coupled stoichiometrically to H^+ transport or not, and whether Cl^- is transported via a channel or by a transport process is also not known yet.

The findings in this thesis thus provide a new insight into the importance of the luminal $[Cl^-]$ and the Cl^-/H^+ exchanger ClC-3 in the regulation of pH_{SV} after endocytosis of recycled synaptic vesicles. Given the importance of this topic, future advances in this

active field are expected to contribute to a better comprehension of neurotransmitter loading into synaptic vesicles and the importance of luminal Cl^-.

Appendix A

Supplements

A.1 Effect of Acid Quench on $pH_{cytosol}$

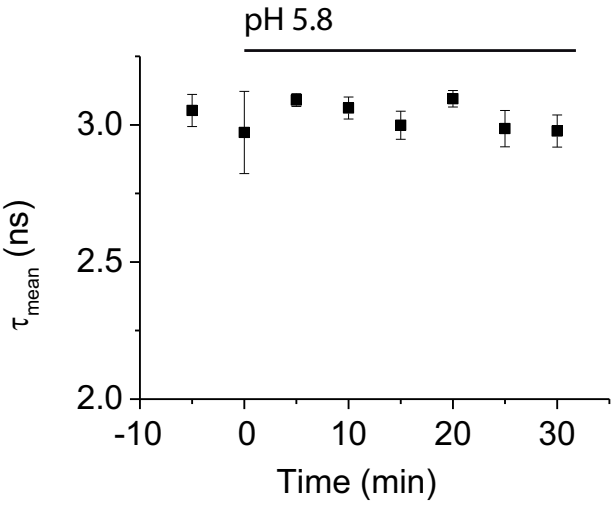

Figure A.1: **Effect of acid quench on $pH_{cytosol}$ in HEK cells.** HEK293 cells expressing Cerulean in the cytosol were perfused with extracellular solution pH 5.8 for up to 30 minutes. Every 5 minutes the pH was determined. Data are given as mean values ± SD.

A.2 Effect of RB on Purified Cerulean

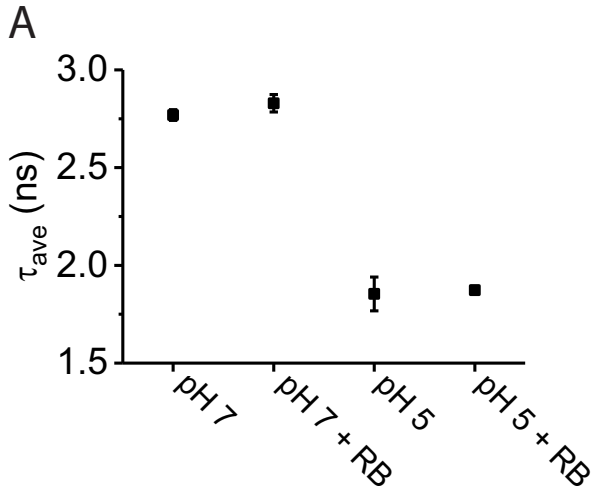

Figure A.2: **Rose Bengal and DL-Histidine do not interfere with Ceruleans fluorescence lifetime** The fluorescence lifetime of purified Cerulean diluted to a final concentration of 2.3 μM in pH 7 and pH 5 citric acid - Na_2HPO_4 buffer solution was measured with and without 100 nM Rose Bengal and 10 mM DL-Histidine. All data are mean ± SD.

A.3 Upregulation of ClC-5 in *Clcn3*$^{-/-}$ neurons

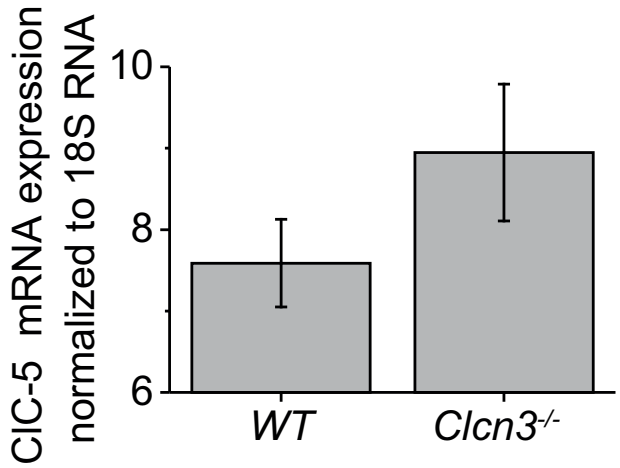

Figure A.3: **Upregulation of ClC5 in *Clcn3*$^{-/-}$ neurons** All data are mean ± SD.

A.4 Chloride Dependency of Cerulean's τ_{mean}

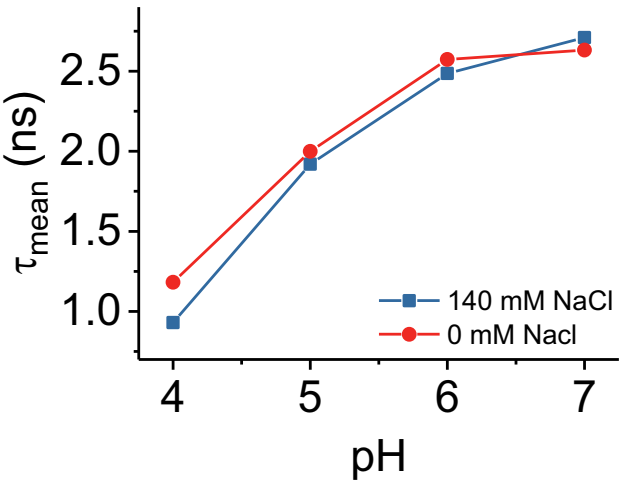

Figure A.4: **Chloride dependency of Cerulean's τ_{mean}.** All data are mean.

Photophysical properties of purified Cerulean were determined either in salt-free buffer (20 mM Na2HPO4/citric acid, pH set from 7 to 4 with NaOH) or supplemented with 140 mM NaCl (Figure A.4). All samples were adjusted to a maximum absorption of 0.1 (λ_{abs} = 433 nm). Absorption spectra were measured using a UV-2450 absorption spectrophotometer (Shimadzu Europe GmbH, Duisburg, Germany). Fluorescence spectra were recorded using a Quanta-Master 40 fluorescence spectrophotometer (Photon Technology International, Birmingham, NJ, USA). Time-resolved detection of the fluorescence decay of Cerulean was performed with a Fluotime100 fluorescence spectrophotometer (Picoquant, Berlin, Germany) based on a picoHarp300 unit by using a pulsed diode laser (LDH-C 440, Picoquant; emission 440 nm; pulse width: 40 ps; used repetition frequency: 20 Mhz) as excitation source. Fluorescence decay curves as a function of time (t) were measured by time-correlated single-photon counting that enables the determination of fluorescence decay components with fluorescence lifetimes greater than 100 ps [4]. Decay curves were analyzed by iterative reconvolution of the instrument response function, IRF(t), with an exponential model function, M(t), using the FluoFit software (version 4.5.3.0; Picoquant) applying equation (A.1) and (A.2):

$$I(t) = IRF(t) * M(t) \tag{A.1}$$

$$(t) = \sum_{n}^{i=1} \left[a_i * exp\left(\frac{-t}{\tau_i}\right) \right] \tag{A.2}$$

τ_{i} are the characteristic lifetimes and $\mathrm{a_i}$ are the respective intensities. The average fluorescence lifetime, $\tau_{\mathrm{fl.ave.}}$, was calculated using equation (A.3):

$$\tau_{fl.ave} = \frac{\sum_{i=1}^{n} a_i * \tau_i}{\sum_{i=1}^{n} a_i} \tag{A.3}$$

Bibliography

[1] Per Brodal. *The central nervous system*. Oxford University Press, New York, NY, United States of America, 5th edition edition, 2016.

[2] Bernhard Katz. The Release of Neural Transmitter Substances. *Liverpool University Press*, 1969.

[3] Thomas C. Südhof. The Synaptic Vesicle Cycle. *Annu. Rev. Neurosci.*, 27:509–547, 2004.

[4] Silvio O. Rizzoli and William J. Betz. Synaptic vesicle pools. *Nat Rev Neurosci*, 6(1):57–69, 2005.

[5] Annette Denker and Silvio O. Rizzoli. Synaptic Vesicle Pools: An Update. *Frontiers in Synaptic Neuroscience*, 2, 2010.

[6] Zhaolin Hua, Sergio Leal-Ortiz, Sarah M. Foss, Clarissa L. Waites, Craig C. Garner, Susan M. Voglmaier, and Robert H. Edwards. V-SNARE Composition Distinguishes Synaptic Vesicle Pools. *Neuron*, 71(3):474–487, 2011.

[7] Taro Ishikawa, Yoshinori Sahara, and Tomoyuki Takahashi. A Single Packet of Transmitter Does Not Saturate Postsynaptic Glutamate Receptors. *Neuron*, 34(4):613–621, 2002.

[8] Rodney L. Parsons, Michelle A. Calupca, Laura A. Merriam, and Chris Prior. Empty Synaptic Vesicles Recycle and Undergo Exocytosis at Vesamicol-Treated Motor Nerve Terminals. *Journal of Neurophysiology*, 81(6):2696–2700, 1999.

[9] Qiang Zhou, Carl C. H. Petersen, and Roger A. Nicoll. Effects of reduced vesicular filling on synaptic transmission in rat hippocampal neurones. *The Journal of Physiology*, 525(1):195–206, 2000.

[10] Nathan R. Wilson, Jiansheng Kang, Emily V. Hueske, Tony Leung, Helene Varoqui, Jonathan G. Murnick, Jeffrey D. Erickson, and Guosong Liu. Presynaptic Regulation of Quantal Size by the Vesicular Glutamate Transporter VGLUT1. *Journal of Neuroscience*, 25(26):6221–6234, 2005.

[11] Sonja M. Wojcik, Shutaro Katsurabayashi, Isabelle Guillemin, Eckhard Friauf, Christian Rosenmund, Nils Brose, and Jeong-Seop Rhee. A Shared Vesicular Carrier Allows Synaptic Corelease of GABA and Glycine. *Neuron*, 50(4):575–587, 2006.

[12] Xin-Sheng Wu, Lei Xue, Raja Mohan, Kenneth Paradiso, Kevin D. Gillis, and Ling-Gang Wu. The Origin of Quantal Size Variation: Vesicular Glutamate Concentration Plays a Significant Role. *Journal of Neuroscience*, 27(11):3046–3056, 2007.

[13] Germaine Y. Goh, Hai Huang, Julie Ullman, Lars Borre, Thomas S. Hnasko, Laurence O. Trussell, and Robert H. Edwards. Presynaptic regulation of quantal size: K^+/H^+ exchange stimulates vesicular glutamate transport. *Nature Neuroscience*, 14(10):1285–1292, 2011.

[14] Lu Wang, Peng Tu, Laurine Bonet, Karin R. Aubrey, and Stéphane Supplisson. Cytosolic Transmitter Concentration Regulates Vesicle Cycling at Hippocampal GABAergic Terminals. *Neuron*, 80(1):143–158, 2013.

[15] Peter M. Burger, Ehrenfried Mehl, Patricia L. Cameron, Peter R. Maycox, Marion Baumert, Friedrich Lottspeich, Pietro De Camilli, and Reinhard Jahn. Synaptic vesicles immunoisolated from rat cerebral cortex contain high levels of glutamate. *Neuron*, 3(6):715–720, 1989.

[16] Nora Riveros, Jenny Fiedler, N. Lagos, C. Munoz, and F. Orrego. Glutamate in rat brain cortex synaptic vesicles: Influence of the vesicle isolation procedure. *Brain Research*, 386(1):405–408, 1986.

[17] Gero Miesenböck, Dino A. De Angelis, and James E. Rothman. Visualizing secretion and synaptic transmission with pH-sensitive green fluorescent proteins. *Nature*, 394(6689):192–195, 1998.

[18] Y. Egashira, M. Takase, and S. Takamori. Monitoring of Vacuolar-Type H+ ATPase-Mediated Proton Influx into Synaptic Vesicles. *Journal of Neuroscience*, 35(8):3701–3710, 2015.

[19] Zohreh Farsi, Julia Preobraschenski, Geert van den Bogaart, Dietmar Riedel, Reinhard Jahn, and Andrew Woehler. Single-vesicle imaging reveals different transport mechanisms between glutamatergic and GABAergic vesicles. *Science*, 351(6276):981–984, 2016.

[20] R. G. Johnson and A. Scarpa. Protonmotive force and catecholamine transport in isolated chromaffin granules. *Journal of Biological Chemistry*, 254(10):3750–3760, 1979.

[21] Peter M. Burger, Johannes Hell, Ehrenfried Mehl, Cornelius Krasel, Friedrich Lottspeich, and Reinhard Jahn. Gaba and glycine in synaptic vesicles: Storage and transport characteristics. *Neuron*, 7(2):287–293, 1991.

[22] J. W. Hell, P. R. Maycox, and R. Jahn. Energy dependence and functional reconstitution of the gamma-aminobutyric acid carrier from synaptic vesicles. *Journal of Biological Chemistry*, 265(4):2111–2117, 1990.

[23] Yoshihiro Egashira, Miki Takase, Shoji Watanabe, Junji Ishida, Akiyoshi Fukamizu, Ryosuke Kaneko, Yuchio Yanagawa, and Shigeo Takamori. Unique pH dynamics in GABAergic synaptic vesicles illuminates the mechanism and kinetics of GABA loading. *Proceedings of the National Academy of Sciences*, page 201604527, 2016.

[24] R. G. Johnson, S. E. Carty, and A. Scarpa. Proton: Substrate stoichiometries during active transport of biogenic amines in chromaffin ghosts. *Journal of Biological Chemistry*, 256(11):5773–5780, 1981.

[25] J. Knoth, M. Zallakian, and D. Njus. Stoichiometry of H+-linked dopamine transport in chromaffin granule ghosts. *Biochemistry*, 20(23):6625–6629, 1981.

[26] M. L. Nguyen, G. D. Cox, and S. M. Parsons. Kinetic parameters for the vesicular acetylcholine transporter: Two protons are exchanged for one acetylcholine. *Biochemistry*, 37(38):13400–13410, 1998.

[27] Liqun Bai, Hua Xu, James F. Collins, and Fayez K. Ghishan. Molecular and Functional Analysis of a Novel Neuronal Vesicular Glutamate Transporter. *Journal of Biological Chemistry*, 276(39):36764–36769, 2001.

[28] Elizabeth E. Bellocchio, Richard J. Reimer, Robert T. Fremeau, and Robert H. Edwards. Uptake of Glutamate into Synaptic Vesicles by an Inorganic Phosphate Transporter. *Science*, 289(5481):957–960, 2000.

[29] Robert T Fremeau, Matthew D Troyer, Ingrid Pahner, Gro Owren Nygaard, Cindy H Tran, Richard J Reimer, Elizabeth E Bellocchio, Doris Fortin, Jon Storm-Mathisen, and Robert H Edwards. The Expression of Vesicular Glutamate Transporters Defines Two Classes of Excitatory Synapse. *Neuron*, 31(2):247–260, 2001.

[30] Etienne Herzog, Gian Carlo Bellenchi, Christelle Gras, Véronique Bernard, Philippe Ravassard, Cécile Bedet, Bruno Gasnier, Bruno Giros, and Salah El Mestikawy. The Existence of a Second Vesicular Glutamate Transporter Specifies Subpopulations of Glutamatergic Neurons. *Journal of Neuroscience*, 21(22):RC181–RC181, 2001.

[31] Martin K.-H. Schäfer, Hélène Varoqui, Norah Defamie, Eberhard Weihe, and Jeffrey D. Erickson. Molecular Cloning and Functional Identification of Mouse Vesicular Glutamate Transporter 3 and Its Expression in Subsets of Novel Excitatory Neurons. *Journal of Biological Chemistry*, 277(52):50734–50748, 2002.

[32] Shigeo Takamori, Pari Malherbe, Clemens Broger, and Reinhard Jahn. Molecular cloning and functional characterization of human vesicular glutamate transporter 3. *EMBO reports*, 3(8):798–803, 2002.

[33] Herman Wolosker, Diogo Souza, and Leopoldo Meis. Regulation of Glutamate Transport into Synaptic Vesicles by Chloride and Proton Gradient. *Journal of Biological Chemistry*, 271(20):11726–11731, 1996.

[34] Zohreh Farsi, Reinhard Jahn, and Andrew Woehler. Proton electrochemical gradient: Driving and regulating neurotransmitter uptake. *BioEssays*, 39(5):1600240–1600240, 2017.

[35] Michael Grabe and George Oster. Regulation of Organelle Acidity. *J. Gen. Physiol.*, 117(4):329–344, 2001.

[36] S. L. Rybak, F. Lanni, and R. F. Murphy. Theoretical considerations on the role of membrane potential in the regulation of endosomal pH. *Biophysical Journal*, 73(2):674–687, 1997.

[37] Yoshinori Moriyama, Masatomo Maeda, and Masamitsu Futai. Involvement of a non-proton pump factor (possibly Donnan-type equilibrium) in maintenance of an acidic pH in lysosomes. *FEBS Lett.*, 302(1):18–20, 1992.

[38] Y. Moriyama and N. Nelson. The purified ATPase from chromaffin granule membranes is an anion-dependent proton pump. *Journal of Biological Chemistry*, 262(19):9175–9180, 1987.

[39] Feng-Yi Wan, Yi-Nan Wang, and Guo-Jiang Zhang. Influence of the physical states of membrane surface area and center area on lysosomal proton permeability. *Archives of Biochemistry and Biophysics*, 404(2):285–292, 2002.

[40] L. Bianchini and J. Pousségur. Molecular structure and regulation of vertebrate Na+/H+ exchangers. *J. Exp. Biol.*, 196(1):337–345, 1994.

[41] Norihiro Nakamura, Shingo Tanaka, Yoshinori Teko, Keiji Mitsui, and Hiroshi Kanazawa. Four Na+/H+ Exchanger Isoforms Are Distributed to Golgi and Post-Golgi Compartments and Are Involved in Organelle pH Regulation. *J. Biol. Chem.*, 280(2):1561–1572, 2005.

[42] Julia Preobraschenski, Johannes-Friedrich Zander, Toshiharu Suzuki, Gudrun Ahnert-Hilger, and Reinhard Jahn. Vesicular Glutamate Transporters Use Flexible Anion and Cation Binding Sites for Efficient Accumulation of Neurotransmitter. *Neuron*, 84(6):1287–1301, 2014.

[43] Nina Milosavljevic, Michaël Monet, Isabelle Léna, Frédéric Brau, Sandra Lacas-Gervais, Sylvain Feliciangeli, Laurent Counillon, and Mallorie Poët. The Intracellular Na+/H+ Exchanger NHE7 Effects a Na+-Coupled, but Not K+-Coupled Proton-Loading Mechanism in Endocytosis. *Cell Reports*, 7(3):689–696, 2014.

[44] U. Misgeld, R. A. Deisz, H. U. Dodt, and H. D. Lux. The role of chloride transport in postsynaptic inhibition of hippocampal neurons. *Science (New York, N.Y.)*, 232(4756):1413–1415, 1986.

[45] S. M. Thompson, R. A. Deisz, and D. A. Prince. Relative contributions of passive equilibrium and active transport to the distribution of chloride in mammalian cortical neurons. *Journal of Neurophysiology*, 60(1):105–124, 1988.

[46] D. F. Owens, L. H. Boyce, M. B. Davis, and A. R. Kriegstein. Excitatory GABA responses in embryonic and neonatal cortical slices demonstrated by gramicidin

perforated-patch recordings and calcium imaging. *The Journal of Neuroscience: The Official Journal of the Society for Neuroscience*, 16(20):6414–6423, 1996.

[47] I. Ehrlich, S. Lohrke, and E. Friauf. Shift from depolarizing to hyperpolarizing glycine action in rat auditory neurones is due to age-dependent Cl- regulation. *The Journal of Physiology*, 520 Pt 1:121–137, 1999.

[48] Verena Untiet, Lisa M. Moeller, Ximena Ibarra-Soria, Gabriela Sánchez-Andrade, Miriam Stricker, Eva M. Neuhaus, Darren W. Logan, Thomas Gensch, and Marc Spehr. Elevated Cytosolic Cl- Concentrations in Dendritic Knobs of Mouse Vomeronasal Sensory Neurons. *Chem Senses*, 41(8):669–676, 2016.

[49] Hiroshi Kaneko, Ilva Putzier, Stephan Frings, U. Benjamin Kaupp, and Thomas Gensch. Chloride accumulation in mammalian olfactory sensory neurons. *J. Neurosci.*, 24(36):7931–7938, 2004.

[50] Daniel Gilbert, Christina Franjic-Würtz, Katharina Funk, Thomas Gensch, Stephan Frings, and Frank Möhrlen. Differential maturation of chloride homeostasis in primary afferent neurons of the somatosensory system. *Int. J. Dev. Neurosci.*, 25(7):479–489, 2007.

[51] P. R. Maycox, T. Deckwerth, J. W. Hell, and R. Jahn. Glutamate uptake by brain synaptic vesicles. Energy dependence of transport and functional reconstitution in proteoliposomes. *Journal of Biological Chemistry*, 263(30):15423–15428, 1988.

[52] J. S. Tabb, P. E. Kish, R. Van Dyke, and T. Ueda. Glutamate transport into synaptic vesicles. Roles of membrane potential, pH gradient, and intravesicular pH. *The Journal of Biological Chemistry*, 267(22):15412–15418, 1992.

[53] S. Cidon and T. S. Sihra. Characterization of a H+-ATPase in rat brain synaptic vesicles. Coupling to L-glutamate transport. *Journal of Biological Chemistry*, 264(14):8281–8288, 1989.

[54] Robert H. Edwards. The Neurotransmitter Cycle and Quantal Size. *Neuron*, 55(6):835–858, 2007.

[55] X. S. Xie, B. P. Crider, and D. K. Stone. Isolation and reconstitution of the chloride transporter of clathrin-coated vesicles. *J. Biol. Chem.*, 264(32):18870–18873, 1989.

[56] Vladimir Riazanski, Ludmila V. Deriy, Pavel D. Shevchenko, Brandy Le, Erwin A. Gomez, and Deborah J. Nelson. Presynaptic CLC-3 determines quantal size of

inhibitory transmission in the hippocampus. *Nature Neuroscience*, 14(4):487–494, 2011.

[57] Raul E. Guzman, Alexi K. Alekov, Mikhail Filippov, Jan Hegermann, and Christoph Fahlke. Involvement of ClC-3 chloride/proton exchangers in controlling glutamatergic synaptic strength in cultured hippocampal neurons. *Frontiers in Cellular Neuroscience*, 8, 2014.

[58] Jacob Eriksen, Roger Chang, Matt McGregor, Katlin Silm, Toshiharu Suzuki, and Robert H. Edwards. Protons Regulate Vesicular Glutamate Transporters through an Allosteric Mechanism. *Neuron*, 90(4):768 – 780, 2016.

[59] Magalie Martineau, Raul E. Guzman, Christoph Fahlke, and Jürgen Klingauf. VGLUT1 functions as a glutamate/proton exchanger with chloride channel activity in hippocampal glutamatergic synapses. *Nat. Commun.*, 8(1):2279, 2017.

[60] Julia Preobraschenski, Cyril Cheret, Marcelo Ganzella, Johannes Friedrich Zander, Karin Richter, Stephan Schenck, Reinhard Jahn, and Gudrun Ahnert-Hilger. Dual and Direction-Selective Mechanisms of Phosphate Transport by the Vesicular Glutamate Transporter. *Cell Reports*, 23(2):535–545, 2018.

[61] Thomas J. Jentsch. CLC Chloride Channels and Transporters: From Genes to Protein Structure, Pathology and Physiology. *Critical Reviews in Biochemistry and Molecular Biology*, 43(1):3–36, 2008.

[62] Sandra M. Stobrawa, Tilman Breiderhoff, Shigeo Takamori, Dominique Engel, Michaela Schweizer, Anselm A. Zdebik, Michael R. Bösl, Klaus Ruether, Holger Jahn, Andreas Draguhn, Reinhard Jahn, and Thomas J. Jentsch. Disruption of ClC-3, a Chloride Channel Expressed on Synaptic Vesicles, Leads to a Loss of the Hippocampus. *Neuron*, 29(1):185–196, 2001.

[63] Mads Grønborg, Nathan J. Pavlos, Irene Brunk, John J. E. Chua, Agnieszka Münster-Wandowski, Dietmar Riedel, Gudrun Ahnert-Hilger, Henning Urlaub, and Reinhard Jahn. Quantitative Comparison of Glutamatergic and GABAergic Synaptic Vesicles Unveils Selectivity for Few Proteins Including MAL2, a Novel Synaptic Vesicle Protein. *Journal of Neuroscience*, 30(1):2–12, 2010.

[64] Gabriel Stölting, Martin Fischer, and Christoph Fahlke. CLC channel function and dysfunction in health and disease. *Front. Physiol.*, 5, 2014.

[65] Raimund Dutzler, Ernest B. Campbell, Martine Cadene, Brian T. Chait, and Roderick MacKinnon. X-ray structure of a ClC chloride channel at 3.0 Å reveals the molecular basis of anion selectivity. *Nature*, 415(6869), 2002.

[66] Raimund Dutzler, Ernest B. Campbell, and Roderick MacKinnon. Gating the Selectivity Filter in ClC Chloride Channels. *Science*, 300(5616):108–112, 2003.

[67] Séverine Lobet and Raimund Dutzler. Ion-binding properties of the ClC chloride selectivity filter. *The EMBO Journal*, 25(1):24–33, 2006.

[68] Raul E. Guzman, Erick Miranda-Laferte, Arne Franzen, and Christoph Fahlke. Neuronal ClC-3 Splice Variants Differ in Subcellular Localizations, but Mediate Identical Transport Functions. *Journal of Biological Chemistry*, 290(43):25851–25862, 2015.

[69] Raul E. Guzman, Stefanie Bungert-Plümke, Arne Franzen, and Christoph Fahlke. Preferential Association with ClC-3 Permits Sorting of ClC-4 into Endosomal Compartments. *J. Biol. Chem.*, page jbc.M117.801951, 2017.

[70] Raul E. Guzman, Matthias Grieschat, Christoph Fahlke, and Alexi K. Alekov. ClC-3 Is an Intracellular Chloride/Proton Exchanger with Large Voltage-Dependent Nonlinear Capacitance. *ACS Chemical Neuroscience*, 4(6):994–1003, 2013.

[71] Xinhua Li, Ting Wang, Zhifang Zhao, and Steven A. Weinman. The ClC-3 chloride channel promotes acidification of lysosomes in CHO-K1 and Huh-7 cells. *Am. J. Physiol., Cell Physiol.*, 282(6):C1483–1491, 2002.

[72] Alessio Accardi, Ludmila Kolmakova-Partensky, Carole Williams, and Christopher Miller. Ionic Currents Mediated by a Prokaryotic Homologue of CLC Cl- Channels. *The Journal of General Physiology*, 123(2):109–119, 2004.

[73] Alessandra Picollo, Mattia Malvezzi, and Alessio Accardi. Proton block of the CLC-5 Cl-/H+ exchanger. *The Journal of General Physiology*, 135(6):653–659, 2010.

[74] Mariko Hara-Chikuma, Baoxue Yang, N. D. Sonawane, Sei Sasaki, Shinichi Uchida, and A. S. Verkman. ClC-3 Chloride Channels Facilitate Endosomal Acidification and Chloride Accumulation. *J. Biol. Chem.*, 280(2):1241–1247, 2005.

[75] Olaf Scheel, Anselm A. Zdebik, Stéphane Lourdel, and Thomas J. Jentsch. Voltage-dependent electrogenic chloride/proton exchange by endosomal CLC proteins. *Nature*, 436(7049):424–427, 2005.

[76] Andrew J Smith and Jonathan D Lippiat. Direct endosomal acidification by the outwardly rectifying CLC-5 Cl-/H+ exchanger. *J Physiol*, 588(Pt 12):2033–2045, 2010.

[77] Yunfeng Hua, Andrew Woehler, Martin Kahms, Volker Haucke, Erwin Neher, and Jürgen Klingauf. Blocking Endocytosis Enhances Short-Term Synaptic Depression under Conditions of Normal Availability of Vesicles. *Neuron*, 80(2):343–349, 2013.

[78] Susan M. Voglmaier, Kaiwen Kam, Hua Yang, Doris L. Fortin, Zhaolin Hua, Roger A. Nicoll, and Robert H. Edwards. Distinct Endocytic Pathways Control the Rate and Extent of Synaptic Vesicle Protein Recycling. *Neuron*, 51(1):71–84, 2006.

[79] Linda W. Dickerson, Daniel J. Bonthius, Brian C. Schutte, Baoli Yang, Thomas J. Barna, Melissa C. Bailey, Keith Nehrke, Roger A. Williamson, and Fred S. Lamb. Altered GABAergic function accompanies hippocampal degeneration in mice lacking ClC-3 voltage-gated chloride channels. *Brain Research*, 958(2):227–250, 2002.

[80] Momono Yoshikawa, Shinichi Uchida, Junji Ezaki, Tatemitsu Rai, Atsushi Hayama, Katsuki Kobayashi, Yujiro Kida, Masaki Noda, Masato Koike, Yasuo Uchiyama, Fumiaki Marumo, Eiki Kominami, and Sei Sasaki. CLC-3 deficiency leads to phenotypes similar to human neuronal ceroid lipofuscinosis. *Genes to Cells*, 7(6):597–605, 2002.

[81] Yasuo Aihara, Hirosato Mashima, Hideaki Onda, Setsuji Hisano, Hidetoshi Kasuya, Tomokatsu Hori, Shirou Yamada, Hideaki Tomura, Yuichiro Yamada, Ituro Inoue, Itaru Kojima, and Jun Takeda. Molecular Cloning of a Novel Brain-Type Na+-Dependent Inorganic Phosphate Cotransporter. *Journal of Neurochemistry*, 74(6):2622–2625, 2000.

[82] B. Ni, P. R. Rosteck, N. S. Nadi, and S. M. Paul. Cloning and expression of a cDNA encoding a brain-specific Na(+)-dependent inorganic phosphate cotransporter. *Proceedings of the National Academy of Sciences of the United States of America*, 91(12):5607–5611, 1994.

[83] Shigeo Takamori, Jeong Seop Rhee, Christian Rosenmund, and Reinhard Jahn. Identification of a vesicular glutamate transporter that defines a glutamatergic phenotype in neurons. *Nature*, 407(6801):189–194, 2000.

[84] Hongbo He, Amanda H. Mahnke, Sukhjeevan Doyle, Ni Fan, Chih-Chieh Wang, Benjamin J. Hall, Ya-Ping Tang, Fiona M. Inglis, Chu Chen, and Jeffrey D. Erickson. Neurodevelopmental Role for VGLUT2 in Pyramidal Neuron Plasticity, Dendritic Refinement, and in Spatial Learning. *Journal of Neuroscience*, 32(45):15886–15901, 2012.

[85] Diederik Moechars, Matthew C. Weston, Sandra Leo, Zsuzsanna Callaerts-Vegh, Ilse Goris, Guy Daneels, A. Buist, M. Cik, P. Spek, Stefan Kass, Theo Meert, Rudi D'Hooge, Christian Rosenmund, and R. Mark Hampson. Vesicular Glutamate Transporter VGLUT2 Expression Levels Control Quantal Size and Neuropathic Pain. *Journal of Neuroscience*, 26(46):12055–12066, 2006.

[86] S. M. Wojcik, J. S. Rhee, E. Herzog, A. Sigler, R. Jahn, S. Takamori, N. Brose, and C. Rosenmund. An essential role for vesicular glutamate transporter 1 (VGLUT1) in postnatal development and control of quantal size. *Proceedings of the National Academy of Sciences of the United States of America*, 101(18):7158–7163, 2004.

[87] Robert T. Fremeau, Kaiwen Kam, Tayyaba Qureshi, Juliette Johnson, David R. Copenhagen, Jon Storm-Mathisen, Farrukh A. Chaudhry, Roger A. Nicoll, and Robert H. Edwards. Vesicular Glutamate Transporters 1 and 2 Target to Functionally Distinct Synaptic Release Sites. *Science*, 304(5678):1815–1819, 2004.

[88] R. M. Tordera, S. Totterdell, S. M. Wojcik, N. Brose, N. Elizalde, B. Lasheras, and J. Del Rio. Enhanced anxiety, depressive-like behaviour and impaired recognition memory in mice with reduced expression of the vesicular glutamate transporter 1 (VGLUT1). *European Journal of Neuroscience*, 25(1):281–290, 2007.

[89] Christelle Gras, Etienne Herzog, Gian Carlo Bellenchi, Véronique Bernard, Philippe Ravassard, Michel Pohl, Bruno Gasnier, Bruno Giros, and Salah El Mestikawy. A Third Vesicular Glutamate Transporter Expressed by Cholinergic and Serotoninergic Neurons. *Journal of Neuroscience*, 22(13):5442–5451, 2002.

[90] Robert T. Fremeau, Jonathon Burman, Tayyaba Qureshi, Cindy H. Tran, John Proctor, Juliette Johnson, Hui Zhang, David Sulzer, David R. Copenhagen, Jon

Storm-Mathisen, Richard J. Reimer, Farrukh A. Chaudhry, and Robert H. Edwards. The identification of vesicular glutamate transporter 3 suggests novel modes of signaling by glutamate. *Proceedings of the National Academy of Sciences*, 99(22):14488–14493, 2002.

[91] J. Hartinger and R. Jahn. An anion binding site that regulates the glutamate transporter of synaptic vesicles. *Journal of Biological Chemistry*, 268(31):23122–23127, 1993.

[92] Yoshinori Moriyama and Akitsugu Yamamoto. Vesicular L-Glutamate Transporter in Microvesicles from Bovine Pineal Glands DRIVING FORCE, MECHANISM OF CHLORIDE ANION ACTIVATION, AND SUBSTRATE SPECIFICITY. *Journal of Biological Chemistry*, 270(38):22314–22320, 1995.

[93] Narinobu Juge, Yumi Yoshida, Shouki Yatsushiro, Hiroshi Omote, and Yoshinori Moriyama. Vesicular Glutamate Transporter Contains Two Independent Transport Machineries. *Journal of Biological Chemistry*, 281(51):39499–39506, 2006.

[94] Narinobu Juge, John A. Gray, Hiroshi Omote, Takaaki Miyaji, Tsuyoshi Inoue, Chiaki Hara, Hisayuki Uneyama, Robert H. Edwards, Roger A. Nicoll, and Yoshinori Moriyama. Metabolic Control of Vesicular Glutamate Transport and Release. *Neuron*, 68(1):99–112, 2010.

[95] Stephan Schenck, Sonja M Wojcik, Nils Brose, and Shigeo Takamori. A chloride conductance in VGLUT1 underlies maximal glutamate loading into synaptic vesicles. *Nat. Neurosci.*, 12(2):156–162, 2009.

[96] Hiroshi Omote, Takaaki Miyaji, Narinobu Juge, and Yoshinori Moriyama. Vesicular Neurotransmitter Transporter: Bioenergetics and Regulation of Glutamate Transport. *Biochemistry*, 50(25):5558–5565, 2011.

[97] Sandra Winter, Irene Brunk, Diego J. Walther, Markus Höltje, Meisheng Jiang, Jens-Uwe Peter, Shigeo Takamori, Reinhard Jahn, Lutz Birnbaumer, and Gudrun Ahnert-Hilger. $G\alpha_{o2}$ Regulates Vesicular Glutamate Transporter Activity by Changing Its Chloride Dependence. *Journal of Neuroscience*, 25(18):4672–4680, 2005.

[98] Emmanuel N. Pothos, Eugene Mosharov, Kuo-Peing Liu, Wanda Setlik, Marian Haburcak, Giulia Baldini, Michael D. Gershon, Hadassah Tamir, and David Sulzer.

Stimulation-dependent regulation of the ph, volume and quantal size of bovine and rodent secretory vesicles. *The Journal of Physiology*, 542(2):453–476, 2002.

[99] Pradeep P. Atluri and Timothy A. Ryan. The Kinetics of Synaptic Vesicle Reacidification at Hippocampal Nerve Terminals. *The Journal of Neuroscience*, 26(8):2313–2320, 2006.

[100] J. Balaji and T. A. Ryan. Single-vesicle imaging reveals that synaptic vesicle exocytosis and endocytosis are coupled by a single stochastic mode. *Proceedings of the National Academy of Sciences*, 104(51):20576–20581, 2007.

[101] Björn Granseth and Leon Lagnado. The role of endocytosis in regulating the strength of hippocampal synapses. *The Journal of Physiology*, 586(24):5969–5982, 2008.

[102] Sung E. Kwon and Edwin R. Chapman. Synaptophysin Regulates the Kinetics of Synaptic Vesicle Endocytosis in Central Neurons. *Neuron*, 70(5):847–854, 2011.

[103] Sethuraman Sankaranarayanan and Timothy A. Ryan. Real-time measurements of vesicle-SNARE recycling in synapses of the central nervous system. *Nature cell biology*, 2(4):197–204, 2000.

[104] Tetsuya Hori and Tomoyuki Takahashi. Kinetics of Synaptic Vesicle Refilling with Neurotransmitter Glutamate. *Neuron*, 76(3):511–517, 2012.

[105] Timothy A. Ryan, Harald Reuter, Beverly Wendland, Felix E. Schweizer, Richard W. Tsien, and Stephen J. Smith. The kinetics of synaptic vesicle recycling measured at single presynaptic boutons. *Neuron*, 11(4):713–724, 1993.

[106] Sandrine Poëa-Guyon, Hélène Pasquier, Fabienne Mérola, Nicolas Morel, and Marie Erard. The enhanced cyan fluorescent protein: a sensitive pH sensor for fluorescence lifetime imaging. *Anal. Bioanal. Chem.*, 405(12):3983–3987, 2013.

[107] Aude Villoing, Myriam Ridhoir, Bertrand Cinquin, Marie Erard, Luis Alvarez, Germain Vallverdu, Pascal Pernot, Régis Grailhe, Fabienne Mérola, and Hélène Pasquier. Complex Fluorescence of the Cyan Fluorescent Protein: Comparisons with the H148d Variant and Consequences for Quantitative Cell Imaging. *Biochemistry*, 47(47):12483–12492, 2008.

[108] Asma Fredj, Hélène Pasquier, Isabelle Demachy, Gabriella Jonasson, Bernard Levy, Valérie Derrien, Yasmina Bousmah, Gallia Manoussaris, Frank Wien, Jacqueline

Ridard, Marie Erard, and Fabienne Merola. The Single T65s Mutation Generates Brighter Cyan Fluorescent Proteins with Increased Photostability and pH Insensitivity. *PLOS ONE*, 7(11):e49149, 2012.

[109] Ranieri Bizzarri, Caterina Arcangeli, Daniele Arosio, Fernanda Ricci, Paolo Faraci, Francesco Cardarelli, and Fabio Beltram. Development of a Novel GFP-based Ratiometric Excitation and Emission pH Indicator for Intracellular Studies. *Biophysical Journal*, 90(9):3300–3314, 2006.

[110] Mark A. Rizzo, Gerald H. Springer, Butch Granada, and David W. Piston. An improved cyan fluorescent protein variant useful for FRET. *Nature Biotechnology*, 22(4):445–449, 2004.

[111] Gert-Jan Kremers, Joachim Goedhart, Erik B. van Munster, and Theodorus W. J. Gadella. Cyan and Yellow Super Fluorescent Proteins with Improved Brightness, Protein Folding, and FRET Förster Radius. *Biochemistry*, 45(21):6570–6580, 2006.

[112] Wolfgang Becker. *Advanced Time-Correlated Single Photon Counting Techniques*. Number 81 in Springer Series in Chemical Physics. Springer, Berlin, Heidelberg, Berlin, Heidelberg, 2005 edition, 2005.

[113] Matthew John Mahon. pHluorin2: an enhanced, ratiometric, pH-sensitive green florescent protein. *Adv. Biosci. Biotechnol.*, 02(03):132–137, 2011.

[114] F. L. Graham and A. J. van der Eb. A new technique for the assay of infectivity of human adenovirus 5 DNA. *Virology*, 52(2):456–467, 1973.

[115] Barde Isabelle, Salmon Patrick, and Trono Didier. Production and Titration of Lentiviral Vectors. *Current Protocols in Neuroscience*, 53(1):4.21.1–4.21.23, 2010.

[116] Raul E. Guzman, Yvonne N. Schwarz, Jens Rettig, and Dieter Bruns. SNARE Force Synchronizes Synaptic Vesicle Fusion and Controls the Kinetics of Quantal Synaptic Transmission. *The Journal of Neuroscience*, 30(31):10272–10281, 2010.

[117] J. A. Thomas, R. N. Buchsbaum, A. Zimniak, and E. Racker. Intracellular pH measurements in Ehrlich ascites tumor cells utilizing spectroscopic probes generated in situ. *Biochemistry*, 18(11):2210–2218, 1979.

[118] Johannes Schindelin, Ignacio Arganda-Carreras, Erwin Frise, Verena Kaynig, Mark Longair, Tobias Pietzsch, Stephan Preibisch, Curtis Rueden, Stephan Saalfeld,

Benjamin Schmid, Jean-Yves Tinevez, Daniel James White, Volker Hartenstein, Kevin Eliceiri, Pavel Tomancak, and Albert Cardona. Fiji: An open-source platform for biological-image analysis. *Nature Methods*, 9(7):676–682, 2012.

[119] Benjamin G. Wilhelm, Sunit Mandad, Sven Truckenbrodt, Katharina Kröhnert, Christina Schäfer, Burkhard Rammner, Seong Joo Koo, Gala A. Claßen, Michael Krauss, Volker Haucke, Henning Urlaub, and Silvio O. Rizzoli. Composition of isolated synaptic boutons reveals the amounts of vesicle trafficking proteins. *Science*, 344(6187):1023–1028, 2014.

[120] M. Mukhtarov, L. Liguori, T. Waseem, F. Rocca, S. Buldakova, D. Arosio, and P. Bregestovski. Calibration and functional analysis of three genetically encoded Cl-/pH sensors. *Frontiers in Molecular Neuroscience*, 6, 2013.

[121] Yunfeng Hua, Raunak Sinha, Cora S Thiel, Roman Schmidt, Jana Hüve, Henrik Martens, Stefan W Hell, Alexander Egner, and Jurgen Klingauf. A readily retrievable pool of synaptic vesicles. *Nature Neuroscience*, 14(7):833–839, 2011.

[122] Henrik Martens, Matthew C. Weston, Jean-Luc Boulland, Mads Grønborg, Jens Grosche, Johannes Kacza, Anke Hoffmann, Michela Matteoli, Shigeo Takamori, Tibor Harkany, Farrukh A. Chaudhry, Christian Rosenmund, Christian Erck, Reinhard Jahn, and Wolfgang Härtig. Unique Luminal Localization of VGAT-C Terminus Allows for Selective Labeling of Active Cortical GABAergic Synapses. *The Journal of Neuroscience*, 28(49):13125–13131, 2008.

[123] S. Bolte and F. P. Cordelieres. A guided tour into subcellular colocalization analysis in light microscopy. *Journal of microscopy*, 224(3):213–232, 2006.

[124] Anne E. West, Rachael L. Neve, and Kathleen M. Buckley. Targeting of the Synaptic Vesicle Protein Synaptobrevin in the Axon of Cultured Hippocampal Neurons: Evidence for Two Distinct Sorting Steps. *J Cell Biol*, 139(4):917–927, 1997.

[125] Jeremy S. Dittman and Joshua M. Kaplan. Factors regulating the abundance and localization of synaptobrevin in the plasma membrane. *PNAS*, 103(30):11399–11404, 2006.

[126] Tomás Fernández-Alfonso, Ricky Kwan, and Timothy A. Ryan. Synaptic Vesicles Interchange Their Membrane Proteins with a Large Surface Reservoir during Recycling. *Neuron*, 51(2):179–186, 2006.

[127] Magda S. Santos, C. Kevin Park, Sarah M. Foss, Haiyan Li, and Susan M. Voglmaier. Sorting of the Vesicular GABA Transporter to Functional Vesicle Pools by an Atypical Dileucine-like Motif. *J Neurosci*, 33(26):10634–10646, 2013.

[128] Shawn M. Ferguson, Gabor Brasnjo, Mitsuko Hayashi, Markus Wölfel, Chiara Collesi, Silvia Giovedi, Andrea Raimondi, Liang-Wei Gong, Pablo Ariel, Summer Paradise, Eileen O'Toole, Richard Flavell, Ottavio Cremona, Gero Miesenböck, Timothy A. Ryan, and Pietro De Camilli. A Selective Activity-Dependent Requirement for Dynamin 1 in Synaptic Vesicle Endocytosis. *Science*, 316(5824):570–574, 2007.

[129] Björn Granseth, Benjamin Odermatt, Stephen J. Royle, and Leon Lagnado. Clathrin-Mediated Endocytosis Is the Dominant Mechanism of Vesicle Retrieval at Hippocampal Synapses. *Neuron*, 51(6):773–786, 2006.

[130] Meera Mani, Sang Yoon Lee, Louise Lucast, Ottavio Cremona, Gilbert Di Paolo, Pietro De Camilli, and Timothy A. Ryan. The Dual Phosphatase Activity of Synaptojanin1 Is Required for Both Efficient Synaptic Vesicle Endocytosis and Reavailability at Nerve Terminals. *Neuron*, 56(6):1004–1018, 2007.

[131] Karina J. Vargas, Sachin Makani, Taylor Davis, Christopher H. Westphal, Pablo E. Castillo, and Sreeganga S. Chandra. Synucleins Regulate the Kinetics of Synaptic Vesicle Endocytosis. *J. Neurosci.*, 34(28):9364–9376, 2014.

[132] S. Naito and T. Ueda. Adenosine triphosphate-dependent uptake of glutamate into protein I-associated synaptic vesicles. *J. Biol. Chem.*, 258(2):696–699, 1983.

[133] Tomas Fernandez-Alfonso and Timothy A. Ryan. A heterogeneous "resting" pool of synaptic vesicles that is dynamically interchanged across boutons in mammalian CNS synapses. *Brain Cell Biology*, 36(1-4):87–100, 2008.

[134] Jerome Di Giovanni and Zu-Hang Sheng. Regulation of synaptic activity by snapin-mediated endolysosomal transport and sorting. *EMBO J*, 34(15):2059–2077, 2015.

[135] Taisuke Miyazaki, Masahiro Fukaya, Hidemi Shimizu, and Masahiko Watanabe. Subtype switching of vesicular glutamate transporters at parallel fibre–Purkinje cell synapses in developing mouse cerebellum. *European Journal of Neuroscience*, 17(12):2563–2572, 2003.

[136] David G. Bole and Tetsufumi Ueda. Inhibition of Vesicular Glutamate Uptake by Rose Bengal-Related Compounds: Structure–Activity Relationship. *Neurochem Res*, 30(3):363–369, 2005.

[137] Kiyokazu Ogita, Koji Hirata, David G. Bole, Sumiko Yoshida, Yutaka Tamura, Anne Marie Leckenby, and Tetsufumi Ueda. Inhibition of vesicular glutamate storage and exocytotic release by Rose Bengal. *J. Neurochem.*, 77(1):34–42, 2001.

[138] Antonio Valencia and Julio Morán. Reactive oxygen species induce different cell death mechanisms in cultured neurons. *Free Radical Biology and Medicine*, 36(9):1112–1125, 2004.

[139] W. F. Boron and P. De Weer. Intracellular pH transients in squid giant axons caused by CO2, NH3, and metabolic inhibitors. *The Journal of General Physiology*, 67(1):91–112, 1976.

[140] G. Miesenbock. Synapto-pHluorins: Genetically Encoded Reporters of Synaptic Transmission. *Cold Spring Harbor Protocols*, 2012(2), 2012.

[141] Olusoji A. T. Afuwape, Catherine R. Wasser, Thomas Schikorski, and Ege T. Kavalali. Synaptic vesicle pool-specific modification of neurotransmitter release by intravesicular free radical generation. *J Physiol*, 595(4):1223–1238, 2017.

[142] Xin Chen, Yue Bi, Tianyang Wang, Pengfei Li, Xin Yan, Shanshan Hou, Catherine E. Bammert, Jingfang Ju, K. Michael Gibson, William J. Pavan, and Lanrong Bi. Lysosomal Targeting with Stable and Sensitive Fluorescent Probes (Superior LysoProbes): Applications for Lysosome Labeling and Tracking during Apoptosis. *Scientific Reports*, 5:9004, 2015.

[143] Federica Daniele, Eliana S. Di Cairano, Stefania Moretti, Giovanni Piccoli, and Carla Perego. TIRFM and pH-sensitive GFP-probes to Evaluate Neurotransmitter Vesicle Dynamics in SH-SY5Y Neuroblastoma Cells: Cell Imaging and Data Analysis. *Journal of Visualized Experiments*, (95), 2015.

[144] Céline Delloye-Bourgeois, Arnaud Jacquier, Julien Falk, and Valérie Castellani. Use of pHluorin to Assess the Dynamics of Axon Guidance Receptors in Cell Culture and in the Chick Embryo. *JoVE (Journal of Visualized Experiments)*, (83):e50883–e50883, 2014.

[145] Dreosti Elena and Lagnado Leon. Optical reporters of synaptic activity in neural circuits. *Experimental Physiology*, 96(1):4–12, 2010.

[146] Serguei S. Khiroug, Evgeny Pryazhnikov, Sarah K. Coleman, Andreas Jeromin, Kari Keinänen, and Leonard Khiroug. Dynamic visualization of membrane-inserted fraction of pHluorin-tagged channels using repetitive acidification technique. *BMC Neuroscience*, 10:141, 2009.

[147] Yun Li, Brittany D. Roy, Wei Wang, Lifeng Zhang, Stephen B. Sampson, and Da-Ting Lin. Imaging pHluorin-tagged Receptor Insertion to the Plasma Membrane in Primary Cultured Mouse Neurons. *JoVE (Journal of Visualized Experiments)*, (69):e4450–e4450, 2012.

[148] Jessica C. Nicholson-Fish, Karen J. Smillie, and Michael A. Cousin. Monitoring activity-dependent bulk endocytosis with the genetically-encoded reporter VAMP4-pHluorin. *Journal of Neuroscience Methods*, 266:1–10, 2016.

[149] Derek C. Prosser, Kristie Wrasman, Thaddeus K. Woodard, Allyson F. O'Donnell, and Beverly Wendland. Applications of pHluorin for Quantitative, Kinetic and High-throughput Analysis of Endocytosis in Budding Yeast. *JoVE (Journal of Visualized Experiments)*, (116):e54587–e54587, 2016.

[150] Stephen J. Royle, Björn Granseth, Benjamin Odermatt, Aude Derevier, and Leon Lagnado. Imaging pHluorin-based probes at hippocampal synapses. *Methods Mol Biol*, 457:293–303, 2008.

[151] Juan Burrone, Zhiying Li, and Venkatesh N Murthy. Studying vesicle cycling in presynaptic terminals using the genetically encoded probe synaptopHluorin. *Nature Protocols*, 1(6):2970–2978, 2007.

[152] Yongling Zhu, Jian Xu, and Stephen F. Heinemann. Two Pathways of Synaptic Vesicle Retrieval Revealed by Single-Vesicle Imaging. *Neuron*, 61(3):397–411, 2009.

[153] Roman M. Lazarenko, Claire E. DelBove, and Qi Zhang. Fluorescent Measurement of Synaptic Activity Using FM Dyes in Dissociated Hippocampal Cultured Neurons. *Bio Protoc*, 8(2), 2018.

[154] Shigeo Takamori, Matthew Holt, Katinka Stenius, Edward A. Lemke, Mads Grønborg, Dietmar Riedel, Henning Urlaub, Stephan Schenck, Britta Brügger, Philippe Ringler, Shirley A. Müller, Burkhard Rammner, Frauke Gräter, Jochen S. Hub,

Bert L. De Groot, Gottfried Mieskes, Yoshinori Moriyama, Jürgen Klingauf, Helmut Grubmüller, John Heuser, Felix Wieland, and Reinhard Jahn. Molecular Anatomy of a Trafficking Organelle. *Cell*, 127(4):831–846, 2006.

[155] Martin Wienisch and Jurgen Klingauf. Vesicular proteins exocytosed and subsequently retrieved by compensatory endocytosis are nonidentical. *Nature Neuroscience*, 9(8):1019–1027, 2006.

[156] Joseph R. Casey, Sergio Grinstein, and John Orlowski. Sensors and regulators of intracellular pH. *Nature Reviews Molecular Cell Biology*, 11(1):50–61, 2010.

[157] Jeremy Dittman and Timothy A. Ryan. Molecular Circuitry of Endocytosis at Nerve Terminals. *Annual Review of Cell and Developmental Biology*, 25(1):133–160, 2009.

[158] Körber Christoph, Horstmann Heinz, Sätzler Kurt, and Kuner Thomas. Endocytic Structures and Synaptic Vesicle Recycling at a Central Synapse in Awake Rats. *Traffic*, 13(12):1601–1611, 2012.

[159] Rebekka M. Wachter and S. James Remington. Sensitivity of the yellow variant of green fluorescent protein to halides and nitrate. *Current Biology*, 9(17):R628–R629, 1999.

[160] Tetsufumi Ueda and Shigetaka Naito. Specific Inhibition of the Phosphorylation of Protein I, a Synaptic Protein, by Affinity-Purified Anti-Protein I Antibody. *Progress in Brain Research*, 56:87–103, 1982.

[161] Shigetaka Naito and Tetsufumi Ueda. Characterization of Glutamate Uptake into Synaptic Vesicles. *Journal of Neurochemistry*, 44(1):99–109, 1985.

[162] Benjamin R. Rost, Franziska Schneider, M. Katharina Grauel, Christian Wozny, Claudia G. Bentz, Anja Blessing, Tanja Rosenmund, Thomas J. Jentsch, Dietmar Schmitz, Peter Hegemann, and Christian Rosenmund. Optogenetic acidification of synaptic vesicles and lysosomes. *Nature Neuroscience*, 18(12):1845–1852, 2015.

[163] B. Ceccarelli, W. P. Hurlbut, and A. Mauro. Turnover of Transmitter and Synaptic Vesicles at the Frog Neuromuscular Junction. *The Journal of Cell Biology*, 57(2):499–524, 1973.

[164] J. E. Heuser and T. S. Reese. Evidence for Recycling of Synaptic Vesicle Membrane During Transmitter Release at the Frog Neuromuscular Junction. *The Journal of Cell Biology*, 57(2):315–344, 1973.

[165] Alexandros C. Kokotos and Michael A. Cousin. Synaptic Vesicle Generation from Central Nerve Terminal Endosomes. *Traffic*, 16(3):229–240, 2015.

[166] Tolga Soykan, Tanja Maritzen, and Volker Haucke. Modes and mechanisms of synaptic vesicle recycling. *Current Opinion in Neurobiology*, 39:17–23, 2016.

[167] Shigeki Watanabe and Emmanuel Boucrot. Fast and ultrafast endocytosis. *Current Opinion in Cell Biology*, 47:64–71, 2017.

[168] Venkatesh N. Murthy and Pietro De Camilli. Cell biology of the presynaptic terminal. *Annual Review of Neuroscience*, 26(1):701–728, 2003.

[169] L. Logiudice, P. Sterling, and G. Matthews. Vesicle recycling at ribbon synapses in the finely branched axon terminals of mouse retinal bipolar neurons. *Neuroscience*, 164(4):1546–1556, 2009.

[170] Henrique Von Gersdorff and Gary Mathews. Dynamics of synaptic vesicle fusion and membrane retrieval in synaptic terminals. *Nature*, 367(6465):735–739, 1994.

[171] Emmanuel Boucrot, Antonio P. A. Ferreira, Leonardo Almeida-Souza, Sylvain Debard, Yvonne Vallis, Gillian Howard, Laetitia Bertot, Nathalie Sauvonnet, and Harvey T. McMahon. Endophilin marks and controls a clathrin-independent endocytic pathway. *Nature*, 517(7535):460–465, 2015.

[172] Igor Delvendahl, Nicholas P. Vyleta, Henrique von Gersdorff, and Stefan Hallermann. Fast, Temperature-Sensitive and Clathrin-Independent Endocytosis at Central Synapses. *Neuron*, 90(3):492–498, 2016.

[173] Sunil P. Gandhi and Charles F. Stevens. Three modes of synaptic vesicular recycling revealed by single-vesicle imaging. *Nature*, 423(6940):607–613, 2003.

[174] Qi Zhang, Yulong Li, and Richard W. Tsien. The Dynamic Control of Kiss-And-Run and Vesicular Reuse Probed with Single Nanoparticles. *Science*, 323(5920):1448–1453, 2009.

[175] T. M. Miller and J. E. Heuser. Endocytosis of synaptic vesicle membrane at the frog neuromuscular junction. *The Journal of Cell Biology*, 98(2):685–698, 1984.

[176] Matthew Holt, Anne Cooke, Minnie M. Wu, and Leon Lagnado. Bulk Membrane Retrieval in the Synaptic Terminal of Retinal Bipolar Cells. *Journal of Neuroscience*, 23(4):1329–1339, 2003.

[177] Wei Wu and Ling-Gang Wu. Rapid bulk endocytosis and its kinetics of fission pore closure at a central synapse. *Proceedings of the National Academy of Sciences*, 104(24):10234–10239, 2007.

[178] Shigeki Watanabe, Qiang Liu, M. Wayne Davis, Gunther Hollopeter, Nikita Thomas, Nels B. Jorgensen, and Erik M. Jorgensen. Ultrafast endocytosis at Caenorhabditis elegans neuromuscular junctions. *eLife*, 2:e00723, 2013.

[179] Shigeki Watanabe, Benjamin R. Rost, Marcial Camacho-Pérez, M. Wayne Davis, Berit Söhl-Kielczynski, Christian Rosenmund, and Erik M. Jorgensen. Ultrafast endocytosis at mouse hippocampal synapses. *Nature*, 504(7479):242–247, 2013.

[180] Ira Milosevic. Revisiting the Role of Clathrin-Mediated Endoytosis in Synaptic Vesicle Recycling. *Front. Cell. Neurosci.*, 12, 2018.

[181] Stephen M. Smith, Robert Renden, and Henrique von Gersdorff. Synaptic vesicle endocytosis: Fast and slow modes of membrane retrieval. *Trends in Neurosciences*, 31(11):559–568, 2008.

[182] Sethuraman Sankaranarayanan and Timothy A. Ryan. Calcium accelerates endocytosis of vSNAREs at hippocampal synapses. *Nature Neuroscience*, 4(2):129–136, 2001.

[183] Zohreh Farsi, Sindhuja Gowrisankaran, Matija Krunic, Burkhard Rammner, Andrew Woehler, Eileen M. Lafer, Carsten Mim, Reinhard Jahn, and Ira Milosevic. Clathrin coat controls synaptic vesicle acidification by blocking vacuolar ATPase activity. *eLife*, 7:e32569, 2018.

[184] Yang-In Yim, Tao Sun, Ling-Gang Wu, Andrea Raimondi, Pietro De Camilli, Evan Eisenberg, and Lois E. Greene. Endocytosis and clathrin-uncoating defects at synapses of auxilin knockout mice. *Proceedings of the National Academy of Sciences*, 107(9):4412–4417, 2010.

[185] Ira Milosevic, Silvia Giovedi, Xuelin Lou, Andrea Raimondi, Chiara Collesi, Hongying Shen, Summer Paradise, Eileen O'Toole, Shawn Ferguson, Ottavio Cremona, and Pietro De Camilli. Recruitment of endophilin to clathrin-coated pit necks is required for efficient vesicle uncoating after fission. *Neuron*, 72(4):587–601, 2011.

[186] P. J. Boyle and E. J. Conway. Potassium accumulation in muscle and associated changes. *The Journal of Physiology*, 100(1):1–63, 1941.

[187] A. L. Hodgkin and B. Katz. The effect of sodium ions on the electrical activity of giant axon of the squid. *The Journal of Physiology*, 108(1):37–77, 1949.

[188] Eric Delpire and Kevin J Staley. Novel determinants of the neuronal Cl- concentration. *The Journal of Physiology*, 592(Pt 19):4099–4114, 2014.

[189] E. Delpire. Cation-Chloride Cotransporters in Neuronal Communication. *News in Physiological Sciences*, 15:309–312, 2000.

[190] Yehezkel Ben-Ari. Excitatory actions of gaba during development: The nature of the nurture. *Nature Reviews. Neuroscience*, 3(9):728–739, 2002.

[191] Peter Blaesse, Matti S. Airaksinen, Claudio Rivera, and Kai Kaila. Cation-chloride cotransporters and neuronal function. *Neuron*, 61(6):820–838, 2009.

[192] K. W. Sung, M. Kirby, M. P. McDonald, D. M. Lovinger, and E. Delpire. Abnormal GABAA receptor-mediated currents in dorsal root ganglion neurons isolated from Na-K-2Cl cotransporter null mice. *The Journal of Neuroscience: The Official Journal of the Society for Neuroscience*, 20(20):7531–7538, 2000.

[193] Claudio Rivera, Juha Voipio, John A. Payne, Eva Ruusuvuori, Hannele Lahtinen, Karri Lamsa, Ulla Pirvola, Mart Saarma, and Kai Kaila. The K^+/Cl^- cotransporter KCC2 renders GABA hyperpolarizing during neuronal maturation. *Nature*, 397(6716):251–255, 1999.

[194] Verena Untiet, Peter Koverman, Gerkau Niklas J., Thomas Gensch, Christine R. Rose, and Christoph Fahlke. Glutamate transporter-associated anion channels adjust intracellular chloride concentrations during glial maturation. *Glia*, 65(2):388–400, 2016.

[195] I. Dietzel, U. Heinemann, G. Hofmeier, and H. D. Lux. Stimulus-induced changes in extracellular Na+ and Cl- concentration in relation to changes in the size of the extracellular space. *Experimental Brain Research*, 46(1):73–84, 1982.

[196] Thomas Gensch, Verena Untiet, Arne Franzen, Peter Kovermann, and Christoph Fahlke. Determination of Intracellular Chloride Concentrations by Fluorescence Lifetime Imaging. In Wolfgang Becker, editor, *Advanced Time-Correlated Single*

Photon Counting Applications, volume 111, pages 189–211. Springer International Publishing, Cham, 2015.

[197] A. S. Verkman, M. C. Sellers, A. C. Chao, T. Leung, and R. Ketcham. Synthesis and characterization of improved chloride-sensitive fluorescent indicators for biological applications. *Analytical Biochemistry*, 178(2):355–361, 1989.

[198] Yoichi Ishida, Smita Nayak, Joseph A. Mindell, and Michael Grabe. A model of lysosomal pH regulation. *J. Gen. Physiol.*, 141(6):705–720, 2013.

Danksagung

Mein Dank geht an alle, die mich in den letzten Jahren unterstützt haben und zum Gelingen dieser Arbeit beigetragen haben.

Insbesondere danke ich Prof. Christoph Fahlke, der mir ermöglicht hat an diesem Forschungsprojekt an seinem Institut zu arbeiten, immer ein offenes Ohr für mich hatte und mich in jeglicher Hinsicht unterstützt hat.
Herrn Prof. Karl-Erich Jaeger danke ich für die Übernahme des Zweitgutachtens dieser Arbeit.
Meinem Betreuer Thomas Gensch danke ich für die anregenden Diskussionen und die fachliche und technische Betreuung.
Raul Guzman und Gustavo Guzman danke ich für die Unterstüzung in der Zellkultur, Virusproduktion, Fragen zu Neuronen und vielem mehr.
Arne Franzen, Christoph Aretzweiler, Meike Zimmerman und Petra Thelen danke ich für technische und molekularbiologische Unterstützung.
Verena, Matthias, Peter, Patricia, Arnd und allen Mitarbeitern des ICS-4 danke für ich die Unterstützung und Diskussionen.

Besonderer Dank gilt meiner Familie und meinen Freunden.

Eidesstattliche Versicherung

Ich versichere an Eides Statt, dass die Dissertation von mir selbstständig und ohne unzulässige fremde Hilfe unter Beachtung der "Grundsätze zur Sicherung guter wissenschaftlicher Praxis an der Heinrich-Heine-Universität Düsseldorf" erstellt worden ist.

Jülich, 07. Juni 2018

Felix Beinlich